To the Graduate Council:

I am submitting herewith a thesis written by Steven Scott Smith entitled "Reverse-Flow Oxidation Catalyst with Supplemental Fuel Injection for Lean-Burn Natural Gas Engines." I have examined the final electronic copy of this thesis for form and content and recommend that it be accepted in partial fulfillment of the requirements for the degree of Master of Science, with a major in Mechanical Engineering.

Ke Nguyen
Major Professor

We have read this thesis
and recommend its acceptance:

David K. Irick

C. Stuart Daw

Accepted for the Council:

Anne Mayhew
Vice Chancellor and
Dean of Graduate Studies

(Original signatures are on file with official student records.)

REVERSE-FLOW OXIDATION CATALYST WITH SUPPLEMENTAL FUEL INJECTION FOR LEAN-BURN NATURAL GAS ENGINES

A

Thesis

Presented for the

Master of Science Degree

The University of Tennessee, Knoxville

Steven Scott Smith

August 2005

DEDICATION

To my love,
Andrea.

Your brilliance and true compassion for the world
serves as my inspiration.

ACKNOWLEDGEMENTS

I would like to thank my advisor, Dr. Ke Nguyen, for giving me the opportunity to widen my horizons though the course of this project. I would also like to thank my graduate committee members, Dr. David Irick and Dr. Stuart Daw. I would like to express my appreciation to Danny Graham, Gary Hatmaker, and Dennis Higdon for their advice and expertise I've used extensively over the course of my undergraduate and graduate career. To (soon to be Dr.) David Smith I would like to express my thanks for all his help with the LabVIEW programming for the project. I would like to thank my laboratory colleagues, Vitaly Prikhodko, Barath Kumar, Ajit Gopinath, Scott Eaton, and (soon to be Dr.) Hakyong Kim, for their assistance and camaraderie throughout my project. To EmerChem I would like to express my thanks for their contribution of the catalyst samples used in this project. I would like to thank the U.S. Department of Energy and the Advanced Reciprocating Engine Systems (ARES) program for their financial support and to Dr. Ming Zheng for obtaining funding for this project.

Lastly, I would like to thank my parents for their love and guidance throughout the course of my life.

ABSTRACT

The purpose of this research is to demonstrate that the use of a reverse-flow oxidation catalyst reactor (RFOCR), both with and without supplemental fuel injection (SFI), will result in significant reductions of methane (CH_4) in a simulated lean-burn natural gas exhaust mixture. Methane reduction is investigated as a function of the directional duration of the exhaust gases through the oxidation catalyst, gas hourly space velocity (GHSV), and exhaust gas temperature. The CH_4 catalytic chemical reaction, at an elevated exhaust gas temperature, is an exothermic reaction and elevating the temperature across the catalyst reactor corresponds to an increase in CH_4 conversion. Periodically reversing the inlet and outlet exhaust direction through the catalyst traps the heat released from the chemical reaction, raising the overall temperature of the exhaust gas through the RFOCR. This study demonstrates the ability of the RFOCR to trap heat, thereby increasing CH_4 oxidation. This ability to trap heat provides a significant advantage over standard unidirectional flow catalytic converters. Additionally, to increase CH_4 conversion at relatively low feed temperatures, the injection of a supplemental fuel mixture consisting of carbon monoxide (CO) and hydrogen (H_2) was evaluated.

The experimental results confirm that, when compared with unidirectional flow, periodically reversing the flow of exhaust mixture through a catalyst reactor can significantly improve CH_4 conversion. Results also indicate that the effect of switching time (ST) on CH_4 conversion vary significantly with gas hourly space velocity (GHSV) and temperature. Furthermore, results indicate that by introducing supplemental fuel into the feed mixture at low engine operating conditions CH_4 conversion is notably improved by elevating the temperature across the catalyst reactor through the combustion of carbon monoxide and hydrogen. However, extended durations of increased CH_4 conversion during reverse-flow operations is not possible after supplemental fuel injection is terminated.

TABLE OF CONTENTS

CHAPTER **PAGE**

1. INTRODUCTION……..……1
2. LITERATURE REVIEW……...……4
    - 2.1 Lean-Burn Natural Gas Engine Emissions……..….4
    - 2.2 Oxidation Reactions…….….…7
    - 2.3 Oxidation Catalyst Selection……..…….…..7
    - 2.4 Palladium Catalyst Oxidation Mechanism……...……8
    - 2.5 Catalyst Deactivation…….….…..8
        - 2.5.1 Palladium Oxide Dissociation…….…….10
        - 2.5.2 Catalyst Sintering…….……10
        - 2.5.3 Inhibiting Effects of Water Vapor…….……..11
    - 2.6 Reverse-Flow Oxidation Catalyst Reactor ……...…..12
        - 2.6.1 Effects of Varying Switching Time for a Reverse-Flow Reactor…….….15
        - 2.6.2 Effects of Varying Volumetric Flowrate for a Reverse-Flow Reactor…….….16

3. EXPERIMENTAL APPARTUS…….…….17
    - 3.1 Overall Description of the Bench-Flow Reactor……17
    - 3.2 Experimental Catalyst…….20
    - 3.3 Components of the Bench-Flow Reactor……21
        - 3.3.1 Reverse-Flow Oxidation Catalyst Reactor……...21
        - 3.3.2 Supplemental Fuel Injection ……...25
        - 3.3.3 Instrument Cabinet……...27
        - 3.3.4 Horiba Analyzer Cabinet…….……27
        - 3.3.5 Peristaltic Pump……...29
        - 3.3.6 Steam Generator……..30
        - 3.3.7 Reactor Branching Valves……...31

3.3.8 Preheater……..31
3.3.9 Mass Flow Controllers…….……31
3.3.10 Solenoid Valves and Solid-State Relays……33
3.4 Instrumentation and Displays…….35
3.4.1 Pressure Transducers Locations……..35
3.4.2 Reverse-Flow Oxidation Catalyst Thermocouple Locations……...36
3.4.3 Temperature Controllers……..36
3.5 Analyzers……36
3.5.1 Carbon Monoxide Analyzers……...36
3.5.2 Carbon Dioxide Analyzer……37
3.5.3 Total Hydrocarbon Analyzer……...37
3.6 Overview of the Data Acquisition System…….38
3.7 Components of the Data Acquisition System…….……39
3.7.1 Computer…….39
3.7.2 Data Acquisition Boards……..……39
3.7.3 LabVIEW…….……39
3.8 Operation of the Bench-Flow Reactor……..……..41
3.8.1 Start-up Procedure……...41
3.9 Experimental Protocols.…….……42
3.9.1 Simulated Exhaust Gas Composition……..……42
3.9.2 Reverse-Flow Oxidation Catalyst Reactor Experimental Protocol…….……42
3.9.3 Supplemental Fuel Injection Protocol..……44

4. EXERIMENTAL RESULTS……..……..45
4.1 Reverse-Flow Oxidation Catalyst Reactor Without Supplemental Fuel Injection……45
4.1.1 Exhaust Mixture Bypassing the Catalyst Due to Flow Reversal….53
4.1.2 Effects of Switching Time and Gas Hourly Space Velocity on CH_4 Conversion…….……..57

4.1.3 Effect of Temperature and Gas Hourly Space Velocity on CH_4 Conversion…….64
4.2 Reverse-Flow Oxidation Catalyst Reactor With Supplemental Fuel Injection……66
4.2.1 Effects of Supplemental Fuel Injection on CH_4 Conversion….…..68

5. CONCLUSIONS AND RECOMMENDATIONS…….……..74

REFERENCES…….……76
APPENDIX……..……..80
VITA……..86

LIST OF TABLES

TABLE PAGE

3.1. Operational Flow Ranges for Individual Mass Flow Controllers……..…….……. 34

3.2. Simulated Exhaust Gas Composition……43

4.1. Average Methane Conversion for the Unidirectional and Flow Reversal Regimes at Reactor Furnace Temperatures of 400, 450, 500, and 600°C, STs of 10, 15, 20, 30, and 45s, and a GHSV of 20,000 hr^{-1}…….……....49

4.2. Average Methane Conversion for the Unidirectional and Flow Reversal Regimes at Reactor Furnace Temperatures of 400, 450, 500, and 600°C, STs of 10, 15, 20, 30, and 45s, and a GHSV of 40,000 hr^{-1}…….…….……...50

4.3. Average Methane Conversion for the Unidirectional and Flow Reversal Regimes at Reactor Furnace Temperatures of 400, 450, 500, and 600°C, STs of 10, 15, 20, 30, and 45s, and a GHSV of 60,000 hr^{-1}……..……..51

4.4. Average Methane Conversion for the Unidirectional and Flow Reversal Regimes at Reactor Furnace Temperatures of 400, 450, 500, and 600°C, STs of 10, 15, 20, 30, and 45s, and a GHSV of 80,000 hr^{-1}……..……...52

4.5. Effects of Switching Time on CO Concentration Bypassing the Catalyst at a Reactor Furnace Temperature of 450°C, a GHSV of 40,000hr^{-1}, and a ST of 10,15, 20, 30, and 45s…….…….……57

4.6. RFOCR Residence Times for the Total Exhaust Mixture at All Reactor Inlet Temperatures and GHSVs……61

4.7. Average CH_4 Conversion With and Without SFI for Unidirectional Flow and Flow Reversal at a Reactor Furnace Temperature of 350°C, a GHSV of 20,000 hr^{-1}, and a ST of 20s for Flow Reversal Operations...……..73

APPENDIX TABLE

A-1. Specifications for the Analyzers……..……81

LIST OF FIGURES

FIGURE PAGE

2.1. Hydrocarbon Production as a Function of Equivalence Ratio……...…..6

2.2. Carbon Monoxide Production as a Function of Equivalence Ratio……...……..6

2.3. An Outline Mechanism of the Oxidation of Methane Over a Palladium Catalyst……..….9

2.4. An Example of the Dissociation and Reoxidation of Palladium Oxide…….11

2.5. Schematic of the RFOCR…….…..13

2.6. Temperature Profile Across the Length of the Catalyst…….13

2.7. Illustration of the Heat Trap Effect……....14

3.1. Schematic of the Bench-Flow Reactor System……..18

3.2. Bench-Flow Reactor……..19

3.3. Oxidation Catalyst Physical Parameters……....20

3.4. Initial Version of the Reverse-Flow Oxidation Catalyst Reactor…….….22

3.5. Current Version of the Reverse-Flow Oxidation Catalyst…….….22

3.6. Current Reactor End Fitting……...……23

3.7. Catalyst Reactor Section…….…23

3.8. Schematic of the Reverse-Flow Oxidation Catalyst Reactor……..25

3.9. Supplemental Fuel Injection Set-up……26

3.10. Instrument Cabinet……...28

3.11. Water Condenser Inside of the Horiba Analyzer Bench……..28

3.12. Control Panel of the Horiba Instrument Cabinet…….29

3.13. Peristaltic Pump and Steam Generator…….30

3.14. Reactor Branching Valves……...32

3.15. Wiring of Displays and MFC Inside the Instrument Cabinet……...32

3.16. Solenoid Valve Configuration……34
3.17. Power Supplies with Solid State Relays……..35
3.18. Thermocouple Locations with Respect to the Catalyst Sample……...37
3.19. LabVIEW Controlling Screen for the Bench-Flow Reactor……40
4.1. Methane Conversion at a Reactor Furnace Temperature of 450°C, GHSV of 40,000 hr^{-1}, and a ST of 10s……..46
4.2. Temperature Profiles Across the Catalyst Length at Various Times at a Reactor Furnace Temperature of 450°C, GHSV of 40,000 hr^{-1}, and a ST of 10s……46
4.3. Temperature Profiles Across the Catalyst Length at a Reactor Furnace Temperature of 450°C and a GHSV of 40,000 hr^{-1} with Unidirectional Flow……..48
4.4. Baseline Unidirectional Temperature Profiles for 10 and 45s ST Experimental Runs at a Reactor Furnace Temperature of 400°C, a GHSV of 20,000 hr^{-1}……...……...54
4.5. Illustration of Dead Volume Associated with a RFR…….……...…56
4.6. Carbon Monoxide Concentration at a Reactor Furnace Temperature of 450°C, a GHSV of 40,000 hr^{-1}, and a ST of 10s…….……..56
4.7. Effects of Switching Time on CH_4 Conversion with GHSV as a Parameter at a Temperature of 400°C……...….58
4.8. Temperature Profile Across the Catalyst at a Reactor Furnace Temperature of 400°C, a GHSV of 20,000 hr^{-1}, and a ST of 10s at Various Experimental Run Times……...……..58
4.9. Temperature Profiles Across the Catalyst at Various Times During an Experimental Run at a Reactor Furnace Temperature of 400°C, GHSV of 20,000 hr^{-1}, and a ST of 30s……60
4.10. Effects of Switching Time on CH_4 Conversion with GHSV as a Parameter at a Temperature of 450°C……....60
4.11. Representation of Various Regimes on an Arrhenius Plot…….…...……..…61

4.12. Temperature Profile at a Reactor Furnace Temperature of 450°C, GHSV of 40,000 hr^{-1}, and a ST of 45s at Various Experimental Run Times…….….63
4.13. Effects of Switching Time on CH_4 Conversion with GHSV as a Parameter at Temperature of 550°C……...……...63
4.14. Effects of Temperature on CH_4 Conversion with Temperature as a Parameter at a GHSV of 80,000 hr^{-1} and a ST of 10s…….……...65
4.15. Effects of Temperature on CH_4 Conversion with GHSV as a Parameter at a ST of 10s…….……...67
4.16. Methane Conversion during Unidirectional Flow Operations with 25 10-Second Pulses of SFI, a Reactor Furnace Temperature of 350°C, and a GHSV of 20,000 hr^{-1}……...69
4.17. Temperature Profile across the Catalyst during Unidirectional Flow Operations at Various Instances of Time with 25 10-Second Pulses of SFI, a Reactor Furnace Temperature of 350°C and a GHSV of 20,000 hr^{-1}…….69
4.18. Methane Conversion with 25 10-Second Pulses of SFI, a Reactor Furnace Temperature of 350°C, a GHSV of 20,000 hr^{-1}, and a ST of 20s……71
4.19. Temperature Profile across the Catalyst at Various Instances of Time with 25 10-Second Pulses of SFI, a Reactor Furnace Temperature of 350°C and a GHSV of 20,000 hr^{-1}……..……71
4.20. Temperature Profile across the Catalyst at Various Instances of Time with 25 10-Second Pulses of SFI, a Reactor Furnace Temperature of 350°C and a GHSV of 20,000 hr^{-1}……..73

APPENDIX FIGURES

FIGURE PAGE

A-1. Effects of 10% Water Vapor on the Methane Conversion at 350°C……..…..82

A-2. Initial Reverse Flow Oxidation Catalyst Reactor with Temperature Oscillation……82

A-3. Effects of Switching Time on CH_4 Conversion with GHSV as a Parameter at a Temperature of 500°C……...83

A-4. Effects of Switching Time on CH_4 Conversion with GHSV as a Parameter at a Temperature of 600°C……...83

A-5. Effects of Temperature on CH4 Conversion with GHSV as a Parameter at a ST of 15s……..……84

A-6. Effects of Temperature on CH4 Conversion with GHSV as a Parameter at a ST of 20s…….……..84

A-7. Effects of Temperature on CH4 Conversion with GHSV as a Parameter at a ST of 30s…….…..85

A-8. Effects of Temperature on CH4 Conversion with GHSV as a Parameter at a ST of 45s…….……..85

LIST OF SYMBOLS

ϕ……..equivalence ratio

A…….pre-exponential factor

Al_2O_3…….……alumina

BFR…….…….bench-flow reactor

C…….……carbon atom

^oC……..…….degrees Celsius

cc/min……..cubic centimeters per minute

CH_2……..…….methylene

CH_4……...……methane

CO……..……carbon monoxide

CO_2……...……..carbon dioxide

cpsi……..……..cells per square inch

CRS……..…… ……catalyst reactor section

DAC…….……data acquisition system

DC…….……..direct current

E_a…….…..activation energy

FID…….flame ionization detector

g/ft^3……grams per cubic foot

GHSV……gas hourly space velocity

H…….……hydrogen atom

H_2…….……...…….hydrogen molecule

H_2O……..……...…water vapor

hr^{-1}…….……per hour

HTSV……..……..high temperature switching valve

I.D…….…..inner diameter

ICE……..internal combustion engine

k…….rate constant

k_a…….....apparent rate constant

kJ/mol…….…….kilojoules per mole

L/min……...liters per minute

LNT…….…lean NO_x trap

MFC…….…mass flow controller

ms……...……millisecond

N_2…….…nitrogen molecule

NMHC……..nonmethane hydrocarbon

NO_x…….…….oxides of nitrogen

O……..……..…oxygen atom

O.D…….outer diameter

Pd……..…….……palladium

PdO……..palladium oxide

$Pd(OH)_2$……palladium hydroxide

ppm……..parts per million

ppsi……..pores per square inch

psi…….pounds per square inch

Pt…….platinum

R_u……..….universal gas constant

RFOCR……..…..reverse-flow oxidation catalyst reactor

RFR……..…….reverse-flow reactor

Rh…….rhodium

RPM……..revolutions per minute

SFI…….supplemental fuel injection

ST…….…….switching time

STP……..……..standard temperature and pressure

T……..…..temperature

t…….……time

THC…….……total hydrocarbon

TM…….…..trademark

V……...volt

CHAPTER 1

INTRODUCTION

The global increase in demand for crude oil and the diminishing supply of these reserves has prompted increased interest in obtaining a domestic and alternative source of energy. In conjunction with easing the domestic dependency on foreign oil, strides have been made to reduce the environmental impact of exhaust emissions from internal combustion engines (ICE). Examples of advances in furthering the quest for minimizing air pollution and greenhouse gas emissions include stringent engine emission legislation, hybrid electric vehicles, and cleaner fuels.

One possible solution for both decreasing the demand for foreign oil and reducing harmful carbon dioxide exhaust emissions is the use of natural gas as an alternative fuel. The benefits of natural gas include its domestic abundance and low carbon content. Natural gas, composed primarily of methane, has a high octane rating, which allows combustion at higher compression ratios without resulting in engine knock, and because of the wide flammability range of natural gas, it is possible to operate an engine with very lean fuel mixtures. Another benefit is the lower carbon content of natural gas, which corresponds to a lower carbon dioxide (CO_2) concentration in the exhaust mixture when compared to gasoline-powered engine emissions.

Although carbon dioxide concentrations are much lower for natural gas burning engines, methane accounts for approximately 70% to 80% of total hydrocarbons (THC) emitted from natural gas burning engines, while methane emissions account for only 5% to 10% [1][*] of total hydrocarbons in the gasoline fueled engine exhaust. Methane by mass also has 12 to 30 times the greenhouse effect of CO_2 [2]. Although the 2007 United States emission standards regulate only non-methane hydrocarbons (NMHC), not methane emissions, the European Community, Japan, and South Korea do consider such

[*] Numbers in [] refer to entries in bibliography.

limits on methane emissions. Regardless of the current domestic legislation, research for the reduction of THC and other greenhouse labeled gases should be addressed; one possibility of reducing CH_4 emissions from natural gas powered engines is by the use of oxidation catalytic converters.

Oxidation catalytic converters reduce CH_4 emissions because the catalyst provides an alternate reaction pathway with a lower activation energy, thereby increasing the rate of chemical reaction without itself being consumed in the reaction. Because methane is an extremely stable molecule and has a large energy barrier for dissociation, a catalyst is needed to aid in the conversion of methane. It is widely accepted that palladium (Pd) based catalysts exhibit the greatest activity for oxidizing methane, and the global oxidation of methane is described by the chemical reaction shown in Equation 1.1.

$$CH_4 + 2O_2 \rightarrow CO_2 + 2H_2O \qquad (1.1)$$

The purpose of this research is to explore several novel methods for reducing methane in a simulated lean-burn natural gas exhaust mixture. Classically, research of this nature is conducted on an engine dynamometer to acquire engine emission data. However, these tests experience variations in accuracy and repeatability due to the extent of the variables associated with the internal combustion engine (ICE). In order to circumvent test variations associated with engines operated on dynamometers, a bench-flow reactor (BFR) was employed to obtain data pertaining to methane conversion in the simulated lean-burn natural gas engine exhaust mixture. The purpose of the BFR is to reduce the amount of variables associated with the ICE and to investigate methane reduction in a simulated natural gas exhaust mixture. Using the BFR, methane conversion is investigated at a range of temperatures and exhaust flowrates to simulate the engine at idle to high load conditions.

In order to maximize CH_4 conversion in the exhaust mixture a reverse-flow oxidation catalyst reactor (RFOCR) was utilized in this study. The function of a reverse-flow reactor is to trap heat produced by the combustion of methane inside the catalyst reactor by periodically reversing the exhaust flow, thereby increasing methane conversion. CH_4 conversion was investigated as a function of the directional duration of the exhaust gases through the oxidation catalyst, gas hourly space velocity (GHSV), and exhaust gas temperature. In a separate experiment, due to the relatively high temperature needed to dissociate methane, a hydrogen (H_2) and carbon monoxide (CO) mixture was also introduced into the main exhaust mixture as a supplemental fuel prior to the RFOCR at relatively low exhaust gas temperatures. This experiment simulated supplemental fuel injection from a partial oxidation catalyst reactor at low engine idle exhaust temperatures for the purpose of increasing CH_4 conversion using the reverse-flow oxidation catalyst reactor.

The literature review in Chapter 2 contains background information on the RFOCR and SFI concepts including the nature of exhaust emissions for lean-burn natural gas engines, the characteristics of oxidation catalysts, and the basic design and operation of a reverse-flow reactor (RFR). The experimental apparatus is described in Chapter 3, which includes all major components associated with the BFR and operational procedures for the bench-flow reactor. Chapter 4 is dedicated to the discussion of results obtained from RFOCR and SFI experiments. Finally, Chapter 5 is devoted to the conclusions obtained from this research effort and presents recommendations for future studies with reverse-flow reactors with and without supplemental fuel injection.

CHAPTER 2

LITERATURE REVIEW

Although the reverse-flow reactor (RFR) is not a new concept, originally patented by Cottrell in 1938, few actual experiments have been performed using such an apparatus. Furthermore, technical papers concerning supplemental fuel injection (SFI) for a RFR were not found, and it is presumed that this is the first type of experimentation concerning the matter. In this chapter the exhaust emissions for a lean-burn natural gas engine, the characteristics of an oxidation catalyst, and the basic design and operation of a RFR will all be discussed in some detail.

2.1 Lean-Burn Natural Gas Engine Emissions

The basic design of the internal combustion engine (ICE) has changed little over the past 100 years, and as environmental concerns increase over the impact of emissions from these engines, so does the need for cleaner and more fuel efficient forms of energies. One possible solution for both decreasing the demand for foreign oil and reducing harmful carbon dioxide exhaust emissions is the use of natural gas as an alternative fuel. The benefits of natural gas include its domestic abundance and low carbon content. Natural gas, composed primarily of methane (85-95%), has a high octane rating (120-130), which allows combustion at higher compression ratios without resulting in engine knock, and because of the wide flammability range of natural gas (5-15% by volume in air), it is possible to operate an engine with very lean fuel mixtures, with air-fuel ratios in excess of 32 without misfires[2]. Another benefit of natural gas is the lower carbon content of natural gas, which corresponds to a lower carbon dioxide (CO_2)

concentration in the exhaust mixture when compared to gasoline-powered engine emissions. The carbon content can be seen in the carbon-to-hydrogen ratio of natural gas (C/H ~ .25) and gasoline (C/H ~ .45) [3].

Although the carbon content of natural gas is lower than gasoline resulting in reduced CO concentrations in the exhaust mixture, methane concentrations are considerably higher in natural gas engine emissions. Natural gas engine emissions have methane concentrations as high as 14 times that of gasoline engine emissions, and on a molecular basis methane is approximately 21 times as effective in absorbing infrared radiation as carbon dioxide [4,5]. This absorption of thermal radiation equates to the trapping of heat in the Earth's atmosphere and is commonly referred to as the greenhouse effect.

As previously discussed, natural gas engines emit considerably larger concentrations of methane than gasoline-powered engines, but a number of methods can be employed to reduce methane and other greenhouse gas emissions in the ICE exhaust. One possibility is to operate the ICE in the fuel-lean condition. The wide flammability range of natural gas allows for the engine to operate at an extremely low equivalence ratio. Equivalence ratio (ϕ) is defined at the actual fuel/air ratio over the stoichiometric fuel/air ratio. Total hydrocarbon production in the exhaust stream can be seen as a function of equivalence ratio in Figure 2.1 [3]. It should be noted that for natural gas engine emissions approximately 70% to 80% of total hydrocarbons comprise of methane, while for gasoline-powered engine emissions only 5% to 10% of total hydrocarbons are methane. Additionally, Figure 2.2 shows the production of carbon monoxide as a function of equivalence ratio [3]. The figure shows that equivalence ratio has a strong influence on carbon monoxide production, and engine operations in the lean-burn condition can have a significant impact on hydrocarbon and CO reduction in the exhaust stream.

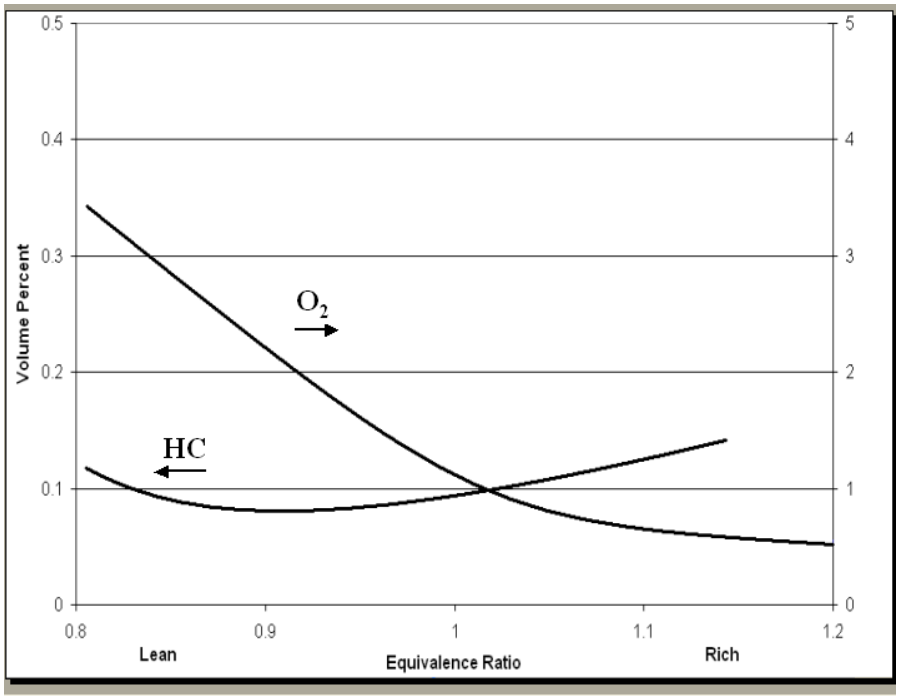

Figure 2.1. Hydrocarbon Production as a Function of Equivalence Ratio.

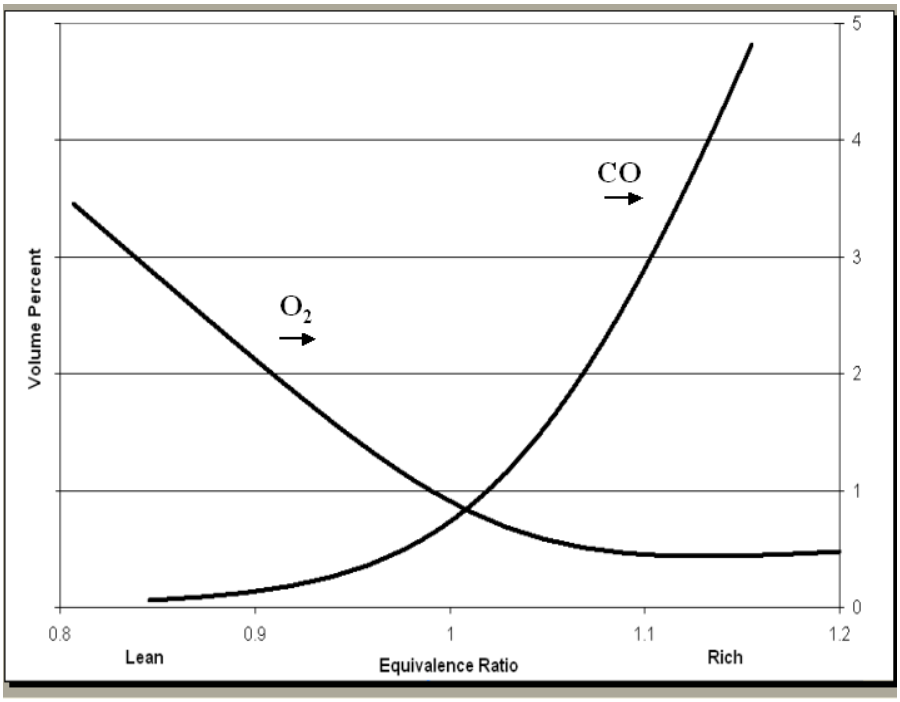

Figure 2.2. Carbon Monoxide Production as a Function of Equivalence Ratio.

2.2 Oxidation Reactions

Oxidation reactions are defined as chemical reactions in which compounds combine with oxygen to produce products. Combustion reactions are divided into two main types of reactions, complete and partial oxidation reactions. The intent of the complete oxidation reaction is to produce carbon dioxide and water, while the partial oxidation reaction produces intermediate compounds, such as carbon monoxide, which can be further oxidized to form carbon dioxide. Examples of complete and partial oxidation reactions are shown in Equations 2.1 and 2.2, respectively. Furthermore, the remarkably strong C–H bond of the methane molecule makes CH_4 one of the most stable hydrocarbons and very resistant to dissociation. Due to the large energy barrier for the dissociation of methane (435 kJ/mol) a catalyst will be used to aid in the cracking of CH_4 [6].

$$CH_4 + 2O_2 \rightarrow CO_2 + 2H_2O \qquad (2.1)$$

$$CH_4 + {}^{3}/_{2}\, O_2 \rightarrow CO + 2H_2O \qquad (2.2)$$

2.3 Oxidation Catalyst Selection

The subject of materials demonstrating high catalytic activity for methane is an extensively researched topic. Noble metals and metal-oxides have been shown to have a high affinity for dissociating methane. Noble metal-based catalysts, such as palladium, platinum, and rhodium, generally have higher catalytic activity and resistance to sulfur poisoning than metal/transition oxide-based catalysts. Results show that noble metal-based catalyst activity for CH_4 oxidation vary by the following: palladium>platinum>rhodium [2,7,8,9,10]. Based on these findings a 100-g/ft^3

palladium (Pd) noble metal-based catalyst on an alumina (γ-Al_2O_3) support was selected for this study.

2.4 Palladium Catalyst Oxidation Mechanism

A catalyst provides an alternative pathway for a chemical reaction with a lower activation energy, thereby increasing the rate of reaction for a particular species. Cullis and Willat studied the oxidation of CH_4 over palladium (Pd) in a pulse flow micro-reactor over a temperature range of 500 to 800 K and presented a proposed mechanism of the oxidation of methane over a palladium catalyst, shown in Figure 2.3 [9]. In the figure the proposed mechanism shows that methane dissociates and bonds to the active catalytic surface sites of palladium oxide (PdO). The figure illustrates the dissociation of an oxygen molecule (O_2) and bonding to an adjacent active PdO site. The methylene radical (CH_2) and oxygen atom (O) react with one another and oxidize to form CO_2 and H_2O, for complete oxidization. The dissociation of methane and oxygen is also shown in the figure to produce H_2O solely. However, the mechanisms for catalytic oxidation are very complex, and this proposed explanation presented is but one possibility for the dissociation of methane over a palladium based catalyst.

2.5 Catalyst Deactivation

As previously discussed, catalysts provide an alternative reaction pathway with a smaller activation energy than a non-catalytic reaction, thereby increasing the chemical reaction rate. Regrettably this catalytic activity often decreases with time. There are six major mechanisms that contribute to catalyst deactivation and are listed and defined below. Each deactivating mechanism is then categorized into chemical, mechanical, or thermal in nature [11].

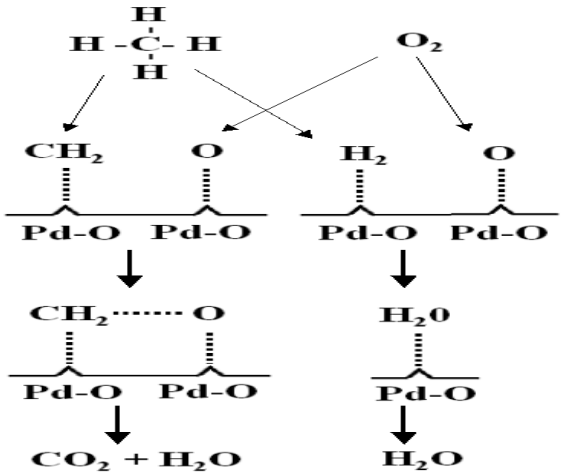

Figure 2.3. An Outline Mechanism of the Oxidation of Methane Over a Palladium Catalyst. Reprinted from Hayes and Kolaczkowski [9].

- Poisoning (Chemical) - Chemisorption of a species on a catalytic sites that effectively blocks the catalyst active site

- Fouling (Mechanical) - Deposit of species onto the catalytic surface

- Thermal degradation (Thermal) - Thermally induced loss of catalytic surface area, support area, and active phase

- Vapor formation (Chemical) - Heterogeneous reaction producing a volatile compound

- Vapor reactions (Chemical) – Heterogeneous reaction producing an inactive phase

- Attrition/crushing (Mechanical) - Loss of catalytic material due to abrasion or crushing of the catalyst particle

Each catalyst deactivating mechanism need not be elaborated on due to the controlled nature of the BFR, but two mechanisms are of concern to this study, thermal degradation and catalyst poisoning. Two specific modes of thermal degradation relevant here are palladium oxide (PdO) dissociation and catalyst sintering. Water poisoning of the catalyst was also a factor in this study. Thermal aging is typically non-reversible, however water poisoning is reversible.

2.5.1 Palladium Oxide Dissociation

It is generally recognized that palladium oxide (PdO) has a stronger affinity for methane oxidation than metallic palladium (Pd) sites do. When the temperature of the catalyst reaches approximately 800°C to 900°C, the active PdO catalyst sites disassociate into less active Pd sites. Pd reoxidation occurs when the catalyst temperature decreases to approximately 650°C to 800°C and re-forms into PdO [9,12]. The dissociation and reoxidation of PdO is shown in Equation 2.3 and an example of this pathway is illustrated in Figure 2.4.

$$PdO \leftrightarrow Pd + \tfrac{1}{2} O_2 \qquad (2.3)$$

Figure 2.4 demonstrates that as PdO dissociates to Pd and then reoxidizes to PdO, an amount of percent weight is lost. This loss of percent weight of PdO is corresponds to a loss of catalytic activity. This leads to the next thermal catalyst degradating mechanism, thermal sintering.

2.5.2 Catalyst Sintering

Temperature excursions result in catalyst deactivating effects such as PdO or Pd sintering. Catalyst sintering typically results in the direct loss of active catalytic surface area. During large catalyst temperature excursions the highly dispersed active sites of PdO on the catalyst surface decompose to the less active Pd, which then migrate toward

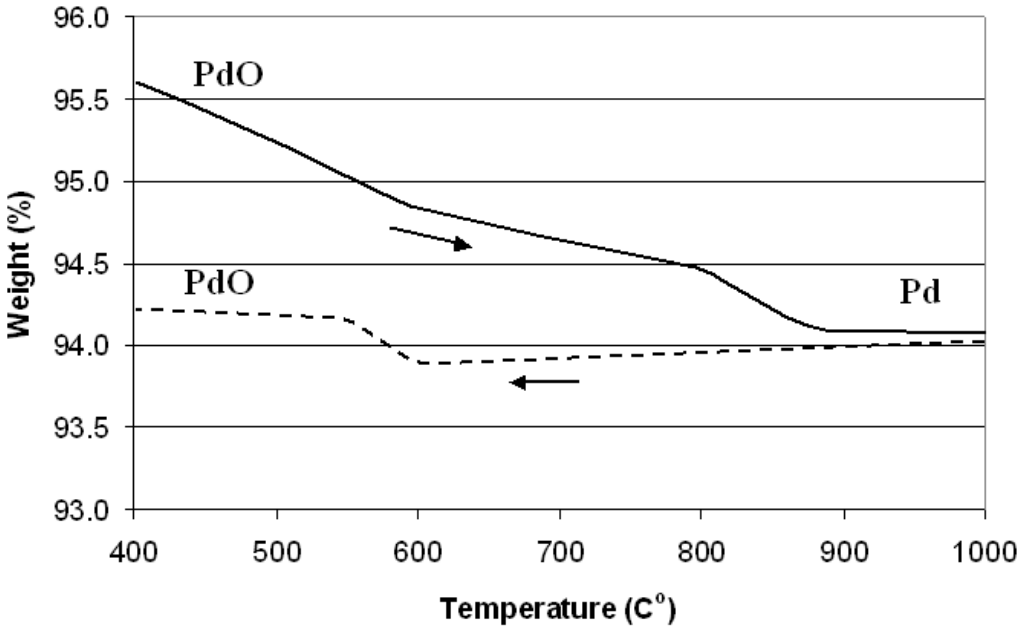

Figure 2.4. An Example of the Dissociation and Reoxidation of Palladium Oxide. Reprinted from Hayes and Kolaczkowski [9].

one another to form larger crystallites. This effectively reduces the number of active sites and reduces CH_4 conversion. Once catalyst deactivation has occurred, PdO or Pd sintering, the effects are non-reversible and the catalyst is permanently damaged.

2.5.3 Inhibiting Effect of Water Vapor

As shown in Equation 2.1, the complete oxidation of methane produces carbon dioxide and water vapor. It is generally agreed upon that H_2O has an inhibiting effects on the catalytic activity, but the nature of how the mechanism inhibits catalytic activity is still in question [13,14].

$$CH_4 + 2O_2 \rightarrow CO_2 + 2H_2O \qquad (2.1)$$

It is speculated that the H_2O catalyst poisoning mechanism is caused by water reacting with PdO at the PdO catalyst site to form $Pd(OH)_2$. This blocks the catalyst site preventing methane access to the active PdO site [13]. The literature is less in agreement as to the stability of palladium hydroxide ($Pd(OH)_2$). It has been reported that $Pd(OH)_2$ decomposes to PdO at approximately 250°C [14], while others claim that $Pd(OH)_2$ remains stable until much higher temperatures [13]. Although the stability of $Pd(OH)_2$ on the catalyst site seems to be in question, there is little doubt that H_2O inhibits catalytic activity. Experimental results of the effects of 10% water vapor on methane conversion at a reactor furnace temperature of 350°C can be seen in Figure A-1 located in the Appendix.

2.6 Reverse-Flow Oxidation Catalyst Reactor

Previous studies on the design and operation of the reverse-flow oxidation catalyst reactor (RFOCR) were evaluated in order to utilize the best available knowledge on experimental set-ups and techniques. The basic design of the present RFOCR, shown in Figure 2.5, was based upon the work of Strots et al. [15]. Switching valves one and four and switching valves two and three, shown in Figure 2.5, can be manipulated to allow the exhaust gas stream to flow in the forward direction or in the reverse direction through the catalyst reactor. Figure 2.6 compares the temperature rise across an oxidation catalyst, due to the oxidation of methane, in the reverse and unidirectional flow configuration. From Figure 2.6 the configuration with flow reversal has a significantly larger maximum temperature rise, or ΔT when compared to unidirectional flow. The larger ΔT is attained by the heat trap effect associated with a RFR [2]. As methane travels across the reactor an exothermic chemical reaction occurs, or that the chemical reaction produces heat as methane is oxidized across the catalyst, which is shown for the unidirectional case in Figure 2.7(a). The temperature rise at the outlet of the reactor (Figure 2.7(a)) can then be used to preheat the feed mixture using a reverse-flow operation. By periodically switching the flow direction through the catalyst reactor it is possible to trap the heat

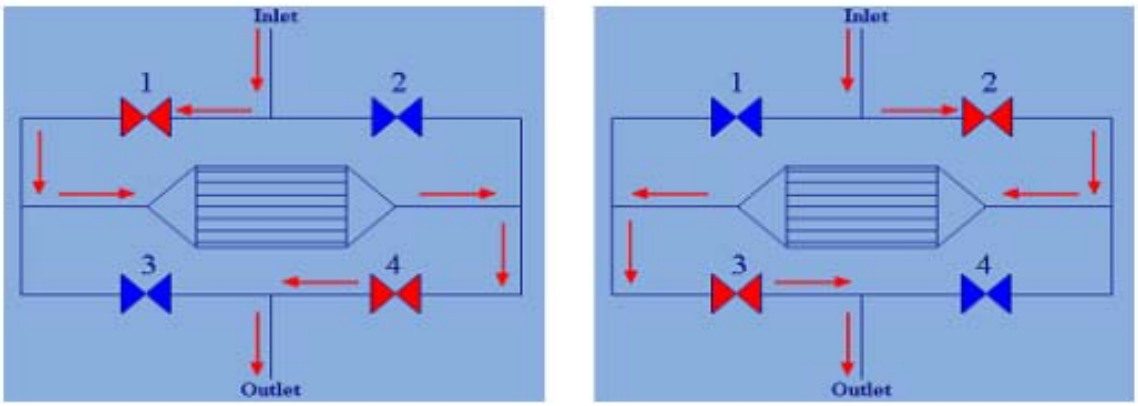

Figure 2.5. Schematic of the RFOCR.

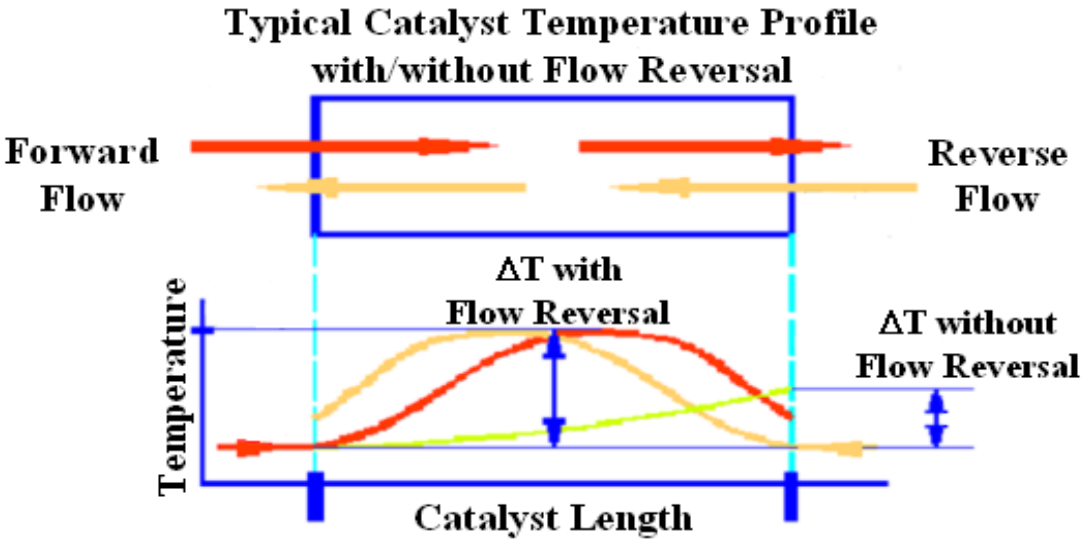

Figure 2.6. Temperature Profile Across the Length of the Catalyst.

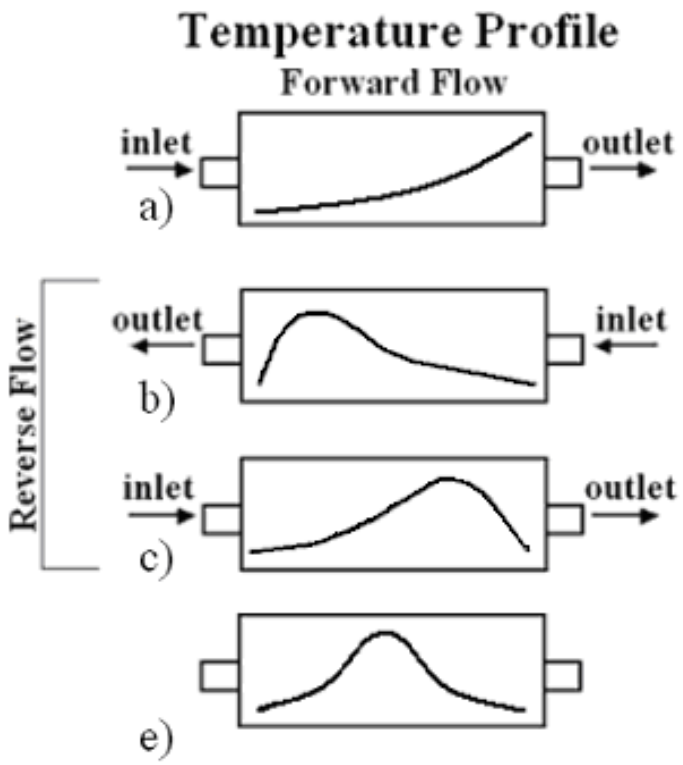

Figure 2.7. Illustration of the Heat Trap Effect.

produced by the exothermic chemical reaction increasing the temperature across the catalyst reactor. The development of the heat trap effect is shown in Figures 2.7(b) and 2.7(c). The bell shaped curve of Figure 2.7(e) is the fully developed temperature profile associated with RFR. Furthermore, it should be noted that the increase in temperature across the reactor due to the trapping of heat directly correlates to a greater CH_4 conversion in the exhaust mixture.

2.6.1 Effects of Varying Switching Time for a Reverse-Flow Reactor

A study investigating the effects of varying the switching time for a reverse-flow reactor on CH_4 and CO conversion was performed by Liu, Checkel, and Hayes [2]. In this study, experimental engine emission data was obtained from a four-cylinder natural gas/diesel dual fuel engine. The experimental apparatus for the investigation consisted of an engine mounted on a dynamometer test bed with a reverse-flow catalytic converter. The catalytic converter consisted of six square monolith honeycomb catalyst segments, each measuring 2.36-centimeters by 2.36-cenitmeters, with each segment separated by a .79-millimeter gap (catalyst type was not disclosed). For the investigation the engine was operated at light load conditions (1500 RPM), with an exhaust gas temperature as low as 257°C. For this particular investigation one experimental run was examined using symmetric and unsymmetric flow reversal operations. Symmetric flow reversal is described as the switching duration being the same in the forward flow as the reverse flow, while unsymmetric flow reversal is expressed as the switching time being different from the forward flow and reverse flow. The test run consisted of an initial unidirectional flow regime followed by a flow reversal regime, which consisted of high frequency switching times (10 to 25 seconds) and concluded with low frequency switching times (30 to 40 seconds). Total hydrocarbon conversion for the unidirectional flow regime was reported to be extremely low (approximately 10%), while CO conversion was significantly higher (>90%). Upon flow reversal CH_4 and CO conversion increased considerably, achieving CH_4 conversions of 85% and CO conversions of 93%. Lui et al. concluded that high frequency switching times (10 to 25 seconds) resulted in high catalyst temperatures and improved overall CH_4 conversion, while lower frequency

switching times produce CH_4 conversions similar to that of unidirectional reactors and therefore have little advantage over the latter. Medium duration cycling times increase the reactor temperature greatly and pose risk to damaging the catalyst through excessive temperature excursions.

2.6.2 Effects of Varying Volumetric Flowrate for a Reverse-Flow Reactor

A study conducted by Neumann and Veser [16] reported the effects of volumetric flowrate on the partial oxidation of CH_4 for a reverse-flow reactor with low catalytic contact times. Experimental runs were conducted on a bench-flow reactor, with the reverse-flow reactor set-up consisting of four switching valves (similar to Figure 2.5), allowing for periodic flow reversal. The experimental catalyst used was a platinum based alumina foam monolith (45 ppsi), with a precious metal loading of approximately 5 to 6 wt% of platinum. The catalyst sample was placed between two inert cordierite monoliths (350 cpsi). Due to the irregular foam structure of the catalyst, temperature measurements were unable to be conducted inside the catalyst; instead, temperature measurements were conducted at the inlet and outlet of the catalyst sample.

The reactor feed consisted of a CH_4-O_2 mixture consisting of a CH_4/O_2 ratio of 2.0 (the stoichiometric point for partial oxidation). The experimental runs were conducted at a volumetric flowrate of 1 to 5 L/min, which corresponds to a residence time of 25 to 5 ms, respectively. Additionally, the switching time for these particular experiments conducted by Neumann and Veser was 15 seconds.

The authors found that at a low volumetric flowrate (1 L/min) CH_4 conversion was approximately constant at 44% for the unidirectional and flow reversal cases. As the flowrate increases CH_4 conversion for the unidirectional case reached a maximum conversion of approximately 57% at 3 L/min, while the maximum CH_4 conversion for the flow reversal case continually increased to approximately 80% at 5 L/min. Nuemann and Veser attribute this behavior to the effects of volumetric flowrate on the temperature of the inlet and outlet of the catalyst.

For unidirectional flow, increasing volumetric flowrate decreased temperature at the inlet of the catalyst and increased temperatures at the outlet of the catalyst. The cooling of the catalyst inlet due to an increase in volumetric flowrate was attributed to higher convective heat transport and an increase in the amount of cool feed gases entering the reactor, while the increasing temperature of the catalyst outlet was considered due to the chemical reaction generating more heat due to the additional reactants being converted per unit time. Reverse-flow operations do not follow this trend. Increasing the volumetric flowrate during flow reversal leads to an increase in the mean temperature at the inlet and outlet of the catalyst. This is due to the trapping of heat across the length of the catalyst, and therefore, heating the inert monoliths. This heating of the inert monoliths produces a regenerative heat exchange from the catalyst and inert monoliths continuously increasing the feed temperature as volumetric flow rates increased. Nuemann and Veser acknowledge that the trend of increasing CH_4 conversion as the volumetric flowrate increases would not continue indefinitely because the heat capacity of the inert monoliths will set an upper limit to the continuous increase in heat generation.

CHAPTER 3

EXPERIMENTAL APPARATUS

This chapter is dedicated to the explanation of the experimental apparatus used in the RFOCR study. Section 3.1 gives an overview of all major components associated with the bench-flow reactor (BFR). Section 3.2 describes the type and physical characteristics of the oxidation catalyst used in the experiment. Sections 3.3 to 3.5 explain each component of the BFR system in more precise detail, and Sections 3.6 and 3.7 describe the data acquisition of the BFR. Section 3.8 explains the operation of the BFR, and finally Section 3.9 explains the experimental test to be run for the RFOCR study.

3.1 Overall Description of the Bench-Flow Reactor

An overall schematic and picture of the bench-flow reactor (BFR) and Horiba analyzer cabinet are shown in Figures 3.1 and 3.2, respectively. While several components are associated with the BFR this study focuses primarily upon the reverse-flow oxidation catalyst reactor (RFOCR). The RFOCR is a catalyst reactor with a system of valves that allow the direction of the exhaust flow through the catalyst to be dictated. The exhaust flow through the RFOCR represents a simulated lean-burn natural gas exhaust mixture consisting of CO_2, CH_4, O_2, N_2, and CO and are introduced into the BFR system by means of mass flow controllers (MFC). Moreover, the methane constituent of the exhaust mixture for the RFOCR study is a reasonable representation of total hydrocarbons given that approximately 70 to 80% of total hydrocarbons in the natural gas exhaust mixture is methane. Additionally, water is injected into the system via a peristaltic pump to represent the water vapor typical of exhaust gas. In addition, supplemental fuel injection (SFI) into the RFOCR is examined for the purpose of

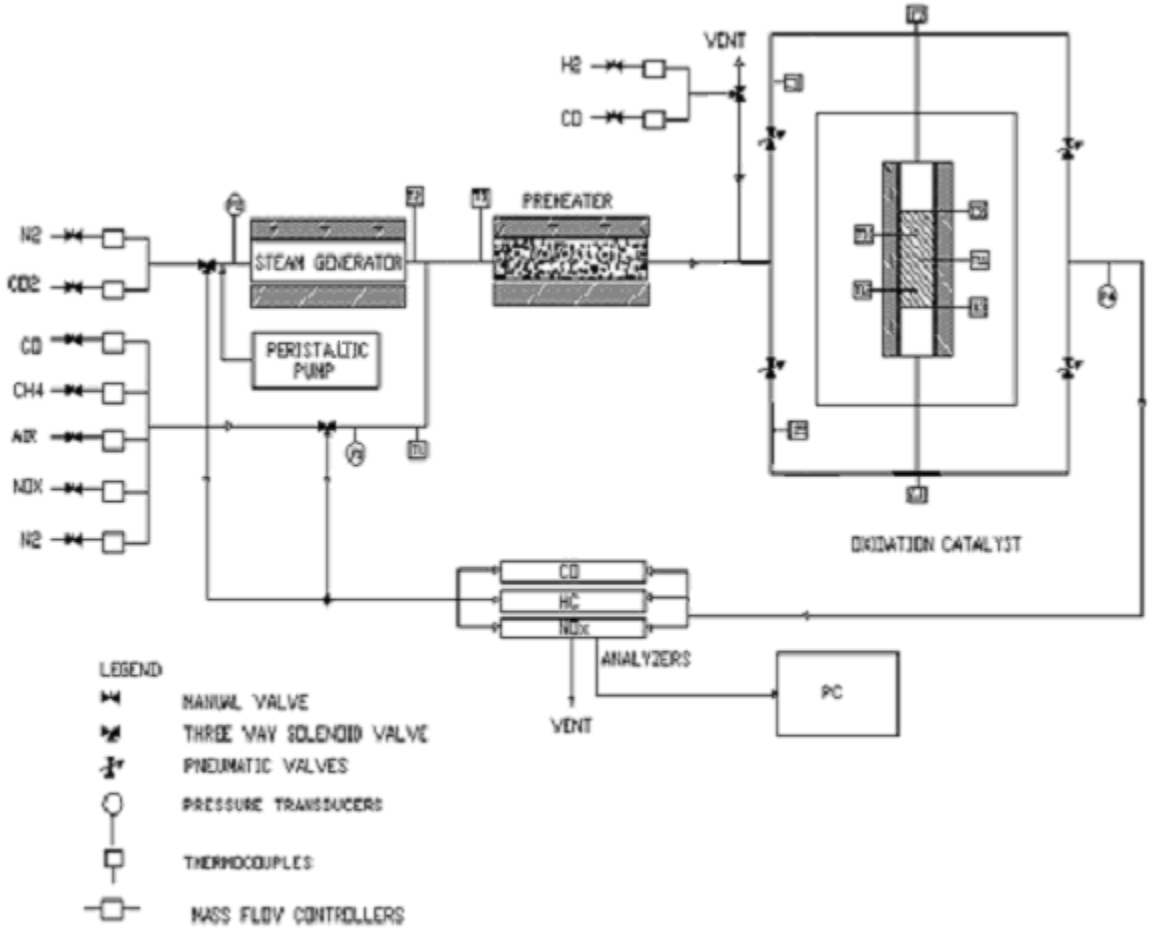

Figure 3.1. Schematic of the Bench-Flow Reactor System.

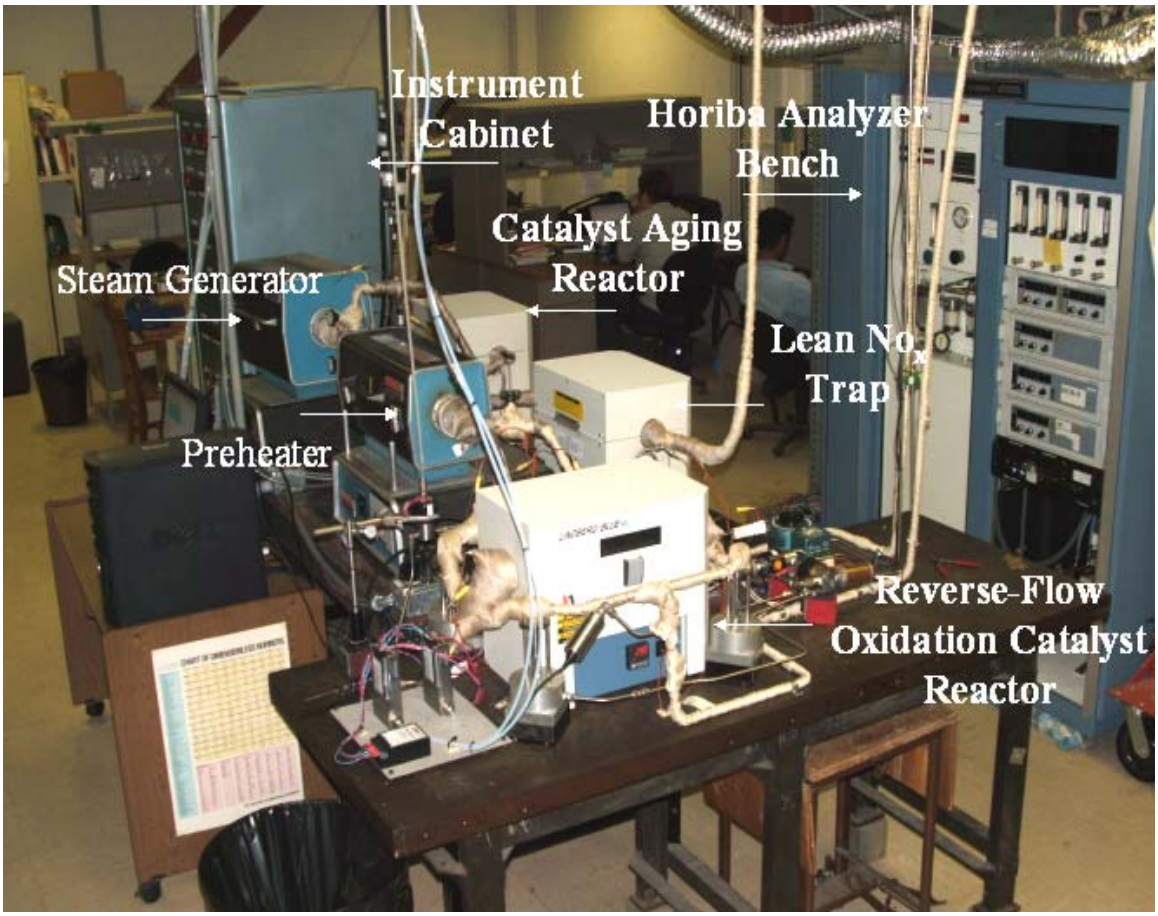

Figure 3.2. Bench-Flow Reactor.

increasing CH_4 conversion at low exhaust gas temperatures. The analysis of gas samples from the reactor is accomplished by several gas analyzers housed in the Horiba analyzer cabinet. All measurements are digitally recorded through a National Instruments LabVIEW data acquisition system.

3.2 Experimental Catalyst

Palladium-alumina ($Pd\text{-}Al_2O_3$) catalysts with a cordierite substrate support, supplied by EmeraChem, were selected for the RFOCR study based upon their strong affinity for methane (CH_4) oxidation. A picture of a typical $Pd\text{-}Al_2O_3$ catalyst is shown in Figure 3.3. The dimensions of the oxidation catalysts used are 7.62 centimeters long with a 2.22-centimeter diameter and a cell density of 300 cells/inch^2 (cpsi), and all oxidation catalysts received a precious metal loading of 100 g-Pd/ft^3. All catalysts were arranged in the RFOCR in the same fashion to establish consistent experimental parameters. The catalyst is wrapped with FiberFrax™ to prevent the exhaust gases from slipping around the catalyst sample and placed at the midpoint of the quartz tube in the reactor furnace.

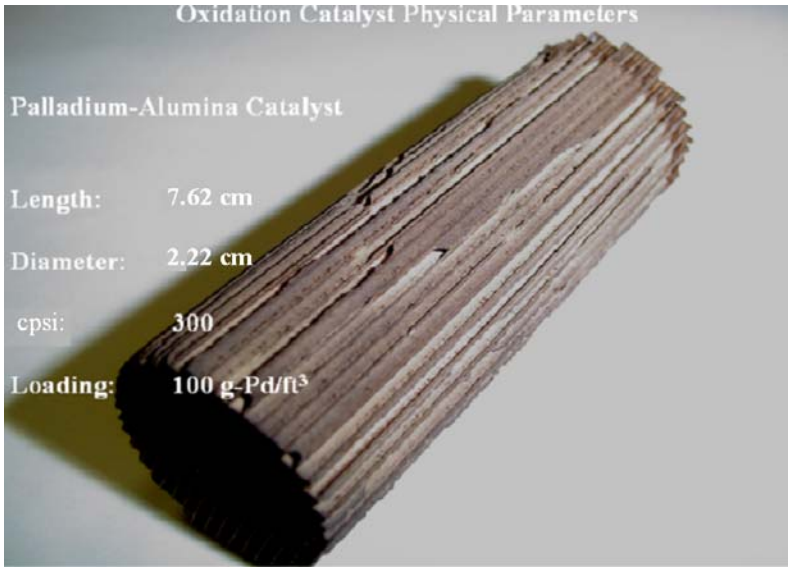

Figure 3.3. Oxidation Catalyst Physical Parameters.

3.3 Components of the Bench-Flow Reactor

3.3.1 Reverse-Flow Oxidation Catalyst Reactor

The reverse-flow oxidation catalyst reactor (RFOCR) consists of a reactor furnace, four high temperature switching valves (HTSV), and a catalyst reactor section (CRS). The RFOCR design underwent several modifications in order to improve the experimental apparatus. Revisions to the RFOCR were made in order to improve temperature stabilization across the catalyst reactor and to resolve gas mixture leakage problems at the reactor end fittings. The initial and present versions of the RFOCR are shown in Figures 3.4 and 3.5, respectively.

To facilitate catalyst removal and installation, end fittings were incorporated into the RFOCR, and a photograph of a reactor end fitting is shown in Figure 3.6. The original reactor end fittings required modification in order to prevent the exhaust mixture leakage at the quartz tube-reactor end fitting interface. The previous end fitting set-up was similar to Figure 3.6 with the exception of the graphite ferrule. Viton O-rings were used in the original reactor end fittings where the graphite ferrule is located to seal the reactor. Due to the high temperatures the system reaches, the O-rings would fatigue and then fail. The high temperature reached by the experiments would harden and crack the Viton O-rings, causing leaks at the reactor end fittings, and as a result of the leakage the emission data collected was inconsistent. This O-ring component failure was resolved by replacing the reactor end fitting with a completely new fitting. While the basic design is very similar, utilizing a graphite ferrule allows the RFOCR to obtain high temperatures without sacrificing the integrity of the seal. Furthermore, an additional advantage over the previous set-up is that the reactor end fittings, if carefully removed from the CRS, may be reused for further experiments.

The catalyst reactor section (CRS) of the RFOCR, shown in Figure 3.7, consists of a 2.22-centimeter diameter, 44.45-centermeter long quartz tube. Five type-K thermocouples are placed throughout the CRS to provide the temperature profile across

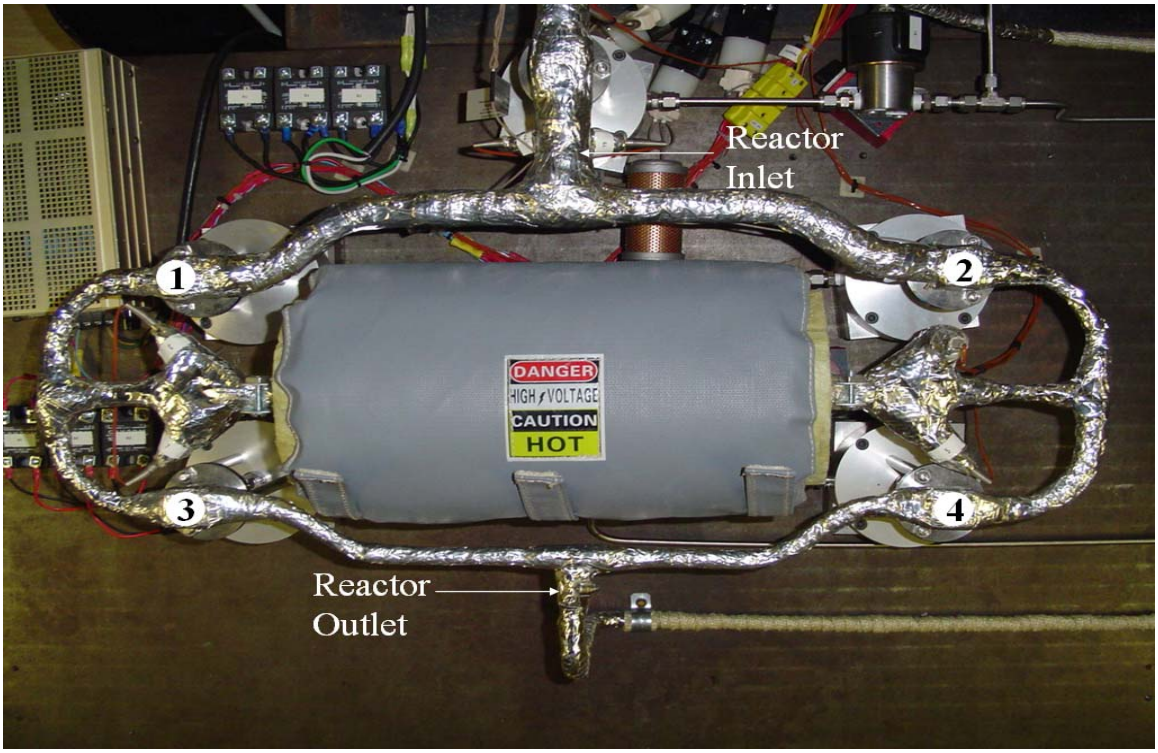

Figure 3.4. Initial Version of the Reverse-Flow Oxidation Catalyst Reactor.

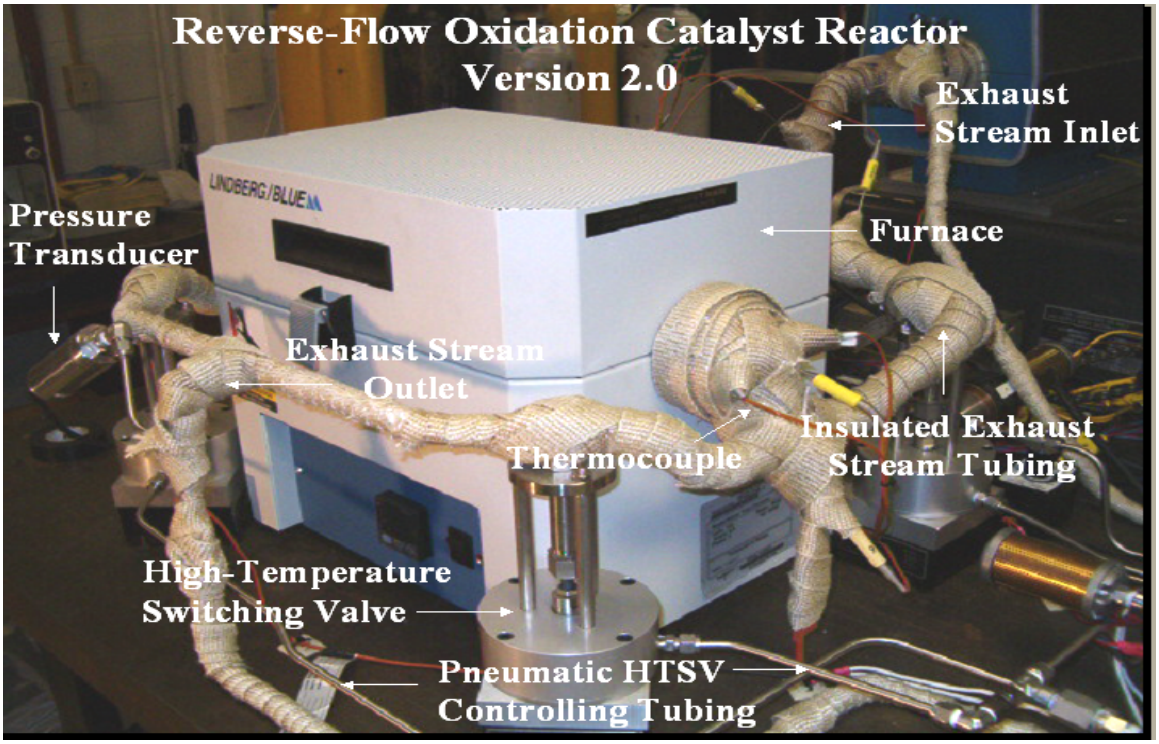

Figure 3.5. Current Version of the Reverse-Flow Oxidation Catalyst.

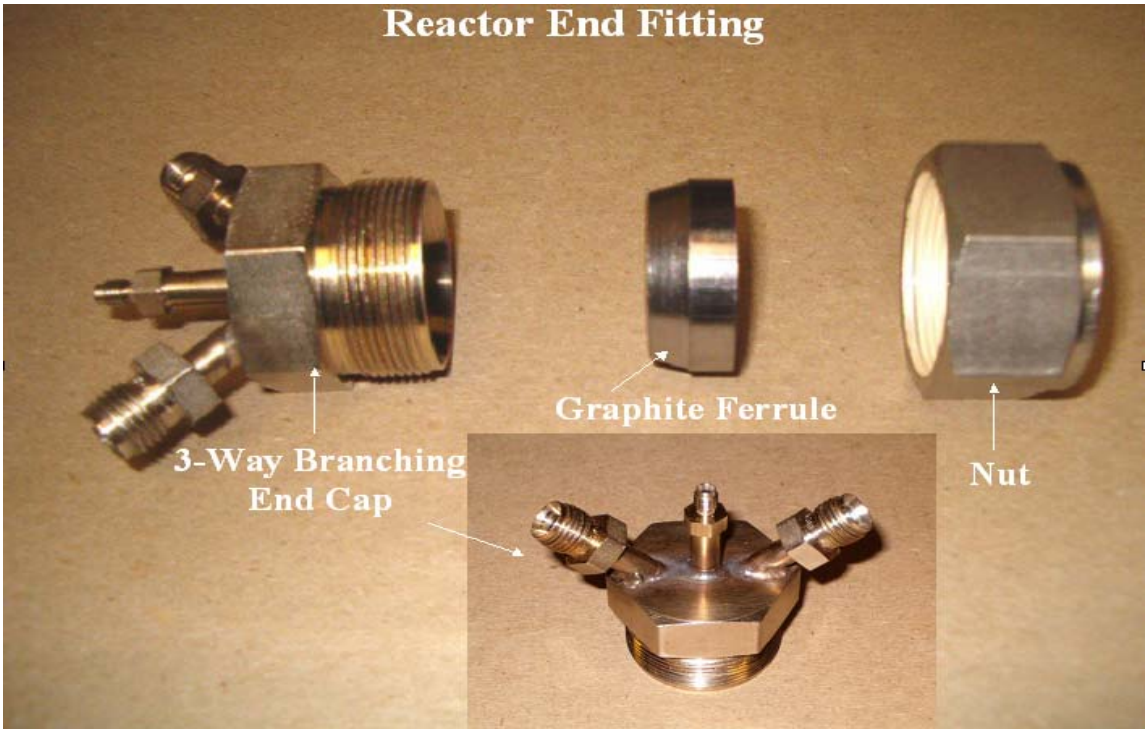

Figure 3.6. Current Reactor End Fitting.

Figure 3.7. Catalyst Reactor Section.

the catalyst. Additionally, the method of heating the CRS has also undergone several modifications in order to stabilize temperature across the catalyst.

The initial reactor heating design consisted of heating tape insulated with a heating jacket. The heating tape was coiled around the reactor for temperature regulation and an insulating jacket was used to prevent heat loss from the CRS. The heating tape around the CRS was controlled using a solid-state relay in conjunction with LabVIEW. The LabVIEW temperature controlling program worked much like a home thermostat in that the temperature was monitored by a thermocouple located in the CRS and a set point temperature was input to LabVIEW. If the temperature was higher than the set point temperature the heating tape around the CRS was shut off via the solid-state relay. Conversely, if the temperature inside the CRS was below the set point temperature the heating tape was energized. This temperature regulating set-up caused reactor temperature oscillations as shown in Figure A-2 located in the Appendix. The oscillations resulted from the difference in the response times between the LabVIEW temperature controlling program and the catalyst wall temperature. While the LabVIEW controller program responded rapidly, while the catalyst wall temperature responded very slowly to the control inputs. This mismatch of time scales in the CRS heating system caused a constant overshooting and undershooting of the temperature set point. To alleviate the oscillations the original CRS heater was replaced with a Lindberg/Blue M single zone tubular furnace (TF55035A-1). This version made it possible to establish a constant catalyst wall temperature.

Lastly, high temperature switching valves (HTSV) had to be chosen for the RFOCR to enable the direction of the exhaust mixture through the catalyst reactor to be dictated. In the original RFOCR design, it was expected that flow reversal could be accomplished by means of two three-way high temperature valves. But due to the extreme temperatures of the exhaust gases through the RFOCR this valve configuration, with a maximum operational rating of 700°C, was not found to be commercially available. Based on the temperature requirements needed to operate the RFOCR, four high temperature pneumatically operated switching valves (SS-4UW-HT-4O), produced by Swagelok, were selected. The high temperature switching valves (HTSV), or simply

referred to as switching valves, are rated to a maximum temperature of 648°C and activate on an air pressure of 60 psi. Using this switching valve configuration flow reversal is accomplished in the following way: switching valves one and four and switching valves two and three, shown in Figure 3.8, can be manipulated in such a way as to allow the exhaust gas stream to flow in the forward or reverse direction through the oxidation reactor. Furthermore, the pneumatically actuated switching valves can be controlled via LabVIEW with the aid of two solid-state relays controlling two three-way solenoid valves. This configuration allows for accurate and variable time durations in the forward and reverse-flow direction.

3.3.2 Supplemental Fuel Injection

The purpose of the supplemental fuel injection (SFI) system is to introduce hydrogen (H_2) and carbon monoxide (CO) into the RFOCR in order to increase CH_4 conversion at relatively low exhaust gas temperatures. The SFI set-up, shown in Figure 3.9, consists of two mass flow controllers, a two-way solenoid valve, and controlling accessories linking the system to LabVIEW.

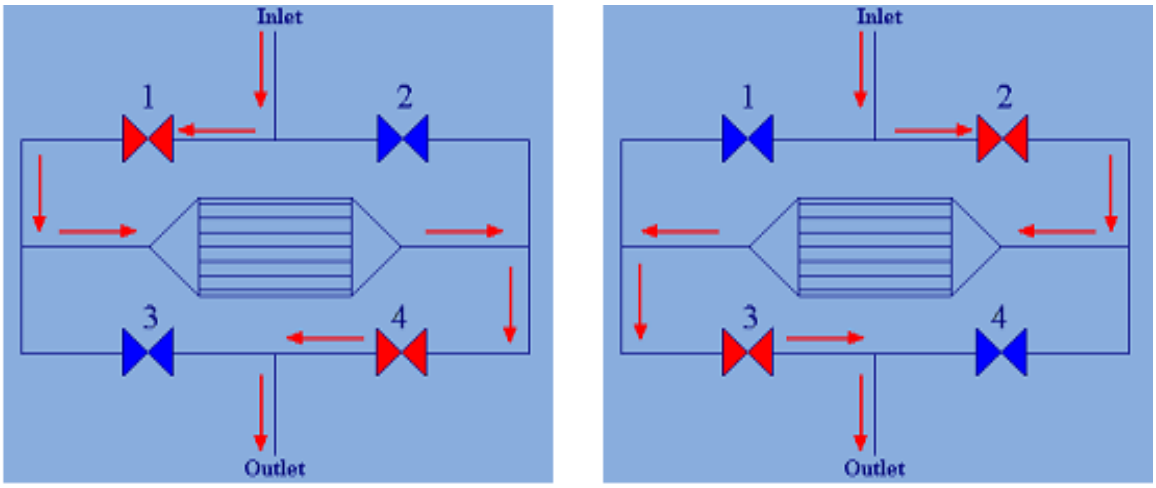

Figure 3.8. Schematic of the Reverse-Flow Oxidation Catalyst Reactor.

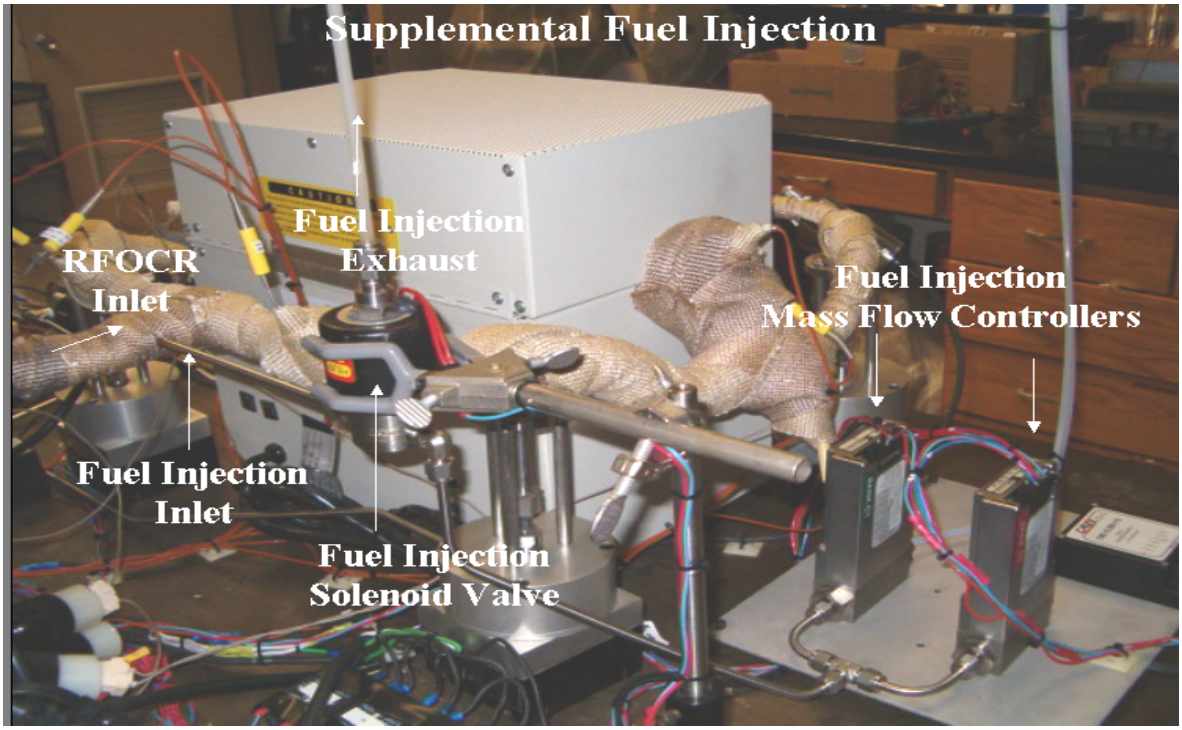

Figure 3.9. Supplemental Fuel Injection Set-up.

The mass flow controllers regulating H_2 and CO are low flowrate controllers with a maximum flowrate of 300 cc/min, designed for minimal fuel injection into the RFOCR. The mass flow controllers, as in the RFOCR set-up, are connected to LabVIEW allowing for accurate flowrate control. Additionally, the outlets of the SFI mass flow controllers are connected to a two-way solenoid valve.

The solenoid valve, also as in the RFOCR set-up, is connected to a power supply and a solid-state relay allowing for the SFI system to be controlled via LabVIEW. Due to the poor accuracy and slow time response of a mass flow controller in transient operations a three-way solenoid valve was installed in order to overcome this obstacle. The solenoid valve diverts the supplemental fuel from the mass flow controllers (MFC) to a vent. Once the MFCs have been given ample time to achieve the desired flowrate the supplemental fuel can be diverted by the solenoid valve into the RFOCR. The SFI set-up can produce accurate and timely fuel injection to the RFOCR for the purpose of increasing CH_4 conversion at relatively low inlet gas temperatures.

3.3.3 Instrument Cabinet

The instrument cabinet, shown in Figure 3.10, houses four major components of the Bench Flow Reactor (BFR) System: mass flow controllers, the data acquisition system, temperature and pressure displays, and heating tape controllers. The mass flow controllers (MFC) regulate the exhaust gas mixture introduced into the BFR and the data acquisition system (DAC) interfaces the components of the BFR output signals with LabVIEW. The instrument panel also houses a number of displays representing the temperature and pressure of the exhaust gas at specific points across the BFR system. Each of the components housed in the instrument cabinet are discussed in further detail below.

3.3.4 Horiba Analyzer Cabinet

The primary function of the Horiba analyzer cabinet is to accommodate all gas analyzers, a pump, and a water condenser. Because gas analysis for the Horiba gas analyzers must be performed on a dry basis, a water condenser is used to remove the water vapor from the simulated exhaust gas mixture, and a picture of the water condenser is shown in Figure 3.11. Furthermore, the water that is trapped in the condenser may be purged from the analyzer cabinet by selecting the Drain button located on the Master Matrix located on the control panel of the cabinet. In addition to the water condenser, the analyzer cabinet uses a pump to control the pressure in the cabinet and the pump pressure can be regulated by the manifold pressure knobs located on the front of the analyzer cabinet, shown in Figure 3.12.

Also located on the front of the Horiba analyzer cabinet is the main, instrument, and auxiliary breakers. The main breaker controls power to the entire cabinet, while the instrument breaker controls power to all the gas analyzers and are also shown in Figure 3.12. Lastly, the auxiliary breaker controls power to the water condenser. The analyzer cabinet also has the capability of dictating which gas analyzer receives the exhaust gas mixture for gas analysis. On the analyzer cabinet control panel the analyzer matrix allows for individual analyzers to be selected for gas analysis, shown in Figure 3.12. The

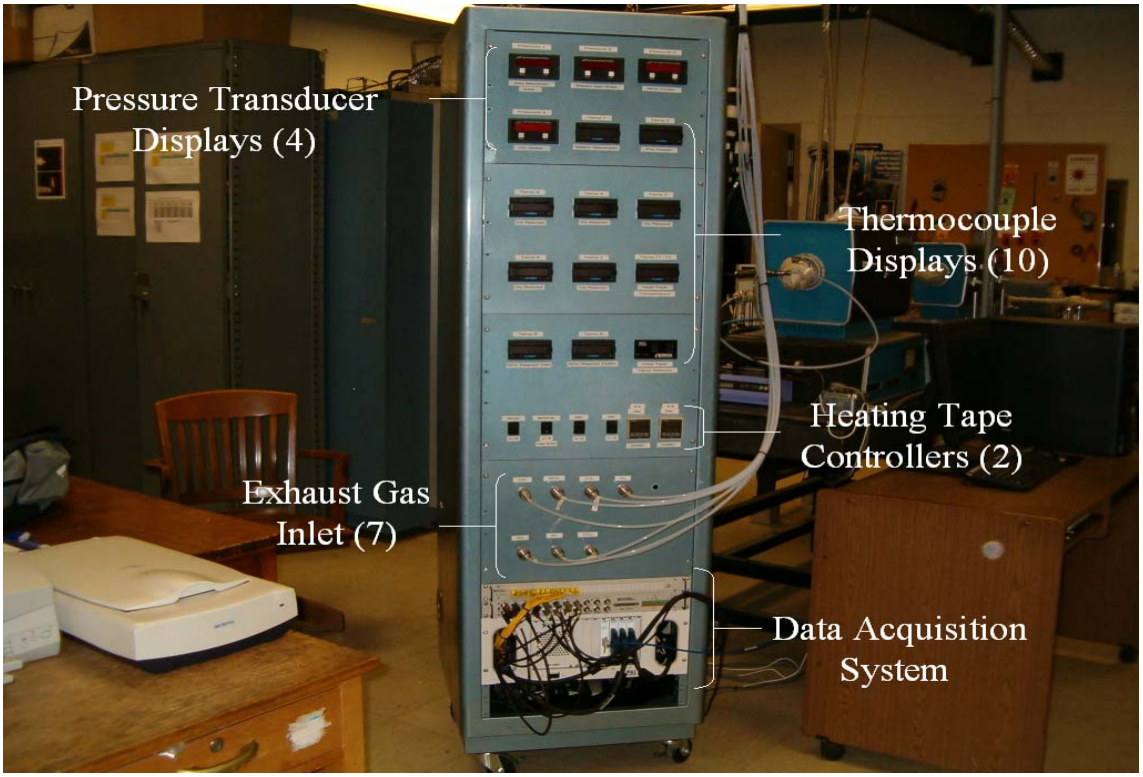

Figure 3.10. Instrument Cabinet.

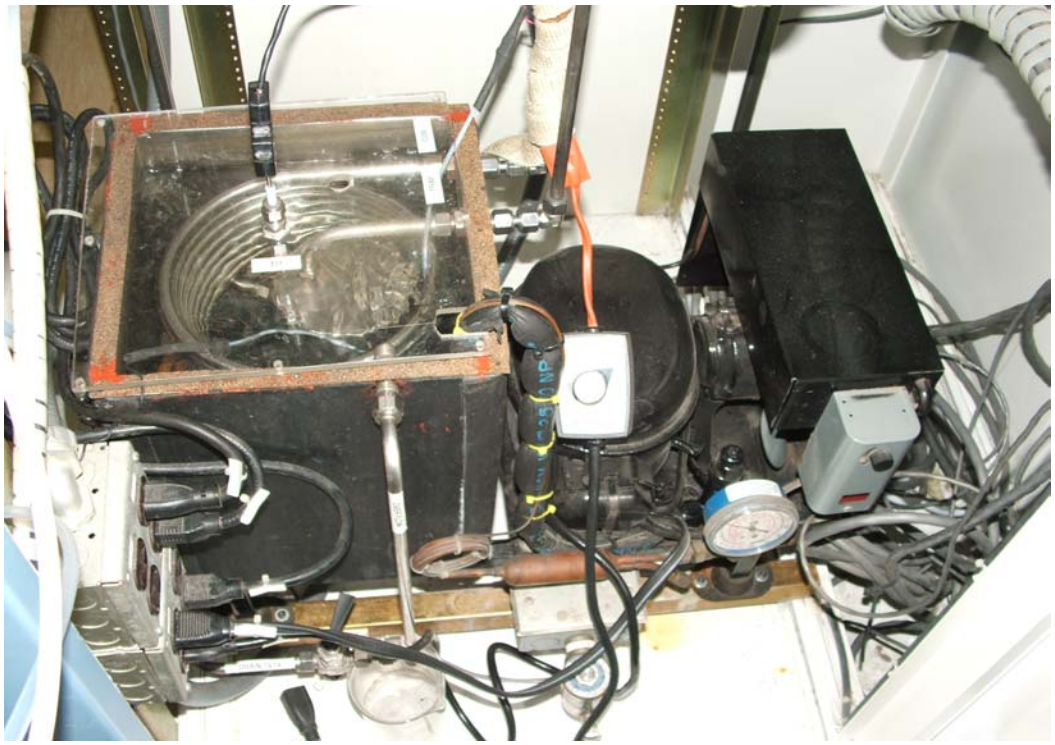

Figure 3.11. Water Condenser Inside of the Horiba Analyzer Bench.

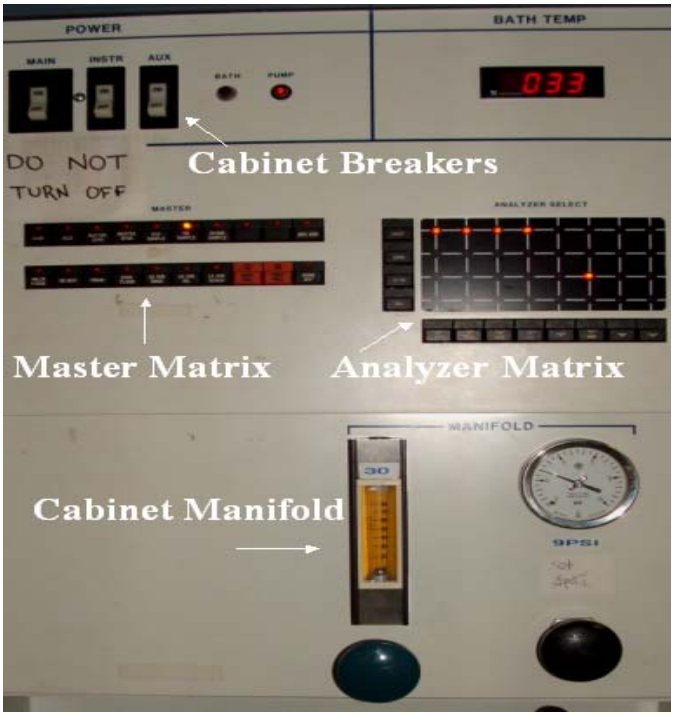

Figure 3.12. Control Panel of the Horiba Instrument Cabinet.

flowrate to the gas analyzers may also be regulated by means of the rotameters located on the control panel of the analyzer cabinet.

3.3.5 Peristaltic Pump

To properly simulate an actual engine exhaust mixture it is necessary for water vapor to be incorporated into the feed stream. A Harvard syringe pump was initially utilized for water injection into the system, but due to the relatively small reservoir of the syringe pump, it proved impractical to use the device for experimental runs with longer time durations. To alleviate this problem a Masterflex peristaltic pump manufactured by Cole Parmer (7524-50) was installed to replace the original syringe pump. The peristaltic pump with a flowrate range of 0.1-580 mL/min allows for continuous water injection due to the pumps inlet being placed into a large water reservoir, which can be periodically filled, and is shown in Figure 3.13.

Figure 3.13. Peristaltic Pump and Steam Generator.

3.3.6 Steam Generator

The purpose of the steam generator is to evaporate the water constituent of the exhaust mixture, which is introduced into the RFOCR system from the peristaltic pump. The steam generator, shown in Figure 3.13, consists of a stainless steel tube placed in a tubular furnace. The furnace used to heat the stainless steel tube is a Lindberg heavy-duty tubular furnace capable of obtaining a maximum temperature of 1000°C. The 2.54-centimeter ID stainless steel tube is sealed with copper gaskets and stainless steel flanges with a 4.45-centimeter ID and 5.57-centimeter OD. Additionally, the flanges are pressure tested to 20 pounds per in^2 (psi) to ensure there is no leakage. Moreover, a wicking strip of material is placed inside the stainless steel tube to aid in uniform water vapor dispersion through the BFR.

3.3.7 Reactor Branching Valves

The bench-flow reactor (BFR) consists of three reactors: the reverse-flow oxidation catalyst reactor (RFOCR), the lean NO_x trap (LNT) reactor, and the lean NO_x trap (LNT) aging reactor. Each of the reactors use the same instrument cabinet, peristaltic pump, and steam generator in their experimental apparatus. Because each particular reactor must be run independently, a valve system was devised to direct the exhaust flow to the desired reactor. A system of Swagelok high temperature bellow valves (SS-4BW), or reactor branching valves were chosen to accomplish this task. The reactor branching valves are manually operated and rated to an operational temperature of 482°C, and is shown in Figure 3.14.

3.3.8 Preheater

The purpose of the preheater furnace is to preheat the exhaust gas prior to the reverse-flow oxidation catalyst reactor. Pyrex beads with a 5-millimeter diameter, held in place by McMaster stainless steel mesh disks are placed inside a 55.88-centimeter long stainless steel tube with a 2.54-centimeter ID. Due to the high temperature of the preheater, approximately 500°C, Pyrex was selected for its specific physical properties and working temperature of the glass beads. The purpose of the Pyrex beads is to assist in a uniform temperature distribution of the exhaust gas.

3.3.9 Mass Flow Controllers

The mass flow controllers (MFC) are used to regulate the flowrate of individual gases making up the simulated exhaust mixture, which are shown in Figure 3.15. All MFC (FMA 5400/5500) are manufactured by Omega, which require a 24 VDC power supply and are controlled by LabVIEW. Since the MFC are calibrated by the manufacturer using N_2, it is necessary to have a correction factor, called the K-factor, to correctly regulate individual gas species through the MFC. MFCs with specific operating flow ranges are used to regulate each constituent of the exhaust mixture. The mixture includes: Carbon Monoxide (CO), Methane (CH_4), Air, Nitrogen (N_2), and Carbon Dioxide (CO_2). Separately, the supplemental fuel injection system has two MFC,

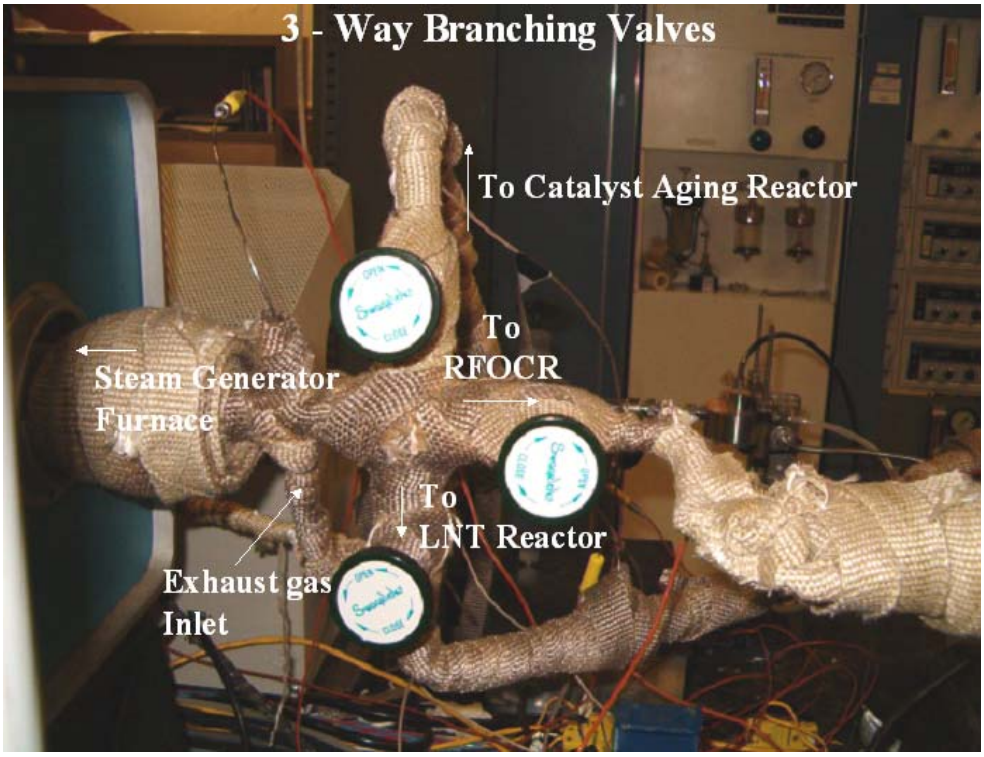

Figure 3.14. Reactor Branching Valves.

Figure 3.15. Wiring of Displays and MFC Inside the Instrument Cabinet.

Hydrogen (H2) and Carbon Monoxide (CO). The operational flow ranges for the individual MFC are shown in Table 3.1.

LabVIEW controls all MFC with their respective output flowrates by a 0-5 VDC-control voltage. Additionally, the MFC have a feedback system in which input andoutput flowrates maybe compared. An output voltage representing the actual flowrate from the MFC is sent to LabVIEW to compare with the input flowrate and to ensure that each MFC is operating properly.

3.3.10 Solenoid Valves and Solid-State Relays

In order to automate the BFR using LabVIEW a number of controlling accessories were used to accomplish this task. LabVIEW controls and maintains the RFOCR inlet gas temperature and the high temperature switching valves (HTSV) through a system of solenoid valves, solid-state relays, and a power supply. Two Peter Paul 24 VDC three-way solenoid valves pneumatically actuate the four switching valves, shown in Figure 3.16. Additionally, Alwitco solenoid mufflers were added to each solenoid valve to minimize noise during operation. Because the computer has a maximum output voltage of 10 VDC, a 100 VDC power supply in conjunction with solid-state relays was used to control the solenoid valves, thereby controlling the switching valves. The set-up of the power supply and solid-state relays can be seen in Figure 3.17.

The power supply and solid-state relay system is also used to control the heatingtapes coiled around the tubing at the inlet of the RFOCR. As previously discussed, the heating tapes are controlled by LabVIEW much like a home thermostat. The LabVIEW program is designed is designed to energize the heating tape if the exhaust gas temperature is below the set point. Alternatively, if the inlet gas temperature to the RFOCR is greater than the input set point temperature the heating tape is shut off. This method of heating is the same as that originally used to heat the catalyst reactor section (CRS). Due to the high specific heat of gas, this technique of heating does not suffer from severe temperature oscillations, as did the original design of heating the CRS.

Table 3.1. Operational Flow Ranges for Individual Mass Flow Controllers.

CO	**0-1 L/min**
CH_4	**0-5 L/min**
AIR	**0-20 L/min**
N_2	**0-10 L/min**
CO_2	**0-10 L/min**
Fuel Injection	
CO	**0-300 cc/min**
H_2	**0-300 cc/min**

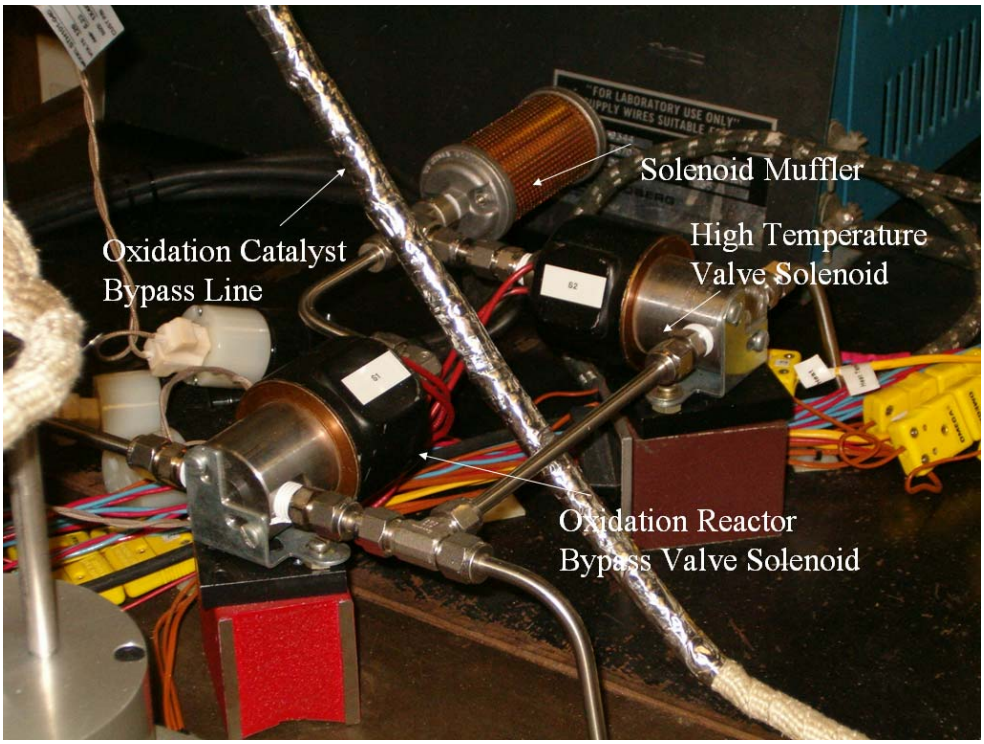

Figure 3.16. Solenoid Valve Configuration.

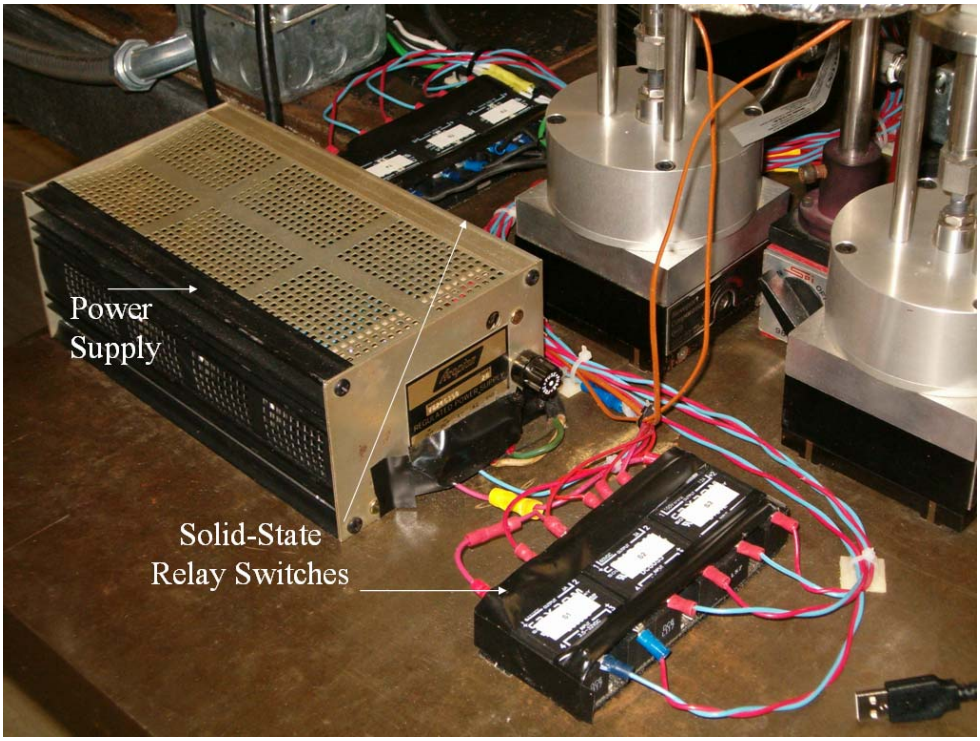

Figure 3.17. Power Supplies with Solid State Relays.

3.4 Instrumentation and Displays

The BFR system includes four Cole Parmer pressure transducers (68072-06) with a pressure range of 0 to 50 psi and seventeen Omega type-K thermocouples capable of measuring temperatures from 200 to 1250°C. The pressure transducers are connected to four Cole Parmer pressure displays (94785-00) and the thermocouples are connected to nine Omega temperature displays (DP 18-KC1) housed in the instrument cabinet. The remaining thermocouple output signals are displayed using a single temperature display using an Omega temperature scanner (MDP-18).

3.4.1 Pressure Transducer Locations

The locations of the pressure transducers are placed before and after the respective reactors to determine if a large pressure drop occurs across the BFR system. Large pressure drops across the system have the potential of interfering with the accuracy of the experimental measurements of the gas concentration. Experimental runs with a

consistent pressure with minimal pressure drop are desired for the RFOCR study. To aid in achieving these conditions four pressure transducers are placed at the following positions in the BFR system:

i. Inlet of the steam generator.
ii. Outlet of the Oxidation Catalyst.
iii. Inlet of the Lean NOx Trap.
iv. Outlet of the Lean NOx Trap.

3.4.2 Reverse-Flow Oxidation Catalyst Reactor Thermocouple Locations

The BFR has a total of seventeen thermocouples (see Figure 3.1) and of those seventeen thermocouples ten are used in the RFOCR. Five thermocouples are used to regulate the exhaust gas temperature prior to the RFOCR and the remaining five are placed inside the catalyst reactor section (CRS) to measure the temperature across the catalyst. The five thermocouples are installed in the CRS to determine both end temperatures of the sample and the temperatures at ¼, ½, and ¾ the length of the catalyst. The thermocouple locations relative to the catalyst sample are shown in Figure 3.18.

3.4.3 Temperature Controllers

Two Athena temperature controllers (XT16) are mounted on the front of the instrument cabinet for the purpose of regulating temperature and avoiding water condensation prior to the preheater furnace. These controllers regulate two Omega heating tapes used to heat the inlet of the Preheater and the inlet of the LNT. The heating tape controllers regulate temperature similarly to the LabVIEW program that is used to heat the inlet of the RFOCR. The temperature is measured using a type-K thermocouple and the heating tape is then monitored and regulated by the temperature controller.

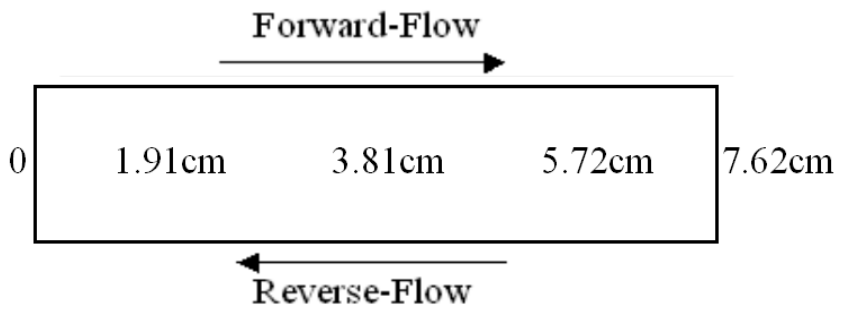

Figure 3.18. Thermocouple Locations with Respect to the Catalyst Sample.

3.5 Analyzers

3.5.1 Carbon Monoxide Analyzer

The Carbon Monoxide (CO) analyzers (AIA-220) use a non-dispersive infrared absorptiometry technique for gas detection produced by Horiba Incorporated. Carbon monoxide detection is accomplished by the use of two separate analyzers, the CO(L) and CO(H), for low and high concentration CO detection, respectively. The specifications of the CO analyzers are shown in Table A-1 in the Appendix [18].

3.5.2 Carbon Dioxide Analyzer

The Carbon Dioxide analyzer is housed in the CO(L) (AIA-220) analyzer and performs gas detection in the same method as the Carbon Monoxide analyzers, non-dispersive infrared absorptiometry. The specifications of the CO_2 analyzer are shown in Table A-1 in the Appendix [18].

3.5.3 Total Hydrocarbon Analyzer

For the purpose of detecting hydrocarbons in the exhaust mixture a total hydrocarbon (THC) analyzer (FIA-220), manufactured by Horiba Incorporated, was selected. The hydrocarbon analyzer uses a flame ionization detector (FID) technique to

quantify total hydrocarbon concentration in the exhaust stream. The specifications of the FID analyzer are shown in Table A-1 in the Appendix [19].

3.6 Overview of the Data Acquisition System

The purpose of the data acquisition system (DAC) is to have the capability to control and monitor components associated with the BFR. The DAC comprises of three main components associated with the system: a personal computer, data acquisition boards, and LabVIEW. Through the use of each component of the DAC the BFR can be controlled, monitored, and logged. The system is designed in such a way as to easily facilitate system changes and modifications, making the DAC an extremely flexible system to manage the BFR.

The DAC allows the experimentalist to monitor and control temperature across the BFR, the switching time durations of the ROCR, and flowrates from mass flow controllers (MFC), which in turn control the concentration of the exhaust mixture. The DAC also accomplishes the tremendous task of logging data from all components associated with the BFR system and Horiba analyzer bench.

Linking the components of the BFR system with the DAC is accomplished by the data acquisition boards. These boards interface every component of the BFR system including the analyzer bench, which accommodates all gas analyzers, and allows for each of the catalyst reactors to be controlled and monitored through LabVIEW. Furthermore, the purpose of LabVIEW in the DAC is to provide a feedback and control loop to the user during the operation of the BFR. The LabVIEW program, in conjunction with all the components associated with the DAC, allows the experimentalist to acquire data and control the BFR system simultaneously.

3.7 Components of the Data Acquisition System

3.7.1 Computer

The computer used for the BFR is a Dell Workstation PWS350 Intel Pentium 4 2.8 GHz personal computer. All automated functions associated with the BFR are performed with the personal computer including data storage.

3.7.2 Data Acquisition Boards

Data acquisition of the BFR system is accomplished through National Instruments hardware and software components. The hardware components of the data acquisition system consist of the following: a shielded rack mounted BNC adapter chassis (BNC-2090), PXI-1002, two shielded rack mounted terminal blocks (TC-2095), which are used to connect the components of the BFR to the DAC, and a 4-slot chassis (NI SCXI-1000).

3.7.3 LabVIEW

LabVIEW is a graphical software developed by National Instruments for the purpose of controlling and acquiring data for various processes. National Instruments LabVIEW 6.1 software was used for the DAC to control and monitor the BFR system. LabVIEW is used to control the flowrate of the MFC, regulate reactor inlet temperature of the RFOCR, operate the switching valves and supplemental fuel injection system, and display temperature and pressure and log data for the BFR. A picture of the LabVIEW controlling screen for the BFR is shown in Figure 3.19. The figure demonstrates the vast amount of information that must be logged while running the BFR. From the screen displayed on the personal computer, all BFR parameters can be manipulated and logged.

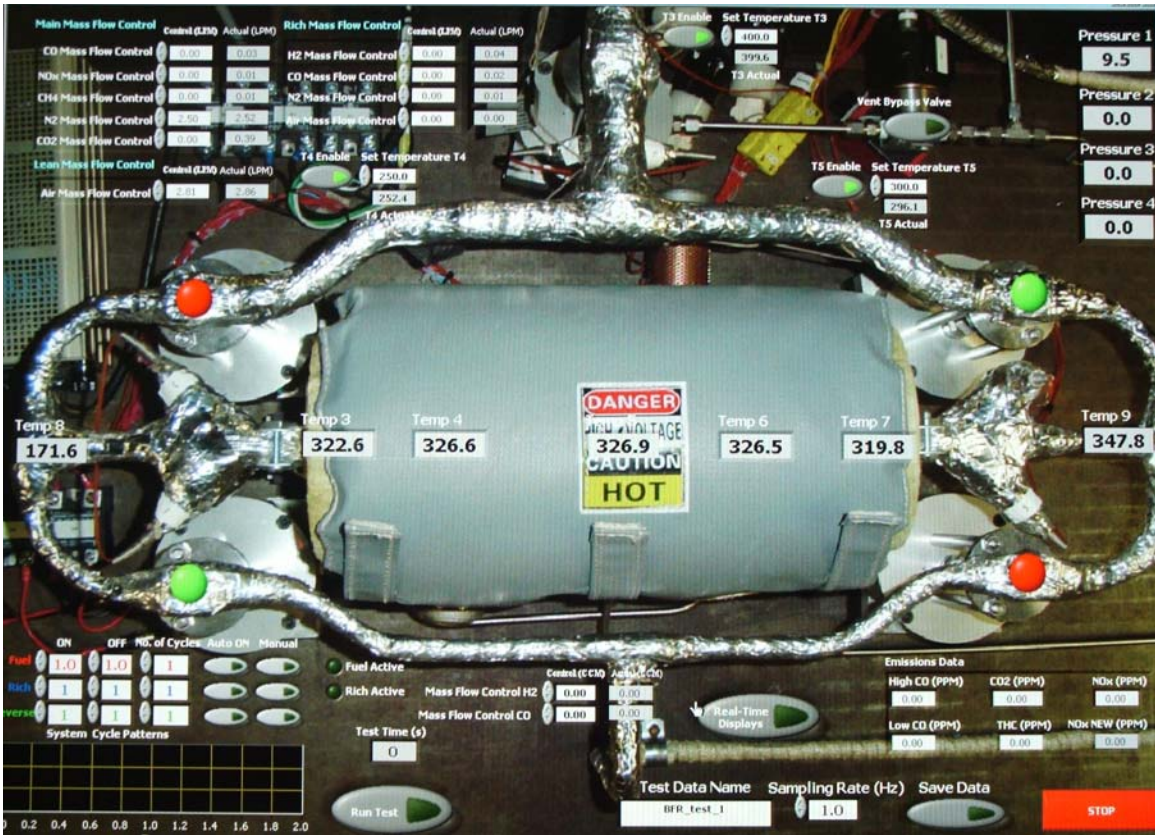

Figure 3.19. LabVIEW Controlling Screen for the Bench-Flow Reactor.

3.8 Operation of the Bench-Flow Reactor

3.8.1 Start-up Procedure

The step-by-step start-up procedure for the BFR proceeds as follows. Firstly, the power strip inside the instrument cabinet must be energized. This powers up the data acquisition system and configures all the components with LabVIEW. Secondly, the system computer is now to be started up. Next, air and hydrogen must be supplied to the FID analyzer, at a supply pressure of 20 psi, to provide fuel for the flame used for hydrocarbon detection. Once the flame is lit, the auxiliary power breaker for the water condenser on the control panel of the Horiba analyzer cabinet must be placed in the ON position. The exhaust fan connected to the outlet line of the analyzer cabinet must also be energized. The analyzer cabinet pump must then be switched on by means of a power strip located behind the analyzer bench. Before gases can be sent to the analyzer bench all gas bottles to be used in the experiment must be opened to a supply pressure of 25 psi and the reactor branching valves must be lined-up for the correct reactor to be used. Once the correct reactor has been lined-up at the reactor branching valves, the outlet line of that reactor is to be connected to the analyzer bench inlet and then the MFC are to be opened. Care must be taken to not have a large pressure or large vacuum develop across the BFR system when flowing gases to the analyzer bench. By monitoring the pressure transducers located before and after the reactor, and by regulating the manifold pressure of the pump it is possible to achieve a low pressure across the BFR system. After the gas is flowing, which initially is typically air and N_2, to the analyzer bench all appropriate analyzers must be lined-up to receive the gas flow. This is accomplished by selecting the desired analyzers on the Analyzer Matrix, located on the front of the analyzer cabinet. The Master Matrix, also located on the front of the analyzer cabinet, must then be selected to Dil Sample (dilute sample). This selection aligns the appropriate solenoid valves inside the analyzer cabinet to the main analyzer cabinet inlet, which should be connected to the appropriate reactor that is to be used. Assuming that gas is flowing through the BFR system and to the analyzer bench the process will need to continue for

1-½ hours for the FID analyzer to stabilize. While the FID analyzer stabilizes heating tape, the reactor furnace, steam generator, and preheater should all be energized to achieve steady-state temperature conditions for the experiment.

3.9 Experimental Protocols

3.9.1 Simulated Exhaust Gas Composition

Based on a literature review the composition of a lean-burn natural gas exhaust mixture, shown in Table 3.2, was selected for the RFOCR study. It should be noted that while oxides of nitrogen (NO_x) and hydrogen (H_2) are present in the typical exhaust mixture for a natural gas engine it was assumed that a lean NO_x trap reactor (LNT) would be prior to the RFOCR, therefore, the concentrations of NO_x and H_2 would essentially be zero. In addition to the exhaust mixture utilized in the RFOCR study, supplemental fuel injection was also introduced into the system. The purpose of using SFI in the RFOCR is to elevate the temperature across the reactor at relatively low reactor inlet temperatures by the combustion of carbon monoxide and hydrogen.

3.9.2 Reverse-Flow Oxidation Catalyst Reactor Experimental Protocol

The purpose of the RFOCR study is to show that by manipulating the simulated exhaust mixture in such a way that it flows in the forward and reverse direction through the catalyst reactor it increases the temperature across the catalyst and hence increases methane conversion. To illustrate this intention CH_4 conversion was directly compared in the reverse and unidirectional flow regimes to determine the merit of a reverse-flow reactor.

Each twenty-minute experimental run consisted of three separate regimes. The runs comprised of five minutes of unidirectional flow followed by ten minutes of flow reversal and concluded with five minutes of unidirectional flow. The initial unidirectional flow regime serves two purposes; it demonstrates steady-state conditions

Table 3.2. Simulated Exhaust Gas Composition.

NOx	0
H_2	0
CO	0.5 %
CH_4	2000 ppm
CO_2	6 %
H_2O	10 %
O_2	6 %
N_2	Balance

for the experimental run and serves as a CH_4 conversion baseline. In the second portion of the experimental runs, the flow reversal regime, the symmetrical switching time durations can vary from 10, 15, 20, 30, or 45 seconds. Symmetrical flow reversal is defined as the time duration in the forward flow being equal to that of the reverse flow. The experimental runs conclude with a unidirectional flow section. This latter unidirectional regime is used to contrast the flow reversal portion of the experiment and illustrate the difference in CH_4 conversion of the two experimental regimes and to return the RFOCR to steady-state unidirectional flow conditions.

To maintain steady-state temperature conditions for the RFOCR the tubular furnace is set to the specific temperature for each experimental run. For the RFOCR study the furnace temperature varies from 400 to 600°C, in 50°C increments. Due to this method of heating, a constant wall temperature is created in the catalyst reactor section for the RFOCR experiments. Furthermore, at higher gas hourly space velocities, greater than 60,000 hr^{-1}, special attention must be made in monitoring the inlet temperatures to RFOCR. If the inlet gas temperature is much less than the catalyst wall temperature the exhaust gas may not have ample time to achieve the temperature of the catalyst wall due to the high gas hourly space velocity. If this occurs it has the effect of cooling the CRS and since CH_4 conversion is a strong function of temperature this cooling effect has the

possibility of shifting the CH_4 conversion much lower than anticipated for a particular temperature.

Lastly, CH_4 conversion is examined as a function of gas hourly space velocity for the RFOCR study. The space velocity for the experiments vary from 20,000-80,000 hr^{-1}. This is accomplished by adjusting the flowrates from the MFC to achieve the appropriate gas hourly space velocity.

3.9.3 Supplemental Fuel Injection Protocol

The supplemental fuel injection (SFI) experiments are similar to, although not as comprehensive as, the RFOCR experiments. The SFI experimental runs consist of two unidirectional runs lasting 600 seconds in duration and four SFI experiments with flow reversal lasting 1200 seconds in duration. The experimental tests are designed to simulate light engine load conditions with low exhaust temperatures, 350°C, and low GHSVs, 20,000 hr^{-1}. Methane conversion is examined as a function of SFI duration and exhaust mixture switching time. Flow reversal experiments consist of SFI pulses introduced into the RFOCR system at the beginning of the flow reversal cycle. The SFI pulses vary from 10, 15, or 20 seconds in duration and the number of pulses vary from 30, 25, 15, or 13 for each respective experimental run. Exhaust mixture switching time is also varied for the SFI experimental runs by 10, 20, 30, and 45 seconds.

CHAPTER 4

EXPERIMENTAL RESULTS

This chapter is divided into two main sections and is devoted to discussing the experimental results obtained for the reverse-flow oxidation catalyst reactor (RFOCR) study. Section 4.1 discusses the results obtained from the RFOCR study without supplemental fuel injection (SFI) and explains how flow reversal duration, reactor furnace temperature, and gas hourly space velocity affects CH_4 conversion. Section 4.2 discusses results obtained from the RFOCR study with SFI both with and without flow reversal and explains how supplemental fuel injection affects CH_4 conversion.

4.1 Reverse-Flow Oxidation Catalyst Reactor Without Supplemental Fuel Injection

All experimental runs for the RFOCR study with flow reversal are divided into three sections, with the total length of the run lasting 1200 seconds in duration. The first 300 seconds consists of an experimental baseline with unidirectional flow, followed by 600 seconds of exhaust flow reversal, and concludes with 300 seconds of unidirectional flow.

Experimental results show that CH_4 conversion is significantly improved with periodic exhaust gas flow reversal when compared with unidirectional flow. Figures 4.1 and 4.2 illustrate methane conversion and the temperature profile across the catalyst for a typical experimental run at a constant reactor furnace temperature of 450°C, a gas hourly space velocity (GHSV) of 40,000 hr^{-1}, and a switching time (ST) of 10 seconds. Figure 4.1 shows methane conversion increases more than 47% during flow reversal when compared to unidirectional CH_4 conversion. This increase in CH_4 conversion is

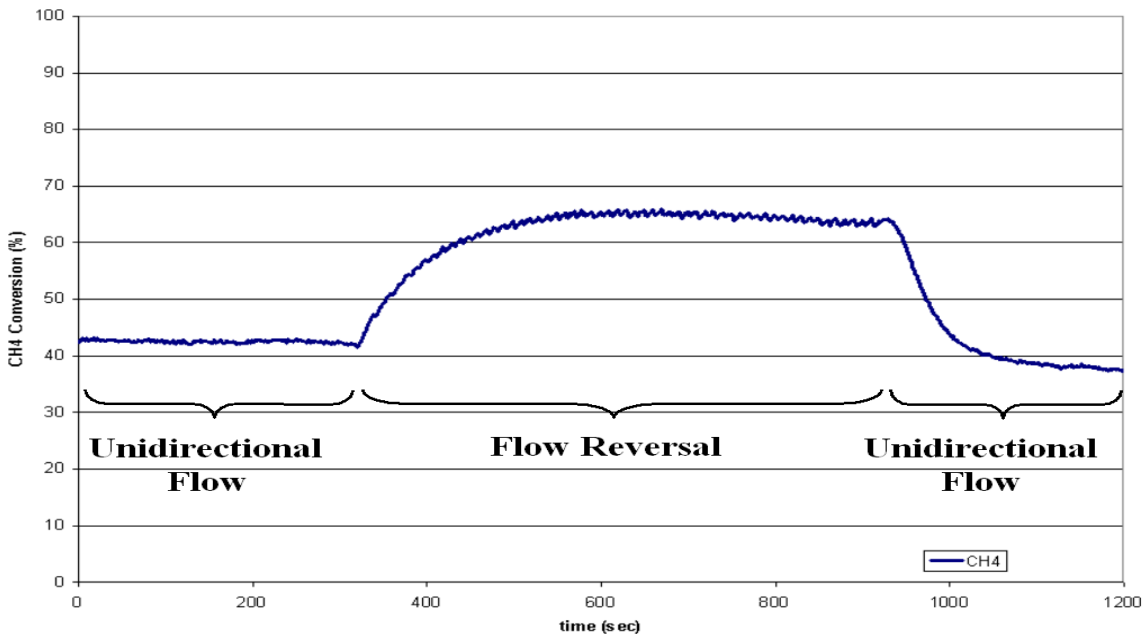

Figure 4.1. Methane Conversion at a Reactor Furnace Temperature of 450°C, GHSV of 40,000 hr^{-1}, and a ST of 10s.

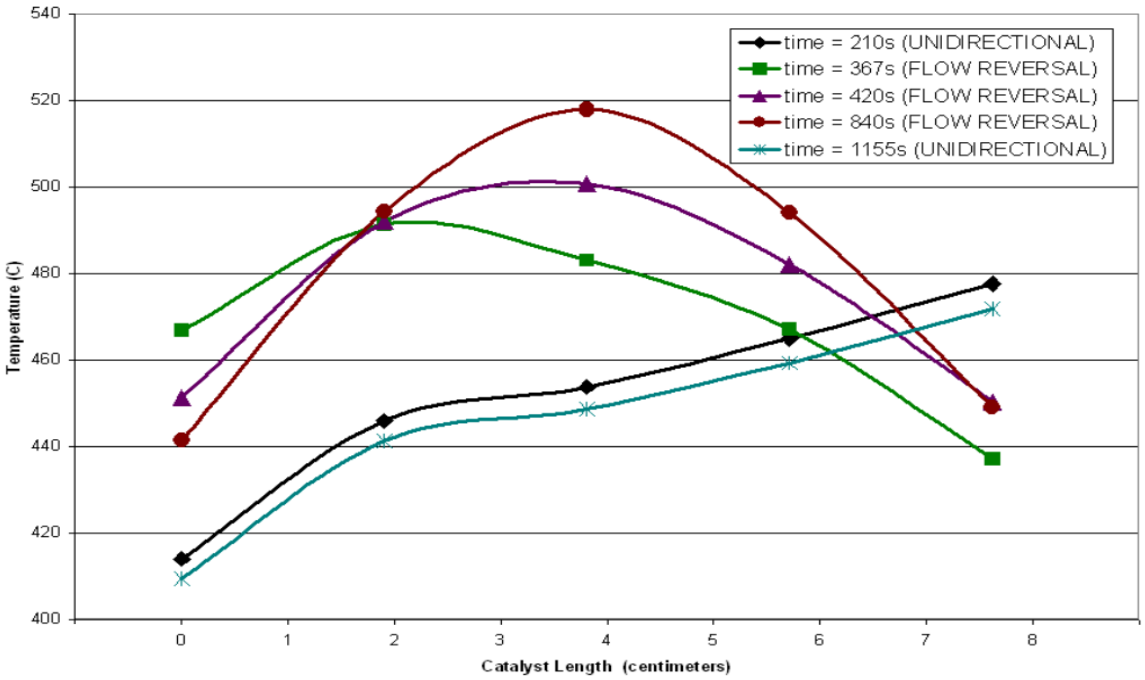

Figure 4.2. Temperature Profiles Across the Catalyst Length at Various Times at a Reactor Furnace Temperature of 450°C, GHSV of 40,000 hr^{-1}, and a ST of 10s.

attributed to the trapping of heat from the combustion of methane across the length of the catalyst due to flow reversal. The temperature profile across the catalyst is examined at several instances of time in the unidirectional flow regime and the flow reversal regime of the experimental run. From Figure 4.2 the unidirectional temperature profiles (t = 210 and 1155 seconds) continually increase due to the exothermic chemical reaction of CH_4 as it travels across the catalyst. The temperature profiles across the catalyst length before and after flow reversal (t = 210 and 1155 seconds) are noted as not having repeatable steady-state temperature profiles, however given time the difference in steady-state CH_4 conversion for both unidirectional regime (pre and post flow reversal) does decrease. Additionally, at an experimental run time of t = 300 seconds to t = 900 seconds the flow direction through the catalyst reactor is then periodically reversed, at a switching time of 10 seconds. During periodic flow reversal the elevated temperature at the exit of the catalyst reactor is used to preheat the feed stream, increasing the reaction rate. After a sufficient amount of periodic flow reversal a considerable amount of heat is trapped across the length of the catalyst, i.e., the heat trap effect. Figure 4.2 illustrates the development of the heat trap effect from the flow reversal temperature profiles ($300 < t < 900$ seconds) across the catalyst. From the figure it is shown that periodically reversing the exhaust mixture increases the average temperature (^oC) across the catalyst reactor by 6% when comparing the fully developed flow reversal temperature profile at t = 840 seconds to the unidirectional temperature profile at t = 210 seconds.

Figure 4.3 illustrates the temperature profiles across the catalyst with both a combustible gas composition and an inert gas composition. Both experimental runs are conducted at a reactor furnace temperature of 450^oC and a GHSV of 40,000 hr^{-1}. The inert exhaust gas composition consists of a mixture of 6% O_2, 10% H_2O, and a N_2 balance. Due to the composition of the inert gas mixture no exothermic chemical reaction is taking place on the surface of the catalyst. The temperature at inlet of the catalyst reactor is lower than the outlet of the catalyst due to convective heat transport of the inert gas composition. The combustible gas composition consists of a mixture of 2000ppm CH_4, 0.5% CO, 6% CO_2, 6% O_2, 10% H_2O, and a N_2 balance. From the figure the temperature across the catalyst is increased when oxidation occurs at the surface of

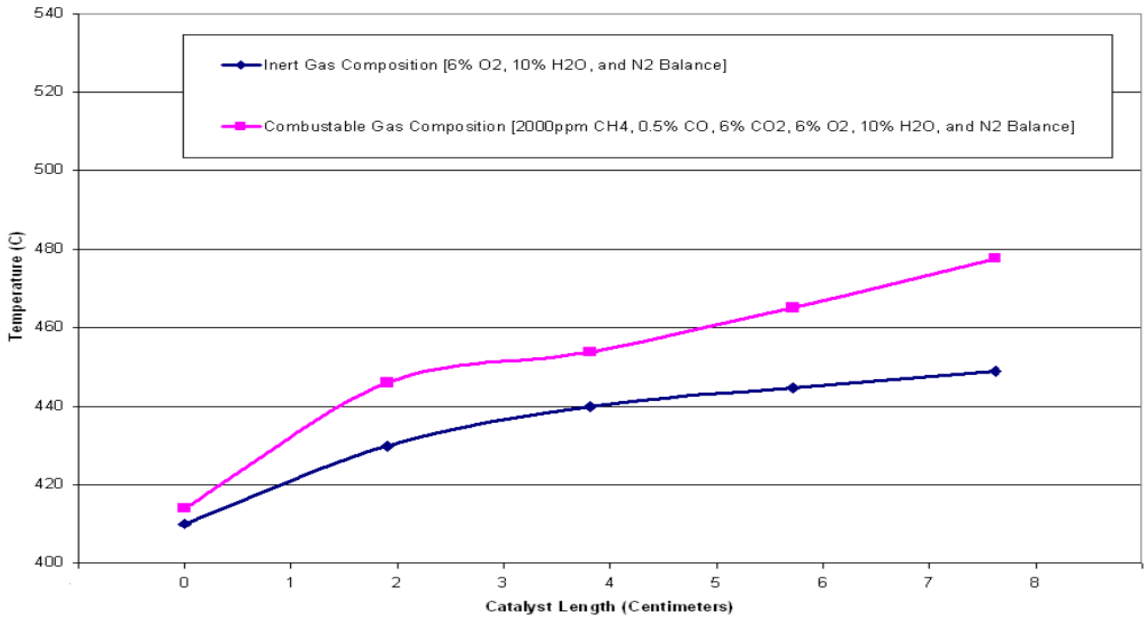

Figure 4.3. Temperature Profiles Across the Catalyst Length at a Reactor Furnace Temperature of 450°C and a GHSV of 40,000 hr^{-1} with Unidirectional Flow.

the catalyst. A significant temperature increase occurs after the first 2-centimeters of the catalyst. This temperature increase is due to CH_4 diffusing and reacting at the surface of the catalyst resulting in an exothermic reaction. Additionally, a list of all average methane conversions for the unidirectional flow regime and the flow reversal regime for all experimental runs are shown in Tables 4.1 through 4.4.

From the Tables 4.1 through 4.4 it is noted that the average unidirectional CH_4 conversion baselines are not consistent at a particular GHSV and reactor furnace temperature. This is due to each of the switching time experiments being run in sequence of one another at a particular GHSV and reactor furnace temperature, which initially resulted in a gradual catalyst warming trend. To attempt to create a repeatable unidirectional CH_4 conversion baseline for each experimental run at a particular GHSV and reactor furnace temperature a unidirectional "cool down time" of 11 minutes was allowed between flow reversal operations. As a result, the cool down time between flow reversal operation proved to insufficient to obtain repeatable unidirectional baseline

Table 4.1. Average Methane Conversion for the Unidirectional and Flow Reversal Regimes at Reactor Furnace Temperatures of 400, 450, 500, and 600°C, STs of 10, 15, 20, 30, and 45s, and a GHSV of 20,000 hr^{-1}.

20,000 hr^{-1} GHSV			
Temperature (°C)	Switching Time (s)	Unidirectional Flow	Flow Reversal
400	10	8%	14%
	15	11%	18%
	20	13%	22%
	30	15%	26%
	45	18%	29%
450	10	76%	82%
	15	76%	86%
	20	75%	85%
	30	71%	83%
	45	68%	81%
500	10	N/A	N/A
	15	N/A	N/A
	20	N/A	N/A
	30	N/A	N/A
	45	N/A	N/A
550	10	N/A	N/A
	15	N/A	N/A
	20	N/A	N/A
	30	N/A	N/A
	45	N/A	N/A
600	10	N/A	N/A
	15	N/A	N/A
	20	N/A	N/A
	30	N/A	N/A
	45	N/A	N/A

Table 4.2. Average Methane Conversion for the Unidirectional and Flow Reversal Regimes at Reactor Furnace Temperatures of 400, 450, 500, and 600°C, STs of 10, 15, 20, 30, and 45s, and a GHSV of 40,000 hr^{-1}.

40,000 hr^{-1} GHSV			
Temperature (°C)	Switching Time (s)	Unidirectional Flow	Flow Reversal
400	10	7%	12%
	15	11%	17%
	20	14%	18%
	30	14%	16%
	45	13%	14%
450	10	41%	60%
	15	34%	52%
	20	30%	45%
	30	27%	39%
	45	25%	34%
500	10	56%	77%
	15	52%	73%
	20	47%	68%
	30	44%	63%
	45	41%	57%
550	10	68%	87%
	15	70%	86%
	20	67%	84%
	30	64%	81%
	45	61%	78%
600	10	N/A	N/A
	15	N/A	N/A
	20	N/A	N/A
	30	N/A	N/A
	45	N/A	N/A

Table 4.3. Average Methane Conversion for the Unidirectional and Flow Reversal Regimes at Reactor Furnace Temperatures of 400, 450, 500, and 600°C, STs of 10, 15, 20, 30, and 45s, and a GHSV of 60,000 hr^{-1}.

60,000 hr^{-1} GHSV			
Temperature (°C)	Switching Time (s)	Unidirectional Flow	Flow Reversal
400	10	3%	8%
	15	4%	12%
	20	6%	15%
	30	6%	14%
	45	6%	12%
450	10	30%	55%
	15	28%	49%
	20	26%	43%
	30	24%	37%
	45	21%	31%
500	10	54%	73%
	15	53%	69%
	20	50%	65%
	30	38%	56%
	45	43%	53%
550	10	64%	81%
	15	62%	78%
	20	59%	75%
	30	56%	71%
	45	54%	66%
600	10	N/A	N/A
	15	N/A	N/A
	20	N/A	N/A
	30	N/A	N/A
	45	N/A	N/A

Table 4.4. Average Methane Conversion for the Unidirectional and Flow Reversal Regimes at Reactor Furnace Temperatures of 400, 450, 500, and 600°C, STs of 10, 15, 20, 30, and 45s, and a GHSV of 80,000 hr^{-1}.

80,000 hr^{-1} GHSV			
Temperature (°C)	Switching Time (s)	Unidirectional Flow	Flow Reversal
400	10	N/A	N/A
	15	N/A	N/A
	20	N/A	N/A
	30	N/A	N/A
	45	N/A	N/A
450	10	8%	20%
	15	8%	19%
	20	6%	13%
	30	4%	8%
	45	3%	6%
500	10	9%	27%
	15	7%	20%
	20	6%	16%
	30	5%	14%
	45	5%	12%
550	10	14%	54%
	15	19%	48%
	20	17%	43%
	30	16%	38%
	45	15%	34%
600	10	25%	69%
	15	30%	65%
	20	28%	60%
	30	27%	55%
	45	26%	51%

conversion prior to flow reversal operations, however direct comparison of the average flow reversal CH_4 conversions at a particular GHSV and furnace temperature may still be preformed. The rationale to directly compare flow reversal CH_4 conversion with dissimilar unidirectional baselines is illustrated in Figure 4.4. Figure 4.4 illustrates the temperature profiles of two different experimental runs. The reactor furnace temperature and GHSV for both runs are 400°C and 20,000 hr^{-1}, respectively. The switching times for the experimental runs are 10 seconds and 45 seconds. From Table 4.1 the unidirectional average CH_4 conversion is 8.1% at a reactor furnace temperature of 400°C, a GHSV of 20,000 hr^{-1}, and a ST of 10 seconds, which corresponds to the temperature profile in Figure 4.4 at a experimental run time of t = 210 seconds. The average unidirectional CH_4 conversion is 17.8% at a reactor furnace temperature of 400°C, a GHSV of 20,000 hr^{-1}, and a ST of 45 seconds, which corresponds to the temperature profile at experimental run time of t = 318 seconds. From the figure the temperature profile of the experimental run at a ST of 10 seconds is initially lower than the temperature profile of the experimental run at a ST of 45, hence the difference in the baseline conversion. However, from the figure the temperature profiles are nearly identical through the center portion of the catalyst at an experimental run time of approximately 319 seconds.

Based on the results presented the initial warming trend of the first experiment to the last experimental run in a particular data set does influence the initial unidirectional average conversion, however the variation in the temperature profile is quickly recovered during the initial flow reversals. Due to this fact it is proper to compare average flow reversal CH_4 conversions at a particular GHSV and reactor furnace temperatures though the unidirectional CH_4 conversions are not constant.

4.1.1 Exhaust Mixture Bypassing the Catalyst Due to Flow Reversal

Periodic flow reversal causes a finite amount of the exhaust mixture to bypass the catalyst reactor due to the dead volume associated with a reverse-flow reactor (RFR). The dead volume is expressed as a volume of space in the flow system, where a dead-end passageway or cavity retains a portion of the exhaust gas mixture. During flow reversal operations a portion of the exhaust mixture is pushed out of the catalyst reactor on the

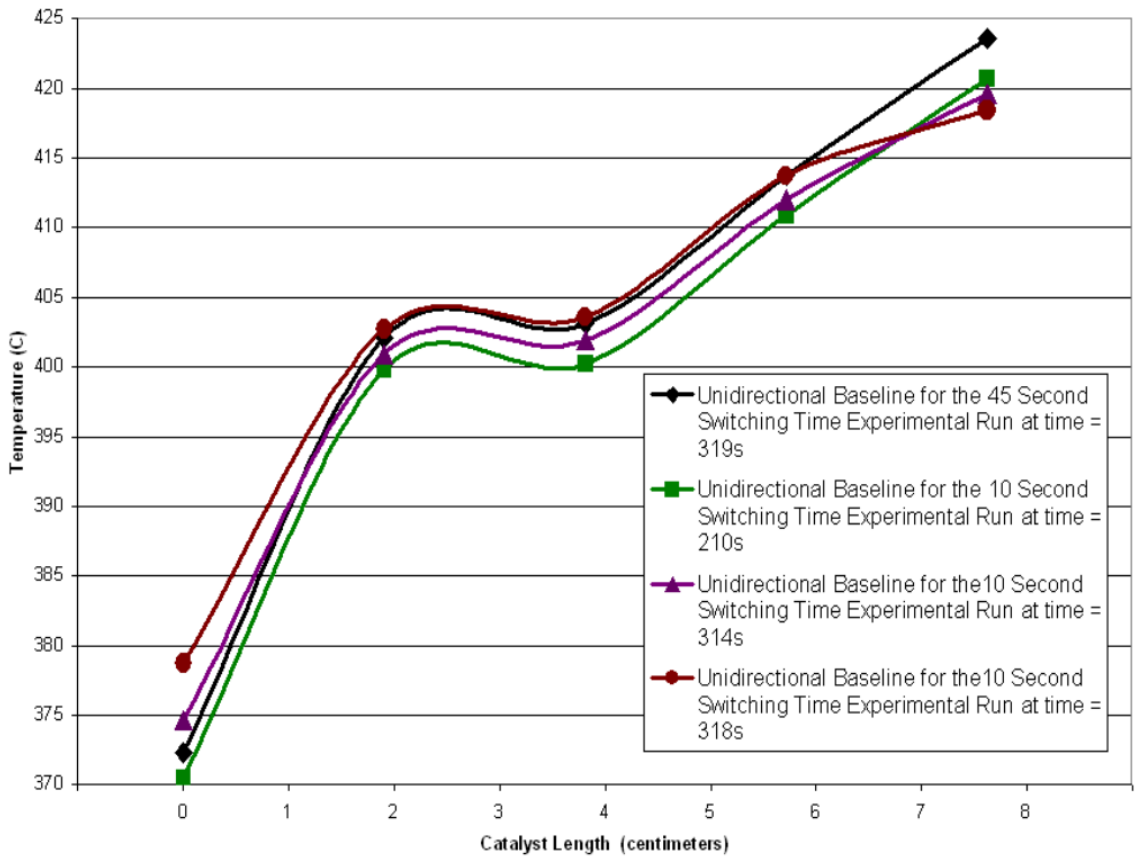

Figure 4.4. Baseline Unidirectional Temperature Profiles for 10 and 45s ST Experimental Runs at a Reactor Furnace Temperature of 400°C, a GHSV of 20,000 hr^{-1}.

subsequent flow reversal, bypassing the combustion process. Figure 4.5 illustrates an example of how the exhaust mixture bypasses the catalyst reactor during flow reversal. As the exhaust gases flow into the catalyst reactor in the forward flow direction (Figure 4.5(a)), a portion of the exhaust mixture is trapped between the switching valve (switching valve 1) and the catalyst reactor upon the subsequent flow reversal (Figure 4.5(b)) and is pushed out of the RFOCR.

As a result of the dead volume associated with a RFR higher concentrations of constituents of the exhaust mixture are found during flow reversal operations. This is best illustrated by carbon monoxide concentrations in the exhaust mixture during experimental runs with flow reversal. During the unidirectional regime of the experimental runs the entire amount of CO in the exhaust mixture is oxidized to CO_2. An example of this CO oxidation is illustrated in Figure 4.5 and the chemical reaction is shown in Equation 4.1.

$$CO + \frac{1}{2} O_2 \rightarrow CO_2 \qquad (4.1)$$

Figure 4.6 illustrates CO concentration for an experimental run at a reactor furnace temperature of 450°C, a GHSV of 40,000 hr^{-1}, and a ST of 10 seconds. From the figure it is clearly seen that flow reversal allows a finite amount of exhaust gases to bypass the catalyst reactor permitting a portion of the exhaust mixture to escape the combustion process. Table 4.5 displays the average CO concentration during flow reversal for experimental runs at a reactor furnace temperature of 450°C, a GHSV of 40,000 hr^{-1}, and STs of 10, 15, 20, 30, and 45 seconds. From the table it is seen that the frequency of flow reversal corresponds to the amount of average CO concentration bypassing the catalyst reactor. The correlation between the frequency of flow reversal and catalyst bypass is explained by the lower the frequency of the flow reversal the closer the flow operations are to unidirectional flow, which do not suffer from reactor bypass associated with the dead volume of a reverse-flow reactor.

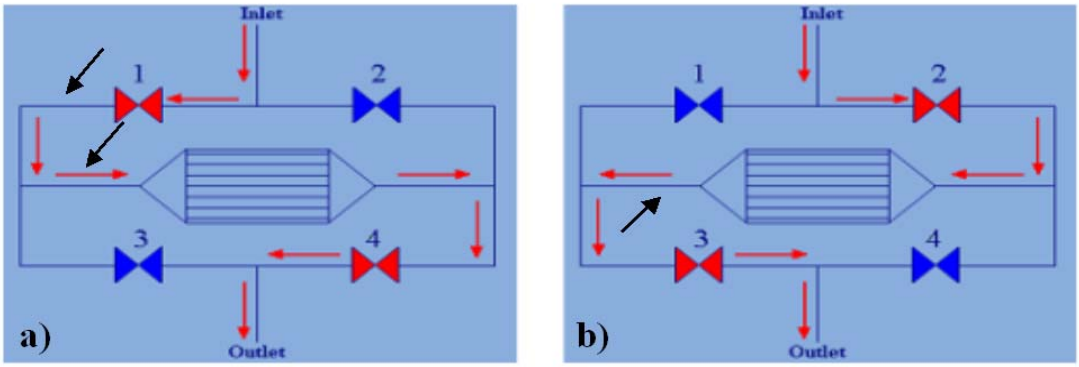

Figure 4.5. Illustration of Dead Volume Associated with a RFR.

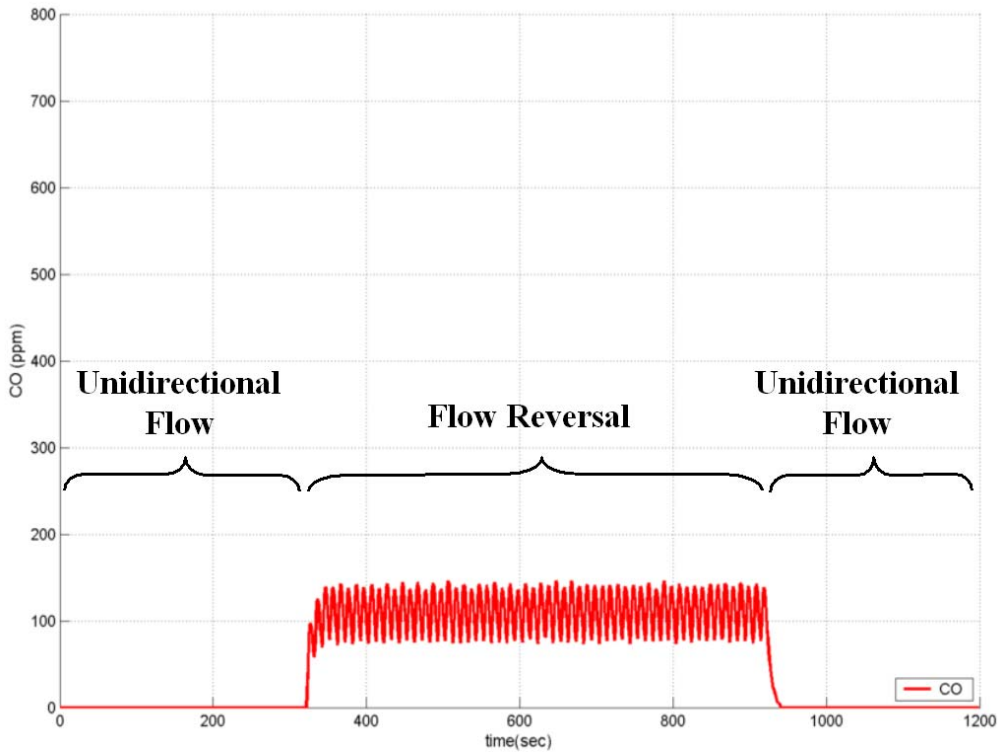

Figure 4.6. Carbon Monoxide Concentration at a Reactor Furnace Temperature of 450°C, a GHSV of 40,000 hr^{-1}, and a ST of 10s.

Table 4.5. Effects of Switching Time on CO Concentration Bypassing the Catalyst at a Reactor Furnace Temperature of 450°C, a GHSV of 40,000hr^{-1}, and a ST of 10,15, 20, 30, and 45s.

Switching Time (s)	Average CO (ppm)
10	106
15	68
20	50
30	31
45	20

4.1.2 Effects of Switching Time and Gas Hourly Space Velocity on CH_4 Conversion

Experimental results confirm that periodically reversing the exhaust mixture through a catalyst reactor CH_4 conversion can be significantly improved when compared with unidirectional flow conversion. Results also indicate that the effects of switching time on CH_4 conversion vary significantly with GHSV and temperature. In the course of examining the experimental data several trends emerged for CH_4 conversion with respect to switching time. Experiments with flow reversal indicate that at a GHSV of 20,000 hr^{-1} and reactor furnace temperature of 400°C a maximum methane conversion is obtained at lower frequency switching times (30 and 45 seconds). This trend is illustrated in Figure 4.7 at a reactor furnace temperature of 400°C and a GHSV of 20,000 hr^{-1}. Methane conversion at a GHSV of 20,000 hr^{-1} is at a minimum at high frequency switching times (10-20 seconds) due to premature flow reversal, which results in a failure to trap large portion of heat across the catalyst. The development of a premature flow reversal temperature profile is shown in Figure 4.8 at a reactor furnace temperature of 400°C, a

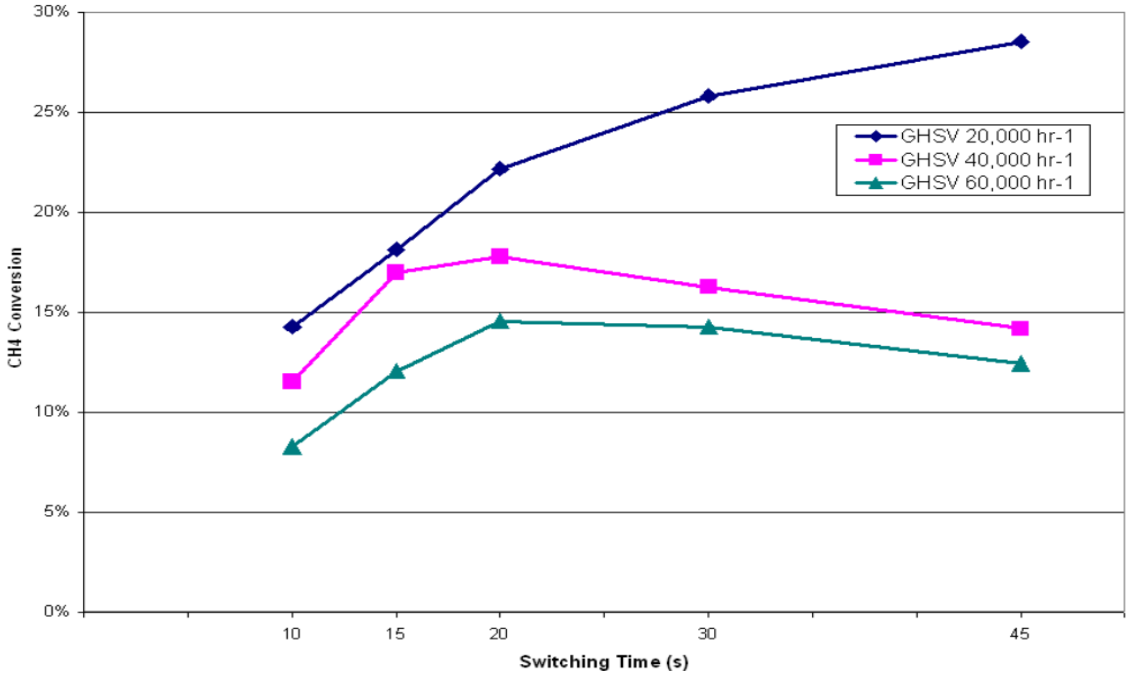

Figure 4.7. Effects of Switching Time on CH_4 Conversion with GHSV as a Parameter at a Temperature of 400°C.

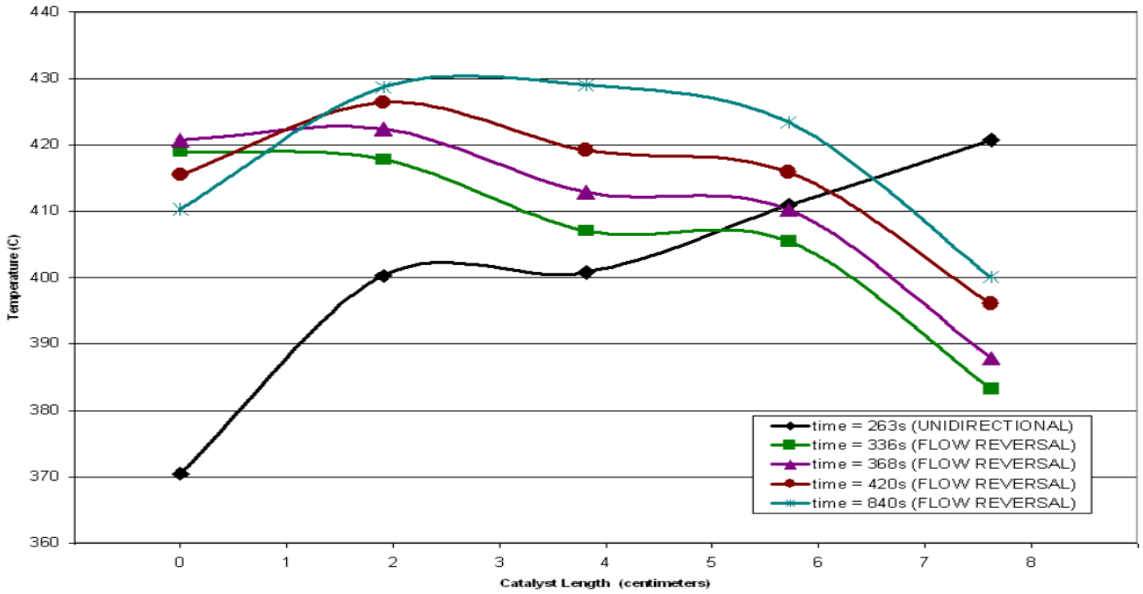

Figure 4.8. Temperature Profile Across the Catalyst at a Reactor Furnace Temperature of 400°C, a GHSV of 20,000 hr^{-1}, and a ST of 10s at Various Experimental Run Times.

GHSV of 20,000 hr^{-1}, and a switching time of 10 seconds. Premature flow reversal is attributed to the preheated reactor inlet temperature not being given ample time to travel across the catalyst before flow reversal. This premature flow reversal results in the elevated temperature being pushed outside the length of the catalyst, which lowers the overall reactor temperature and decreases CH_4 conversion. From Figure 4.8 the fully developed temperature profile associated with a RFR (see Figure 2.7(e)) at experimental run time t = 840 seconds is shifted away from the center of the catalyst length. As described before the loss of trapped heat across the catalyst directly correlates to a reduction in CH_4 conversion. Figure 4.9 is at a reactor furnace temperature of 400°C, a GHSV of 20,000 hr^{-1}, and a switching time of 30 seconds. Figure 4.9 illustrates that correctly timing the switching duration leads to a maximum temperature profile across the length of the catalyst. Comparison of the fully developed temperature profiles associated with a RFR in Figures 4.8 and 4.9 demonstrates the importance of selecting the proper switching time at a specific gas hourly space velocity and feed temperature.

Experimental results at a reactor furnace temperature of 450°C and a GHSV of 20,000 hr^{-1} do not follow the trend of increasing CH_4 conversion as switching time increase. Figure 4.10 illustrates that CH_4 conversion is relative consistent across the entire range of switching times. This phenomenon is attributed to the chemical reaction for the dissociation of CH_4 falling into the diffusion limited regime of an Arrhenius plot, shown in Figure 4.11. The figure is an Arrhenius plot with the natural log of the apparent rate constant of the chemical reaction plotted against the inverse of temperature. The figure shows that once in the diffusion limited regime the chemical reaction approaches an asymptote where no amount of temperature increase will improve the chemical reaction rate constant. Figure 4.11 shows that varying switching time does not enhance CH_4 conversion due to the fact that all STs presented at a GHSV of 20,000 hr^{-1} and a reactor furnace temperature of 450°C are limited to the time the chemical species has to diffuse to the surface of the catalyst and, therefore, CH_4 conversion is relatively constant across all STs presented. The time a chemical species has to diffuse to the surface of the catalyst is expressed as the residence time or the contact time. Table 4.6 lists all residence times for the RFOCR system at particular reactor furnace temperatures and gas

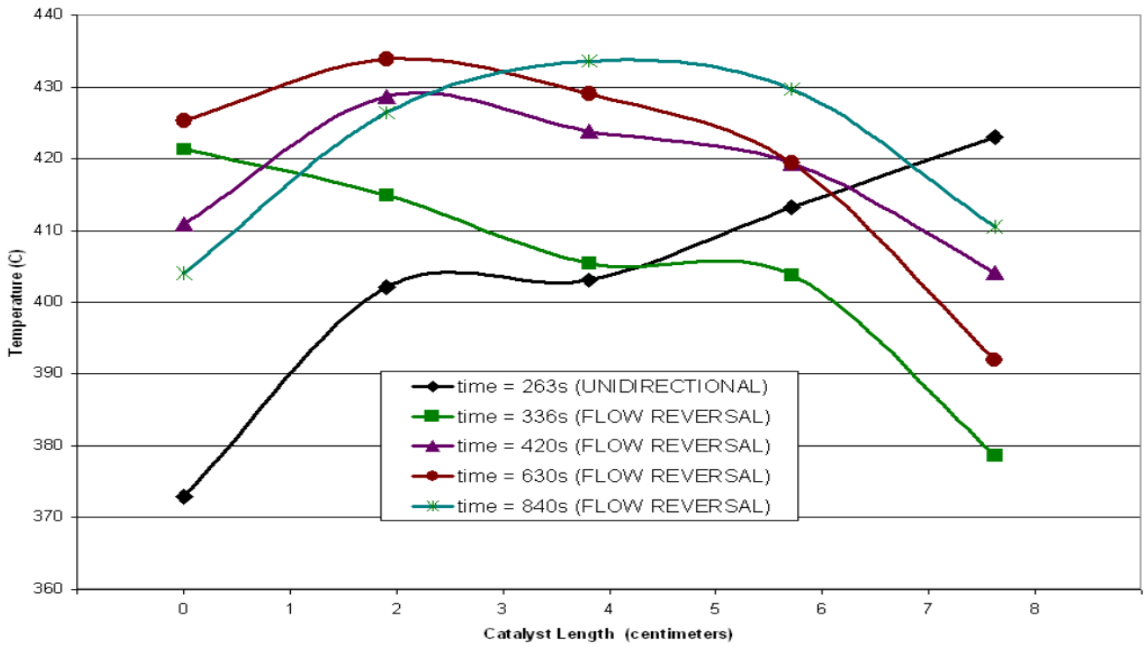

Figure 4.9. Temperature Profiles Across the Catalyst at Various Times During an Experimental Run at a Reactor Furnace Temperature of 400°C, GHSV of 20,000 hr^{-1}, and a ST of 30s.

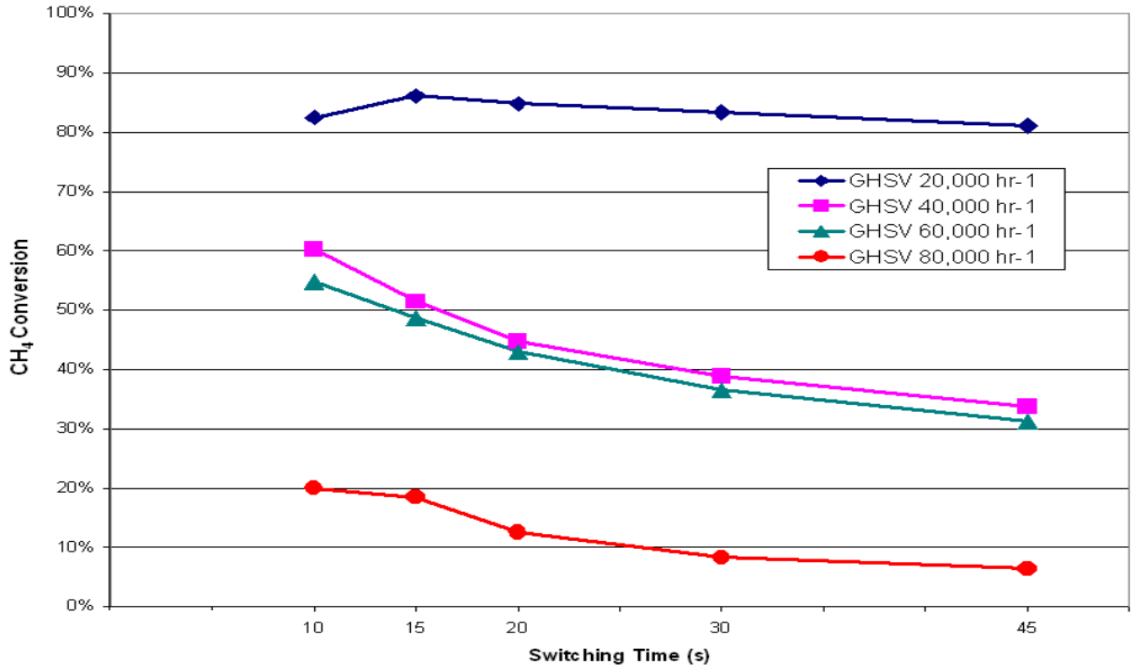

Figure 4.10. Effects of Switching Time on CH_4 Conversion with GHSV as a Parameter at a Temperature of 450°C.

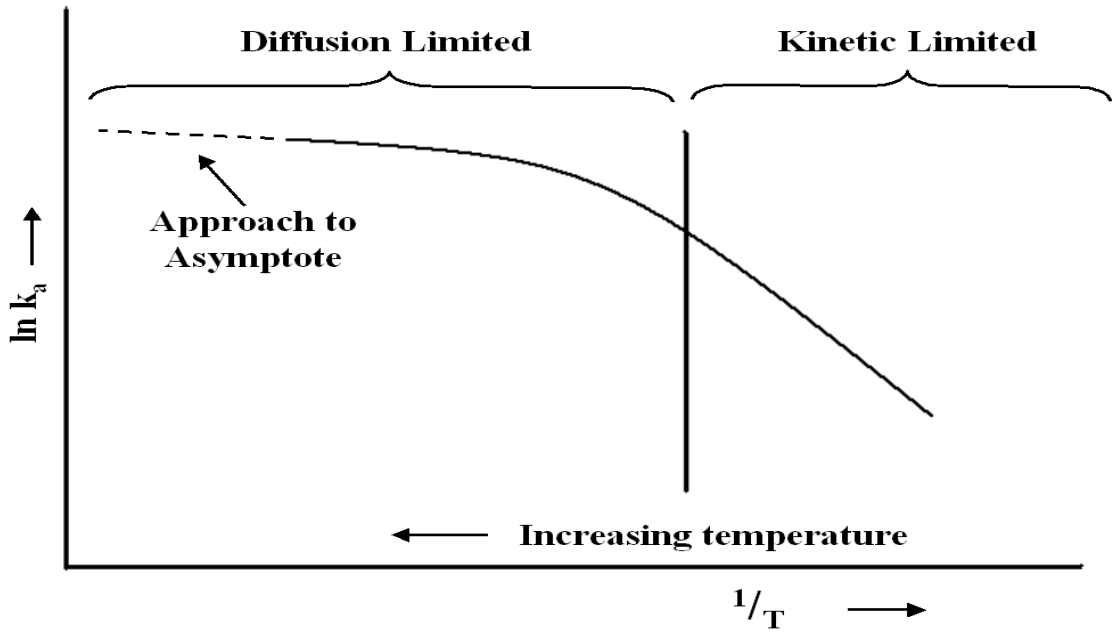

Figure 4.11. Representation of Various Regimes on an Arrhenius Plot. Reprinted from Hayes and Kolaczkowski [9].

Table 4.6. RFOCR Residence Times for the Total Exhaust Mixture at All Reactor Inlet Temperatures and GHSVs.

Furnace Temperature	GHSV 20,000 hr^{-1}	GHSV 40,000 hr^{-1}	GHSV 60,000 hr^{-1}	GHSV 80,000 hr^{-1}
400°C	185 ms	93 ms	62 ms	46 ms
450°C	174 ms	86 ms	57 ms	43 ms
500°C	N/A	81 ms	54 ms	40 ms
550°C	N/A	76 ms	50 ms	38 ms
600°C	N/A	N/A	N/A	36 ms

Experimental results also confirm that maximum CH_4 conversion occurs at higher frequency switching times (10-20 seconds) for experiments at a GHSV of 40,000 hr^{-1}, with the exception of the experimental run at a reactor furnace temperature of 550°C. This trend of greater CH_4 conversions at switching times of 15 and 20 seconds at a GHSV of 40,000 hr^{-1} can be seen in Figure 4.7. The loss in CH_4 conversion at lower frequency switching times (30 and 45 seconds) is attributed to a delayed switching. Similar to the preheated exhaust temperature being pushed out of the reactor due to premature flow reversal (as is the case for a ST of 10 seconds, a GHSV of 40,000 hr^{-1}, and a reactor furnace temperature of 400°C), the STs of 30 and 45 seconds at a GHSV of 40,000 hr^{-1} experience an inability to trap elevated temperatures across the catalyst reactor due to delayed flow reversal. If the flow reversal is too low in frequency the elevated temperature is allowed to travel from one end of the catalyst to the other during flow reversal cycles without trapping a large amount of elevated temperature across the center of the catalyst. As a result of the delayed flow reversal a portion of the fully developed temperature profile associated with a RFR is pushed outside the length of the catalyst. The development of the delayed flow reversal temperature profile at a reactor furnace temperature of 450°C, a GHSV of 40,000 hr^{-1}, and a ST of 45 seconds is illustrated in Figure 4.12. The figure shows an inability to trap the elevated temperature across the length of the catalyst resulting in a pseudo-unidirectional temperature profile during flow reversal, thereby reducing the overall temperature across the catalyst and lowering CH_4 conversion.

Methane conversion at a GHSV of 40,000 hr^{-1} follows the general trend of producing the greatest CH_4 conversion at more frequent STs with the exception of the experiments at a reactor furnace temperature of 550°C (Figure 4.13). Experimental variations in the switching time had little effect on CH_4 conversion for experiments at a GHSV of 40,000 hr^{-1} and reactor furnace temperature of 550°C. Figure 4.13 illustrates that the increase in CH_4 conversion is reasonably flat across the switching times of 10 to 45 seconds. As discussed before, this phenomenon is also attributed to the chemical reaction for the dissociation of CH_4 falling into the diffusion limited regime of an Arrhenius plot, shown in Figure 4.11.

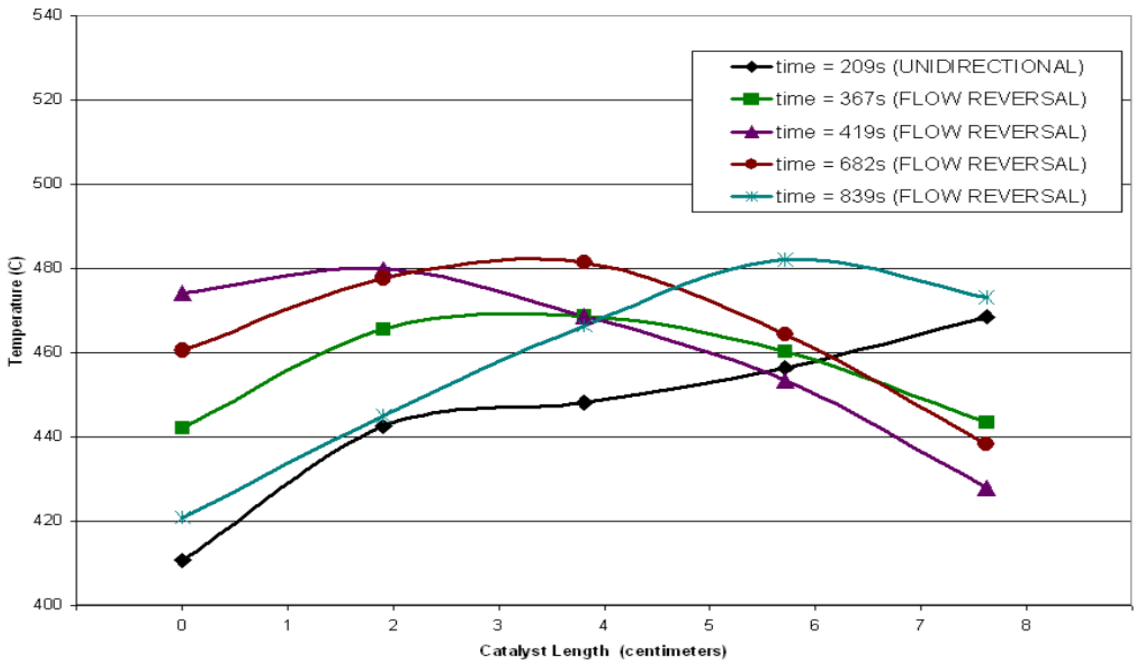

Figure 4.12. Temperature Profile at a Reactor Furnace Temperature of 450°C, GHSV of 40,000 hr^{-1}, and a ST of 45s at Various Experimental Run Times.

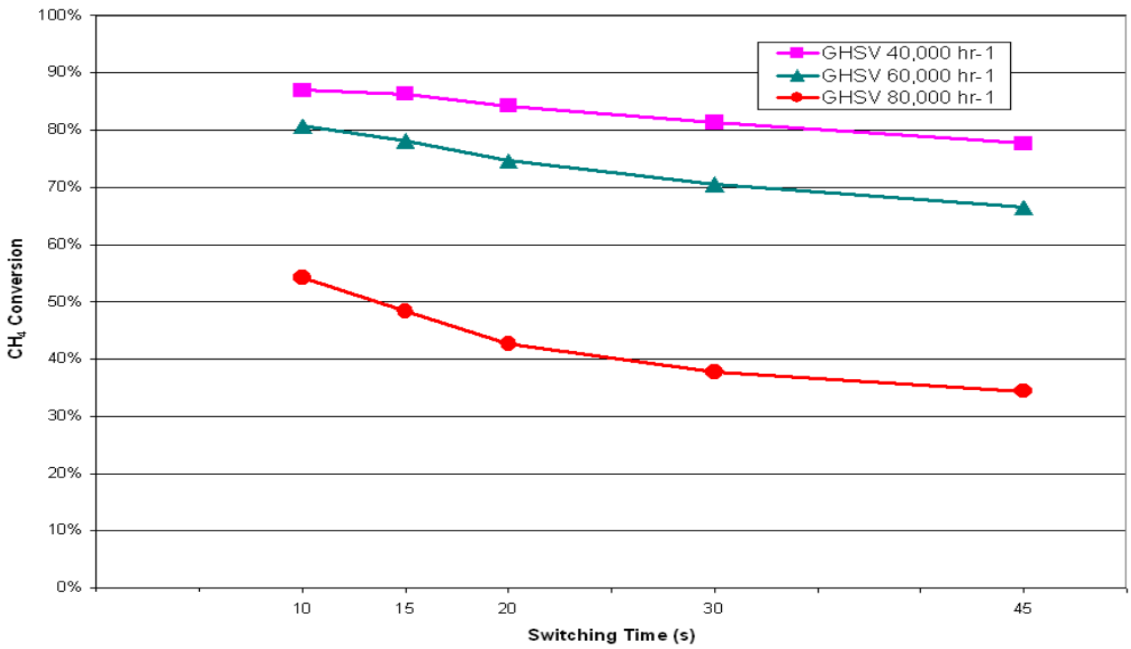

Figure 4.13. Effects of Switching Time on CH_4 Conversion with GHSV as a Parameter at Temperature of 550°C.

Methane conversion for experiments with flow reversal for GHSVs of 60,000 and 80,000 hr^{-1} is similar to the trends presented for GHSVs of 40,000hr^{-1}. Generally, higher frequency STs produced higher CH_4 conversions than that of the lower frequency STs for GHSVs of 60,000 and 80,000 hr^{-1}, and this is shown in Figures 4.7, 4.10, and 4.13. Figure 4.7 at a GHSV of 60,000 hr^{-1} shows a maximum CH_4 conversion at a ST of 20 seconds. As previously discussed, the lesser CH_4 conversions in the figure are attributed to either premature or delayed flow reversal, both of which lead to a decrease in the overall catalyst temperature and a reduction in CH_4 conversion. As in the case for a GHSV of 40,000 hr^{-1} CH_4 conversion begins to become more constant across the range of switching times at a reactor furnace temperature of 550°C. This constant CH_4 conversion at a GHSV of 60,000 hr^{-1} is attribute to the chemical reaction for the dissociation of CH_4 falling into the diffusion limited regime of an Arrhenius plot. Experiments with flow reversal at GHSVs of 80,000 hr^{-1} consistently demonstrate that the greatest improvement in CH_4 conversion is at a switching time of 10 seconds. The decline in CH_4 conversion at lower frequency switching times is attributed to a delay in flow reversal resulting in a failure to trap a majority of the elevated temperature across the catalyst reactor.

4.1.3 Effect of Temperature and Gas Hourly Space Velocity on CH_4 Conversion

Experimental results indicate that CH_4 conversion continually improves with or without flow reversal as the reactor furnace temperature increases and as GHSV decreases. Figure 4.14 illustrates CH_4 conversions plotted against time with temperature as a parameter at a constant GHSV of 80,000 hr^{-1} and at a switching time of 10 seconds. As previously discussed both figures are divided into three separate regimes: the unidirectional regime, the flow reversal regime, and the concluding unidirectional regime. Figure 4.14 shows CH_4 conversion increases in all regimes as temperature increases. This increase is due to the exponential effect of temperature on the dissociation of methane and may be seen in the Arrhenius rate law shown in Equation 4.2. The equation illustrates that as temperature increases the rate constant increases, which corresponds to an increase in CH_4 conversion.

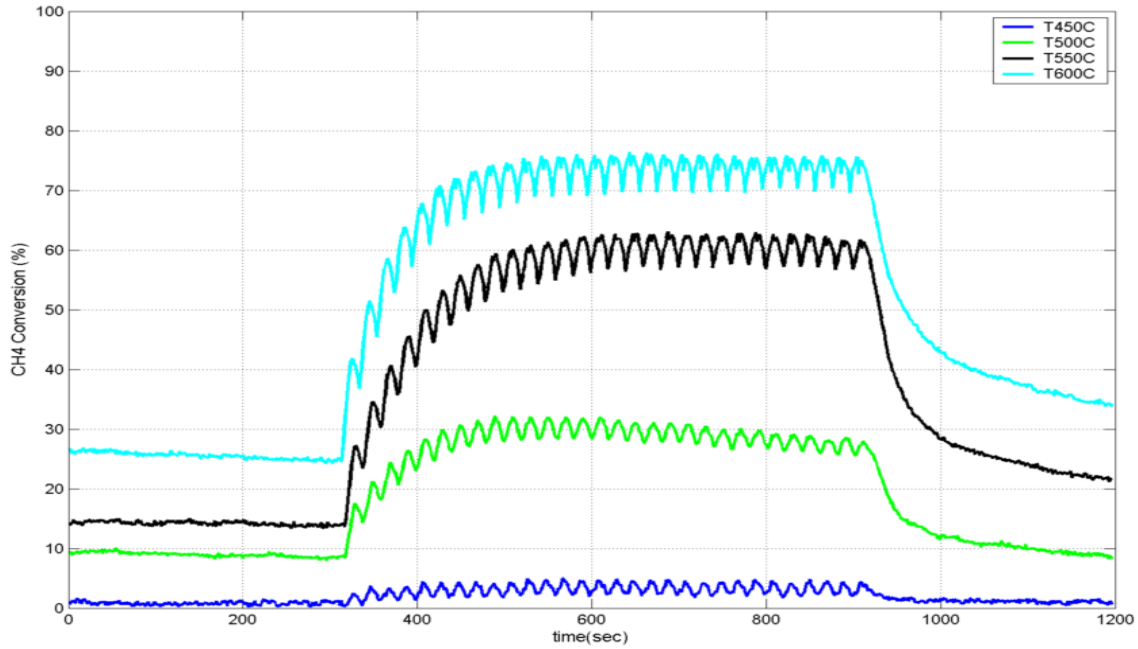

Figure 4.14. Effects of Temperature on CH_4 Conversion with Temperature as a Parameter at a GHSV of 80,000 hr^{-1} and a ST of 10s.

$$k(T) = A \exp(-E_A/R_uT) \qquad (4.2)$$

where,

k = rate constant, A = pre-exponential factor

E_A = activation energy, R_u = universal gas constant

T = temperature

Furthermore, at relatively low reactor furnace temperatures CH_4 conversion only benefits modestly with flow reversal. This is attributed to a relatively low CH_4 conversion temperature across the catalyst, which produces a small amount of heat to be trapped, resulting in only slight improvements in CH_4 conversion due to flow reversal. This can be seen in Figure 4.14 at reactor furnace temperatures of 450°C. Conversely, the effect flow reversal has on enhancing CH_4 conversion diminishes as the temperature

increases at relatively high reactor furnace temperatures. As previously discussed this is attributed to the chemical reaction of the dissociation of CH_4 falling into the diffusion limiting regime. In the diffusion limited regime the chemical reaction becomes dependent on the gas-phase diffusivity, which is only a weak function of temperature. An example of the diminishing effect on the increase of temperature with respect to flow reversal is shown in Figure 4.15.

Experimental results establish that GHSV can have a significant effect on CH_4 conversion. Figure 4.15 illustrates the effects of GHSV at a ST of 10 seconds with GHSV as a parameter across a reactor furnace temperature range. Figure 4.15 illustrates that as GHSV increases CH_4 conversion decreases. This is due to residence time, or length of time a molecule spends in the catalyst reactor (see Table 4.6). As the GHSV is increased the amount of time a molecule spends in the catalyst reactor decreases. This decrease in residence time results in a lower CH_4 conversion due to the limited time the molecule has to diffuse to the surface of the catalyst.

4.2 Reverse-Flow Oxidation Catalyst Reactor With Supplemental Fuel Injection

Supplemental fuel is introduced into the RFOCR system to simulate fuel injection from a partial oxidation catalyst reactor at low engine load conditions. The supplemental fuel consists of a carbon monoxide and hydrogen mixture at a 3:1 ratio, respectively. This ratio is derived from the partial oxidation of methane and is described in Equation 4.3. Equation 4.4 describes the water-gas shift reaction, but due to equilibrium, Equation 4.4 does not proceed to completion. Furthermore, at typical exhaust temperatures (approximately 400°C) CO concentrations are three times that of H_2 concentrations for partial oxidation reactors; hence the 3:1 ratio of carbon-to-hydrogen used for supplemental fuel injection.

$$CH_4 + {}^{3}/_{2}\, O_2 \rightarrow CO + 2\, H_2O \qquad (4.3)$$

$$CO + H_2O \rightarrow H_2 + CO_2 \qquad (4.4)$$

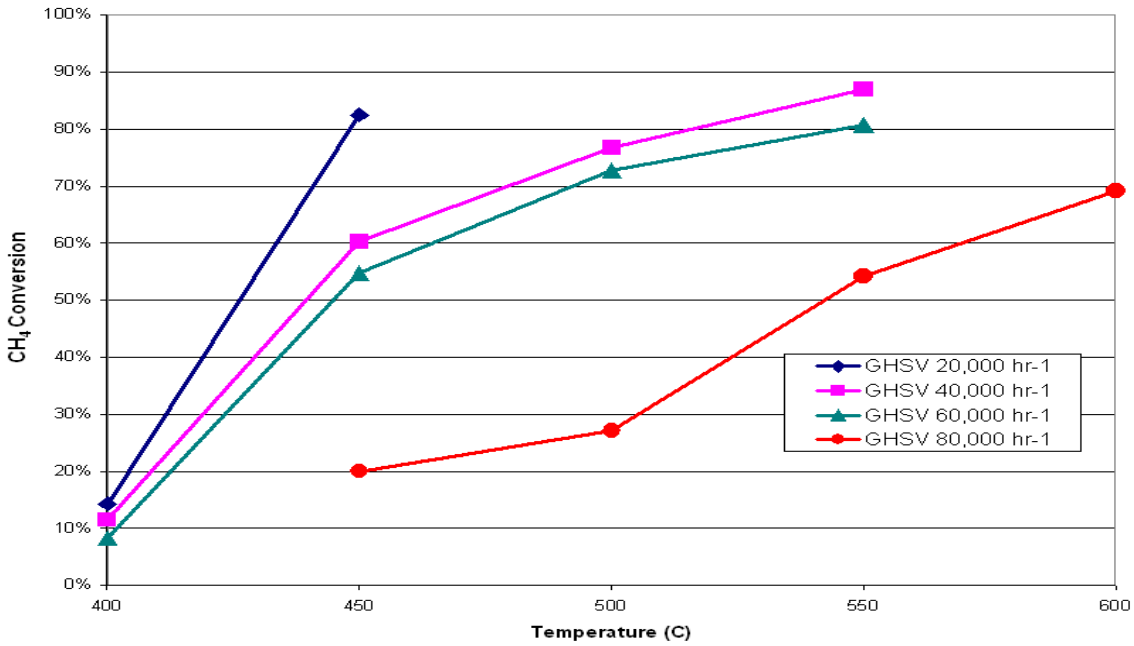

Figure 4.15. Effects of Temperature on CH_4 Conversion with GHSV as a Parameter at a ST of 10s.

Two separate experimental runs with supplemental fuel injection were conducted to evaluate the effects of SFI on CH_4 conversion both with and without flow reversal at low engine load conditions. First, an experimental run was conducted solely with unidirectional flow operations to serve as a supplemental fuel injection baseline, with the total length of the run lasting 1200 seconds in duration. The second experimental run with SFI was conducted with flow reversal with a switching time of 20 seconds. This run with flow reversal is divided into three sections, with the total length of the run also lasting 1200 seconds in duration. The first 300 seconds of the experimental run is conducted with unidirectional flow, followed by 600 seconds of exhaust mixture flow reversal, and concludes with 300 seconds of unidirectional flow. Both experimental runs introduce supplemental fuel into the exhaust mixture prior to the reactor catalyst at experimental run times of t = 300 seconds to t = 800 seconds. The total volumetric flowrate of the supplemental fuel introduced into the exhaust mixture is 350 cc/min at

STP, which corresponds to an exhaust gas mixture concentration of 0.96% of carbon monoxide and 0.32% of hydrogen.

4.2.1 Effects of Supplemental Fuel Injection on CH_4 Conversion

Experimental results confirm introducing supplemental fuel into the RFOCR improves CH_4 conversion by elevating the temperature across the catalyst reactor through the combustion of carbon monoxide and hydrogen and is described by the chemical reactions in Equations 4.5 and 4.6.

$$CO + \frac{1}{2} O_2 \rightarrow CO_2 \qquad (4.5)$$

$$H_2 + \frac{1}{2} O_2 \rightarrow H_2O \qquad (4.6)$$

Figure 4.16 illustrates CH_4 conversion during unidirectional flow operations with 25 10-second pulses of supplemental fuel injection, with a 10 second intermission between pulses at a reactor furnace temperature of 350°C and a GHSV of 20,000 hr^{-1}. From the figure CH_4 conversion is extremely low without supplemental fuel injection (1%), while the average CH_4 conversion increases considerably (10%) with supplemental fuel injection. This increase in CH_4 conversion is be attributed to the increase in temperature due to the combustion of the supplemental fuel. This increase in catalyst temperature is illustrated in Figure 4.17. The temperature profile across the catalyst reactor is shown at various instance of time for the unidirectional flow experimental run. As previously discussed supplemental fuel was injected from an experimental run time of t = 300 seconds to t = 800 seconds, and it is clearly demonstrated from Figure 4.17 that the combustion of supplemental fuel corresponds to the increase in the temperature profile across the catalyst, thereby increasing CH_4 conversion.

The second experimental run with SFI incorporated flow reversal into the

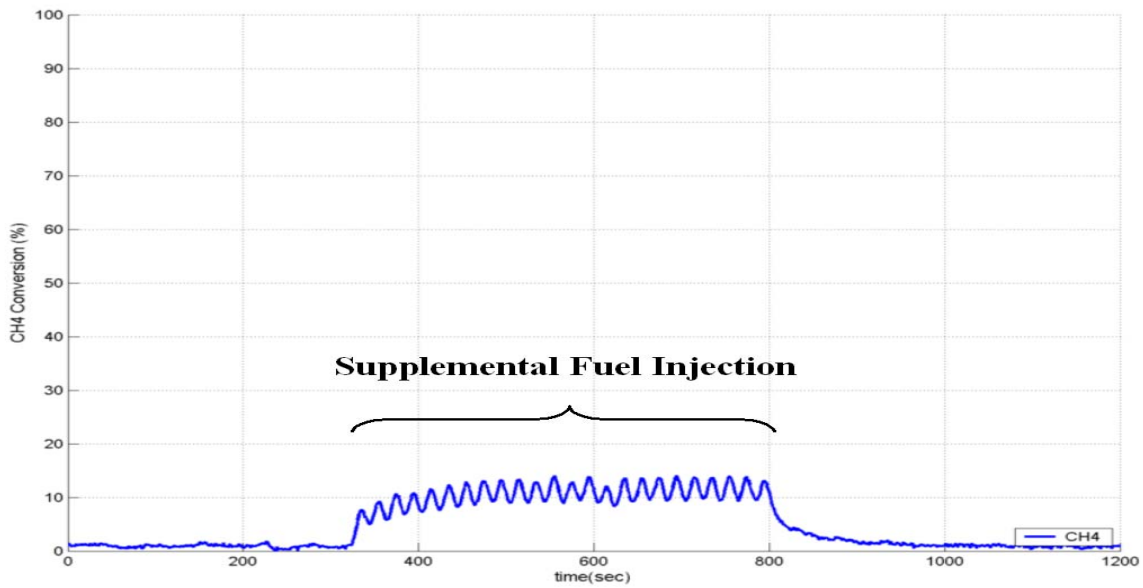

Figure 4.16. Methane Conversion during Unidirectional Flow Operations with 25 10-Second Pulses of SFI, a Reactor Furnace Temperature of 350°C, and a GHSV of 20,000 hr^{-1}.

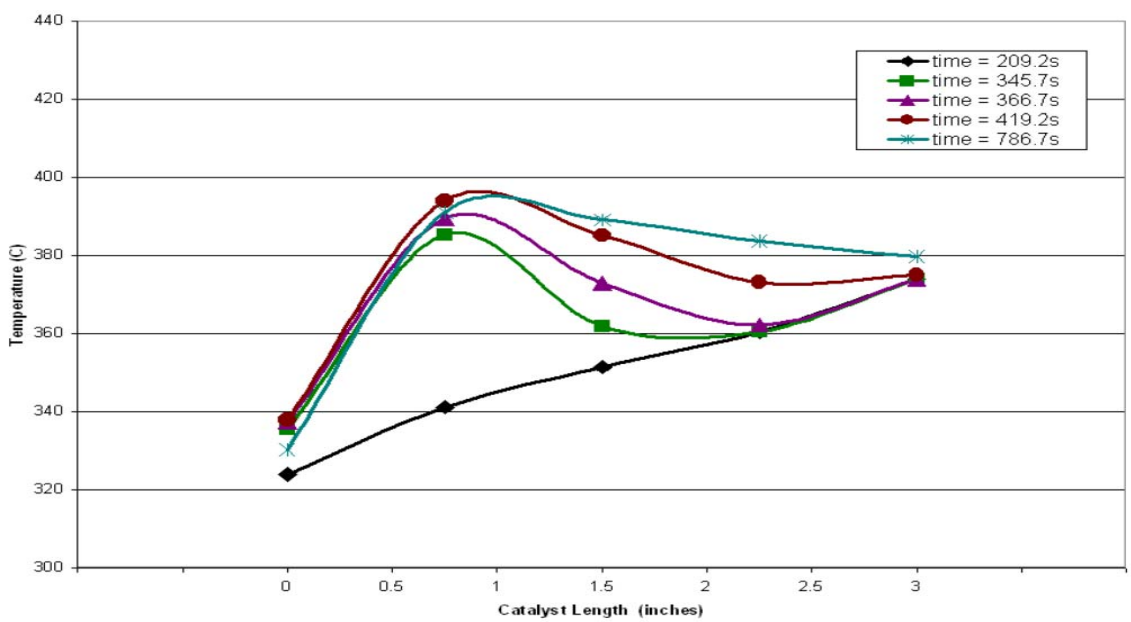

Figure 4.17. Temperature Profile across the Catalyst during Unidirectional Flow Operations at Various Instances of Time with 25 10-Second Pulses of SFI, a Reactor Furnace Temperature of 350°C and a GHSV of 20,000 hr^{-1}.

experimental run. The purpose of this experimental run is to investigate the effects of flow reversal on CH_4 conversion while introducing supplemental fuel into the catalyst reactor. In addition, supplemental fuel injection was introduced into the exhaust mixture from an experimental run time of t = 310 seconds to 810 seconds, while flow reversal continued for an additional 90 seconds after SFI was terminated. The purpose of continuing flow reversal is to examine the possibility of continuing prolonged durations of enhanced CH_4 conversion after terminating supplemental fuel injection.

Experimental results demonstrate that CH_4 conversion is significantly enhanced with SFI and flow reversal. Figure 4.18 illustrates an experimental run conducted with flow reversal with 25 10-second pulses of supplemental fuel injection, with a 10 second intermission between fuel pulses at a reactor furnace temperature of 350°C, a GHSV of 20,000 hr^{-1}, and a ST of 20 seconds. From the figure CH_4 conversion without SFI or flow reversal is extremely low (2%), while the average CH_4 conversion is significantly increased with SFI and flow reversal (15%). This dramatic increase in CH_4 conversion is attributed to the increase in temperature across the catalyst due to the combustion of supplemental fuel and the trapping of heat across the catalyst due to flow reversal. Figure 4.19 illustrates the increase in the temperature profile across the length of the catalyst due to SFI and flow reversal at various times during the course of the experimental run. From Figure 4.19 the increase in CH_4 conversion during SFI and flow reversal is clearly attributed to the increase in temperature across the length of the catalyst. Furthermore, the temperature profile associated with reverse flow operations develops at an experimental run time of t > 419 seconds, but due to improperly timed flow reversal only a portion of the heat is trapped across the catalyst. As previously discussed, premature or delayed flow reversal causes a portion of the temperature profile associated with a reverse-flow reactor (see Figure 2.7(e)) to be pushed outside the length of the catalyst. As a result of this premature or delayed flow reversal the temperature across the catalyst is lowered and CH_4 conversion suffers. Based on the results obtained for the RFOCR without supplemental fuel injection, properly timing flow reversal durations could increase CH_4 conversion, however the optimization of CH_4 conversion with respect to switching time with SFI is out of the scope of this study.

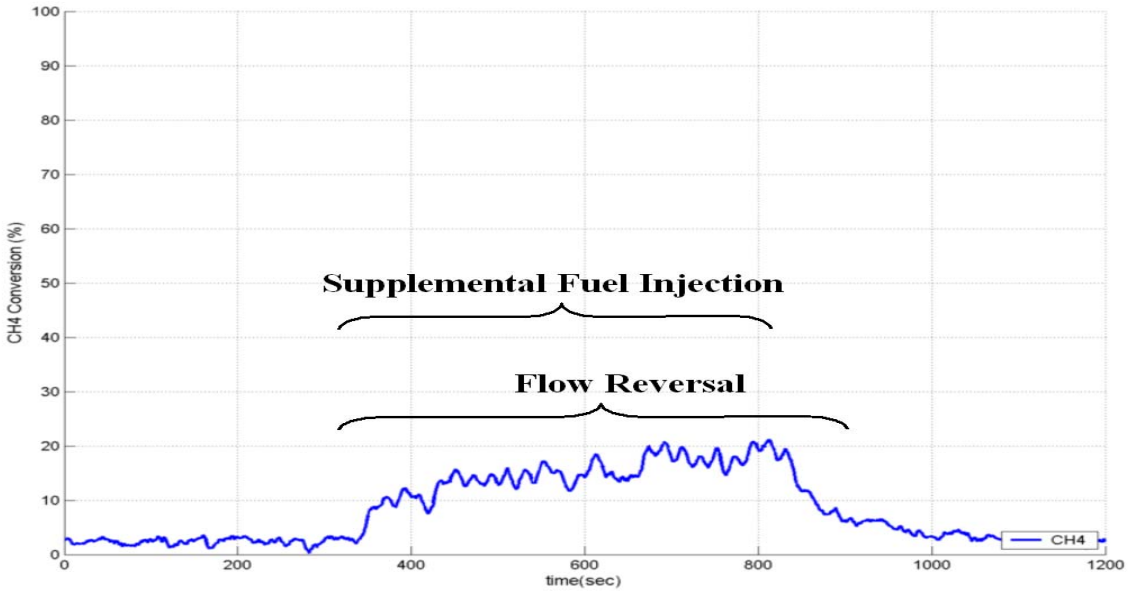

Figure 4.18. Methane Conversion with 25 10-Second Pulses of SFI, a Reactor Furnace Temperature of 350°C, a GHSV of 20,000 hr^{-1}, and a ST of 20s.

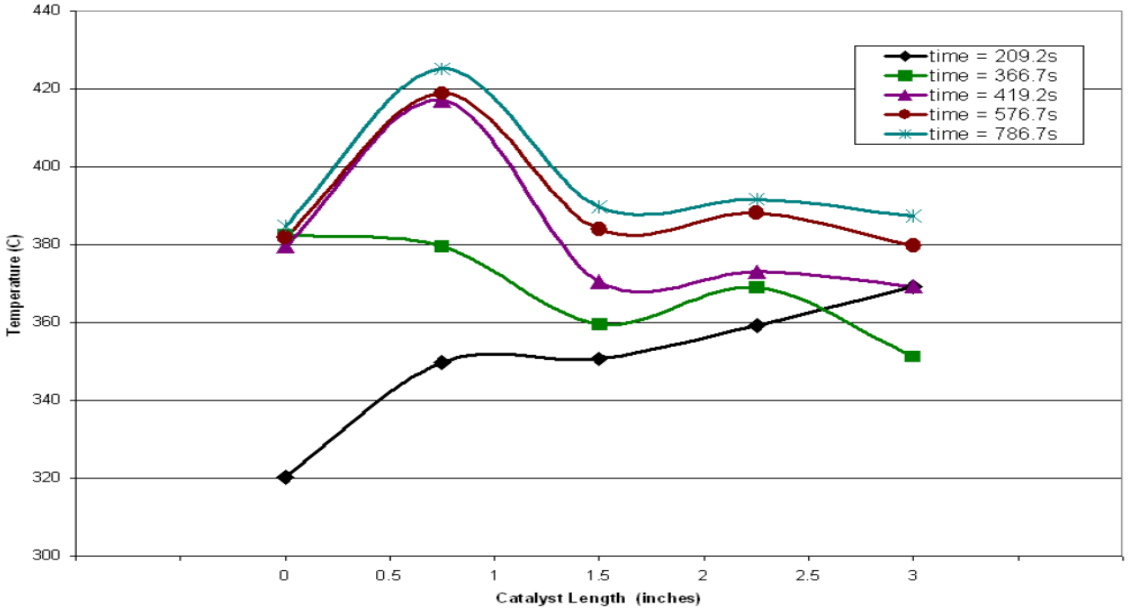

Figure 4.19. Temperature Profile across the Catalyst at Various Instances of Time with 25 10-Second Pulses of SFI, a Reactor Furnace Temperature of 350°C and a GHSV of 20,000 hr^{-1}.

In addition to the examination of the effects of SFI with flow reversal on CH_4 conversion the possibility of continuing prolonged durations of enhanced CH_4 conversion after terminating supplemental fuel injection was investigated. Experimental results indicate that extended durations of increased CH_4 conversion due to flow reversal is not possible after the SFI pulses have concluded and this is shown in Figure 4.18. Figure 4.18 illustrates that CH_4 conversion substantially decreases after less than 20 seconds subsequent to SFI being terminated. This decrease in CH_4 conversion is attributed to a reduction in temperature across the reactor. Figure 4.20 demonstrates the decline in temperature across the catalyst during flow reversal after SFI is terminated. The high rate of reduction of temperature across the catalyst is attributed to an improperly timed switching duration, which pushes the trapped heat out of the length of the catalyst. As described before this reduction in temperature directly correlates to a reduction in CH_4 conversion. From the results obtained for the RFOCR without SFI CH_4 conversion could be maintained for longer durations after SFI is terminated if the switching time is properly. A table demonstrating the average CH_4 conversion for the SFI experimental runs both with and without flow reversal is shown in Table 4.7.

Comparing the two SFI experimental runs it is clear that flow reversal enhances CH_4 conversion when compared to the purely unidirectional flow experimental run. As previously described this increase in CH_4 conversion is attributed to the trapping of heat across the catalyst during flow reversal operations.

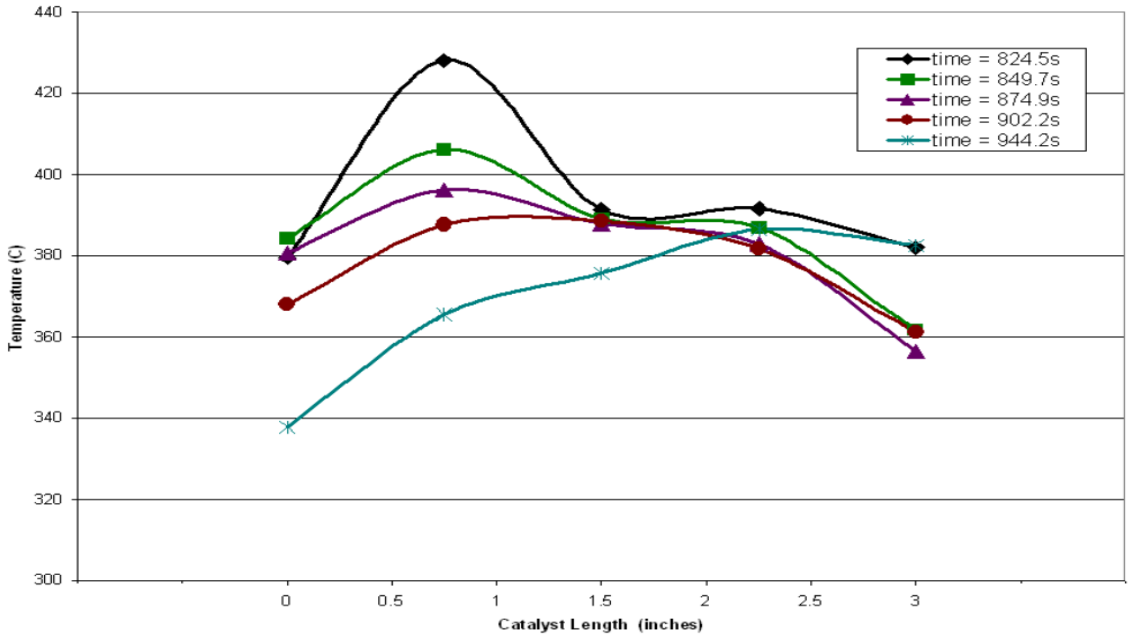

Figure 4.20. Temperature Profile across the Catalyst at Various Instances of Time with 25 10-Second Pulses of SFI, a Reactor Furnace Temperature of 350°C and a GHSV of 20,000 hr^{-1}.

Table 4.7. Average CH_4 Conversion With and Without SFI for Unidirectional Flow and Flow Reversal at a Reactor Furnace Temperature of 350°C, a GHSV of 20,000 hr^{-1}, and a ST of 20s for Flow Reversal Operations.

	Unidirectional Flow	Flow Reversal
Average CH_4 conversion without SFI	1%	10%
Average CH_4 conversion with SFI	2%	15%

CHAPTER 5

CONCLUSIONS AND RECOMMENDATIONS

The results of this research demonstrate the effects of flow reversal duration, temperature, and gas hourly space velocity on methane conversion for a reverse-flow reactor over a wide range of engine conditions. In addition, the research investigates the effects of supplemental fuel injection on methane conversion during flow reversal operations at low engine load conditions. The goal of the research is to optimize system parameters to obtain a maximum CH_4 conversion in a simulated natural gas exhaust stream.

Experimental results indicate periodic flow reversal through a catalyst reactor can significantly increase methane conversion when compared to standard unidirectional flow. Reverse-flow operations at relatively low feed temperatures (400°C - 450°C) and low gas hourly space velocities (20,000 hr^{-1}) experience increases as high as 77% in methane conversion, while methane conversion at high feed temperatures (550°C-600°C) and high gas hourly space velocities (80,000 hr^{-1}) experience increases as high as 292%. Experimental results conclude that CH_4 conversion is a function of flow reversal duration at a particular temperature and gas hourly space velocity. Low frequency flow reversal durations (30 and 45 seconds) prove to be most effective in increasing methane conversion at a gas hourly space velocity of 20,000 hr^{-1}, while high frequency flow reversal durations (30 and 45 seconds) demonstrate a higher CH_4 conversion at gas hourly space velocity of 40,000 hr^{-1}, 60,000 hr^{-1}, and 80,000 hr^{-1}.

Experimental results indicate that CH_4 conversion can be significantly improved with the injection of a supplemental fuel into the feed mixture at low engine load conditions. Further improvement with regard to CH_4 conversion can be obtained with the injection of supplemental fuel while reversing the feed mixture through the catalyst

reactor. It is recommended that further examination into the optimal duration for flow reversal at a particular temperature and gas hourly space velocity be conducted to obtain a maximum CH_4 conversion during supplemental fuel injection.

REFERENCES

REFERENCES

[1] Raine, R.R., Zhang, G., and Pflug, A., "Comparison of Emissions from Natural Gas and Gasoline Fuelled Engines - Total Hydrocarbon and Methane Emissions and Exhaust Gas Recirculation Effects," SAE Paper 970743, 1997.

[2] Liu, B., Checkel, M.D., Hayes, R.E., Zheng, M., and Mirosh, E., "Experimental and Modeling Study of Variable Cycle Time for a Reversing Flow Catalytic Converter for Natural Gas/Diesel Dual Fuel Engines," SAE Paper 2000-01-0213, 2000.

[3] Williams, A., "Lean NO_x Trap Catalysis for Lean-Burn Natural Gas Engines," M. Sc. Thesis, Department of Mechanical Engineering, The University of Tennessee-Knoxville, 2004.

[4] Salomons, S., Hayes, R.E., Poirier, M., and Sapoundjiev, H., "Flow Reversal Reactor for the Catalytic Combustion of Lean Methane Mixtures," Catalysis Today, Vol. 83, 2003, pp. 59-69.

[5] Watts, R.G., Engineering Response to Global Climate Change. Boca Raton: Lewis Publishers, 1997.

[6] Steinfeld, J.I., Francisco, J.S., Hase, W.L, Chemical Kinetics and Dynamics, 2nd ed. New Jersey: Prentice Hall, 1999.

[7] Eguchi, K. and Hiromichi, A., "Low Temperature Oxidation of Methane Over Pd-Based Catalysts-Effect of Support Oxide on the Combustion Activity," Applied Catalysis A: General, Vol. 222, 2001, pp. 359-367.

[8] Anderson, R.B., Stein, K.C., Feenan, J.J., and Hofer, J.E., "Catalytic Oxidation of Methane," Industrial and Engineering Chemistry, Vol. 53, 1961, pp. 809-812.

[9] Hayes, R.E. and Kolaczkowski, S.T., Introduction to Catalytic Combustion. Amsterdam, Netherlands: Gordon and Breach Publishers, 1997.

[10] Subramanian, S., Kudla, R.J., and Chattha, M.S., "Treatment of Natural Gas Vehicle Exhaust," SAE paper 930223, 1993.

[11] Bartholomew, C., H., "Mechanisms of Catalyst Deactivation," Applied Catalysis A: General, Vol. 212, 2001, pp. 17-60.

[12] Euzen, P., Le Gal, J., Rebours, B., and Martin, G., "Deactivation of Palladium Catalyst in Catalytic Combustion of Methane," Catalysis Today, Vol. 47, 1999, pp. 19-27.

[13] Burch, R., Urbano, F.J., and Loader, P.K., "Methane Combustion Over Palladium Catalysts: The Effect of Carbon Dioxide and Water on Activity," Applied Catalysis A: General, Vol. 123, 1995, pp. 173-184.

[14] Kikuchi, R., Maeda, S., Sasaki, K., Wennerstrom, S., Eguchi, K., "Low-Temperature Methane Oxidation Over Oxide-Supported Pd Catalysts: Inhibitory Effect of Water Vapor," Applied Catalysis A: General, Vol. 232, 2002, pp.23-28.

[15] Strots, V.O., Bunimovich, G.A., Matros, Y.S., Zheng, M., and Mirosh, E.A., "Novel Catalytic Converter for Natural Gas Powered Diesel Engines," SAE Paper 980194, 1998.

[16] Neumann, D., Veser, G., "Catalytic Partial Oxidation of Methane in a High-Temperature Reverse-Flow Reactor," AIChE Journal, Vol. 51, No.1, 2005, pp.210-223.

[17] Lisenby, P., "An Experimental Investigation of Natural Gas Catalysts Using a Bench-Flow Reactor," M. Sc. Thesis, Department of Mechanical Engineering, The University of Tennessee-Knoxville, 1995.

[18] Instruction Manual AIA-210/220 CO/CO_2 Infrared Analyzer, Horiba Instruments Inc., Irvine, CA, 1989.

[19] Instruction Manual FIA-220 Hydrocarbon Flame Ionization Magneto-Pneumatic Analyzer, Horiba Instruments Inc., Irvine, CA, 1989.

[20] Zufle, H. and Turek, T., "Catalytic Combustion in a Reactor with Periodic Flow Reversal. Part 1. Experimental Results," Chemical Engineering and Processing, Vol. 36, 1997, pp. 327-340.

[21] Manivannan, A., Tamilporai, P., Chandrasekaran, S., and Ramprabhu, R., "Lean Burn Natural Gas Spark Ignition Engine - An Overview," SAE Paper 2003-01-0638, 2003.

[22] Matros, Yu. Sh., Unsteady Processes in Catalytic Reactors. Amsterdam: Elseveier, 1985.

[23] McCormick, R., Newlin, A.W., Mowery, D., Graboski, M.S., and Ohno, T.R., "Rapid Deactivation of Lean-Burn Natural Gas Engine Exhaust Oxidation Catalysts," SAE Paper 961976, 1996.

[24] Kamel, M., Lyford-Pike, E., Frailey, M., Bolin, M., Clark, N., Nine, R., and Wanye, S., "An Emission and Performance Comparison of the Natural Gas Cummins Westport Inc. C-Gas Plus versus Diesel in Heavy-Duty Trucks," SAE Paper 2002-01-2737, 2002.

[25] Nauman, E. Bruce, Chemical Reactor Design, Optimization, and Scaleup. New York: McGraw-Hill, 2002.

[26] Fogler, H. Scott, Elements of Chemical Reaction Engineering 3rd ed. New Jersey: Prentice Hall, 1999.

[27] Stewart, R., Oxidation Mechanisms: *Applications to Organic Chemistry*. New York: W.A. Benjamin, INC., 1964.

[28] Aris, Rutherford, Elementary Chemical Reactor Analysis. Massachusetts: Butterworths, 1989.

[29] Oyama, S. Ted, Hightower, Joe W., Catalytic Selection Oxidation. Washington, DC: American Chemical Society, 1993.

[30] Anderson, J.R., Pratt, K.C., Introduction to Characterization and Testing of Catalysts. Australia: Academic Press, 1985.

[31] Wicke, Lutz, Beyond Kyoto - A New Global Climate Certificate System. Germany: Springer, 2005.

[32] Turns, Stephen R., An Introduction to Combustion 2nd ed. Massachusetts: McGraw-Hill, 2000.

[33] Ryan, T.W. and Callaghan, T.J., "The Effects of Natural Gas Composition on Engine Combustion, Performance, and Emissions," SAE Paper 925012, 1992.

APPENDIX

Table A-1. Specifications for the Analyzers.

AIA-220 Carbon Monoxide & Carbon Dioxide Analyzer		
Ranges	CO(L)	0-100 ppm to 3000 ppm
	CO(H)	0-5000 ppm to 10 volume%
	CO_2	0-1 volume% to 20 volume %
Repeatability	+/- 1% full scale	
Zero/Span Drift	+/- 1% full scale / 8 hours	
Response	90% electrical response in 2 seconds	
Output	0-5 VDC	
FIA-220 Total Hydrocarbon Analyzer		
Ranges	0-10 ppm to 30,000 ppm	
Repeatability	+/- 1% full scale	
Zero/Span Drift	+/- 1% full scale / 8 hours	
Response	90% electrical response in 1.5 seconds	
Output	0-5 VDC	

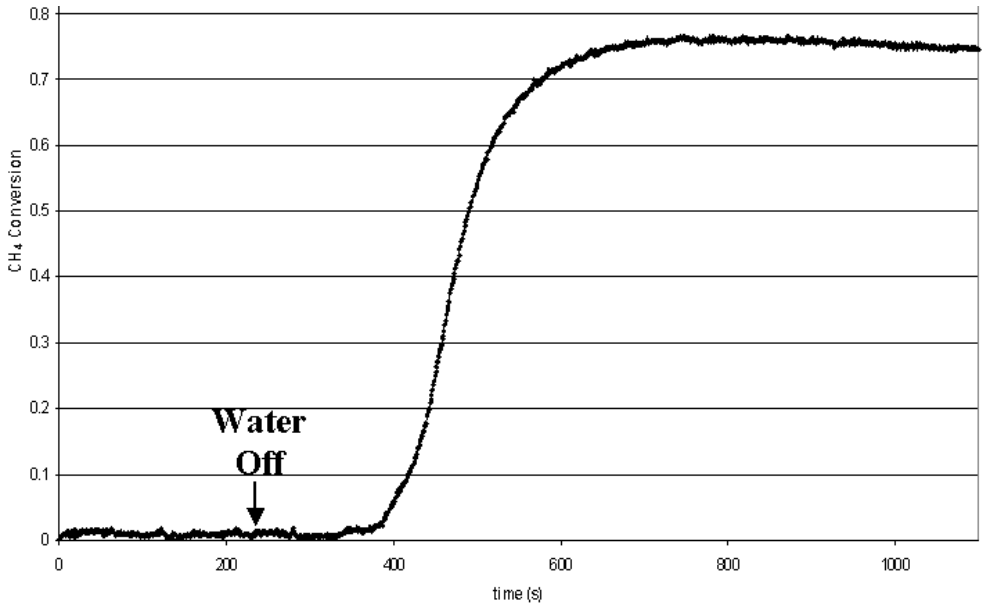

Figure A-1. Effects of 10% Water Vapor on the Methane Conversion at 350°C.

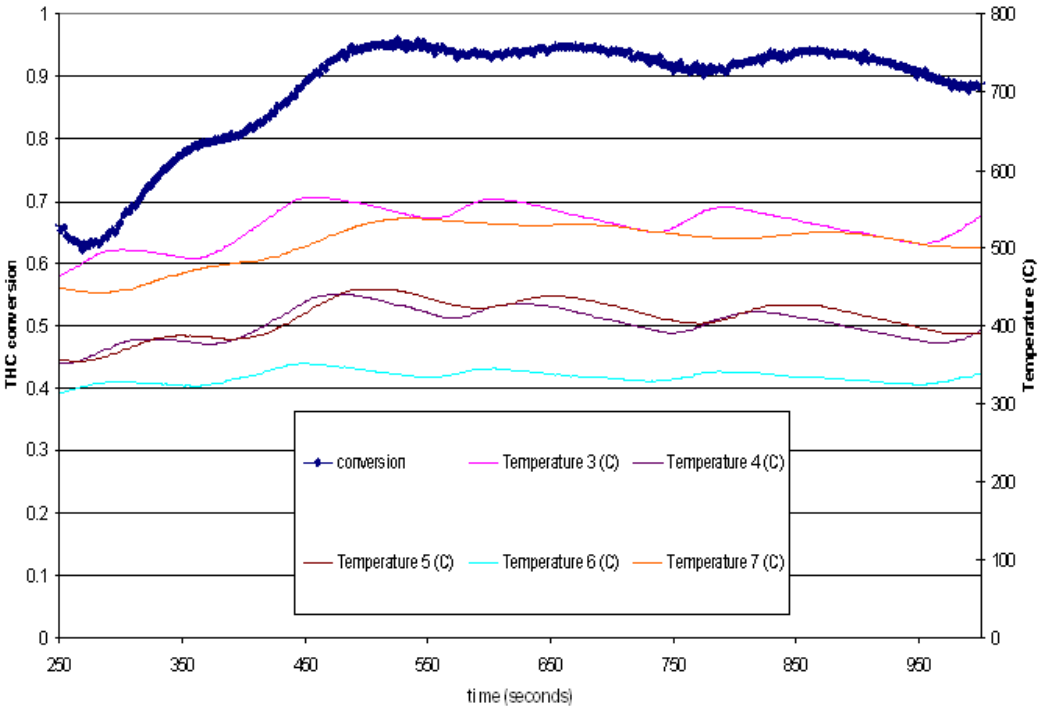

Figure A-2. Initial Reverse Flow Oxidation Catalyst Reactor with Temperature Oscillation

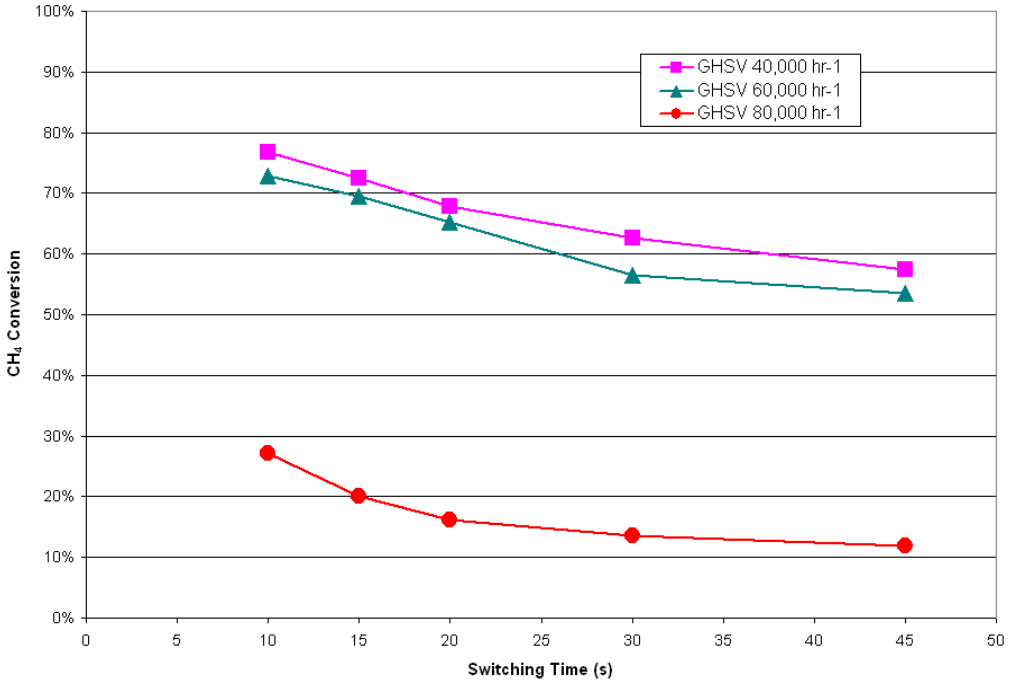

Figure A-3. Effects of Switching Time on CH_4 Conversion with GHSV as a Parameter at a Temperature of 500°C.

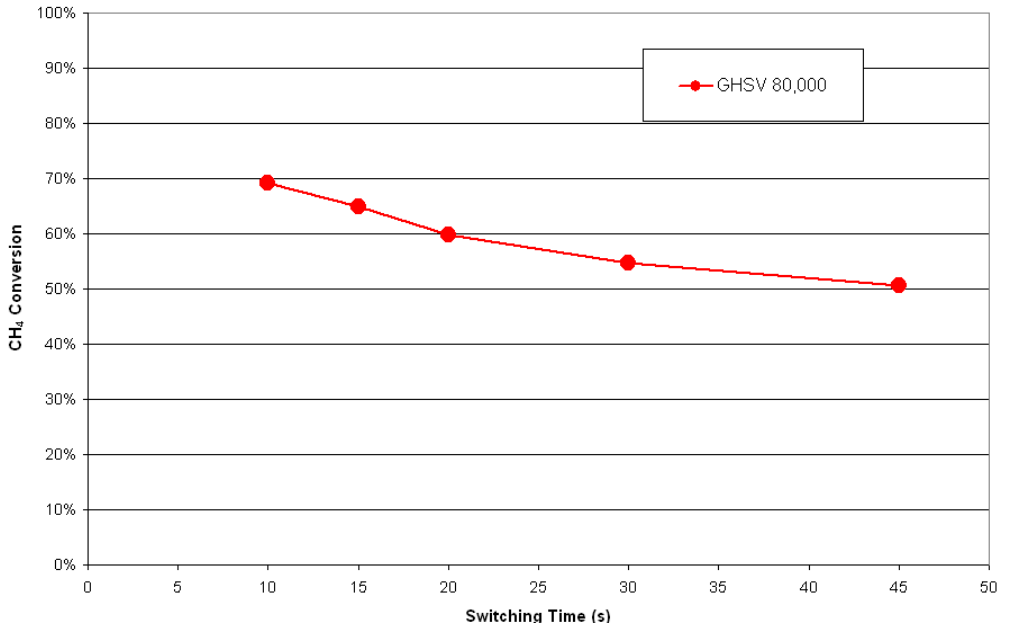

Figure A-4. Effects of Switching Time on CH_4 Conversion with GHSV as a Parameter at a Temperature of 600°C.

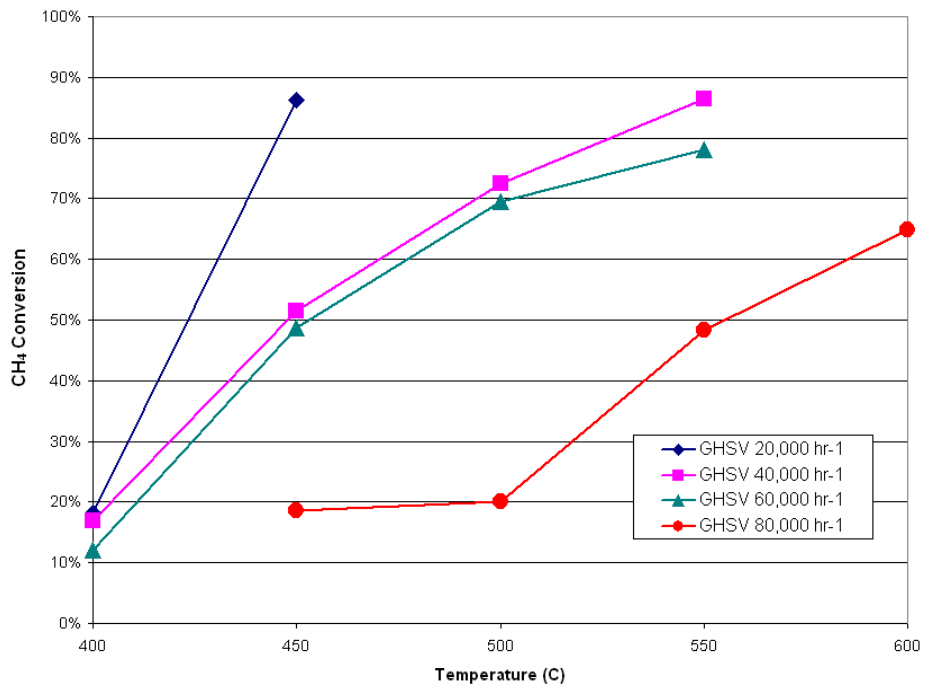

Figure A-5. Effects of Temperature on CH4 Conversion with GHSV as a Parameter at a ST of 15s.

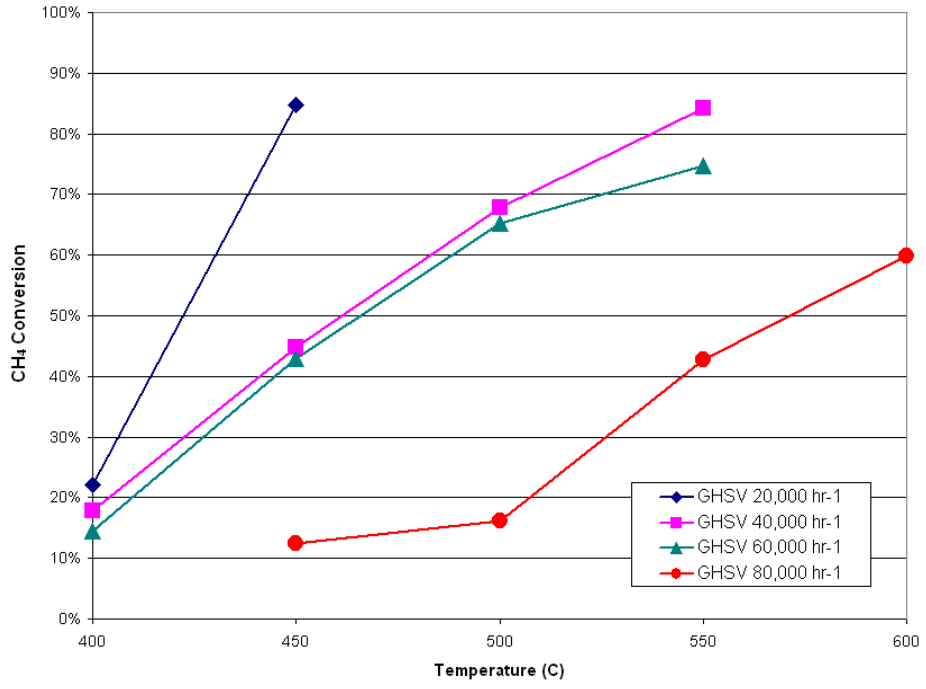

Figure A-6. Effects of Temperature on CH4 Conversion with GHSV as a Parameter at a ST of 20s.

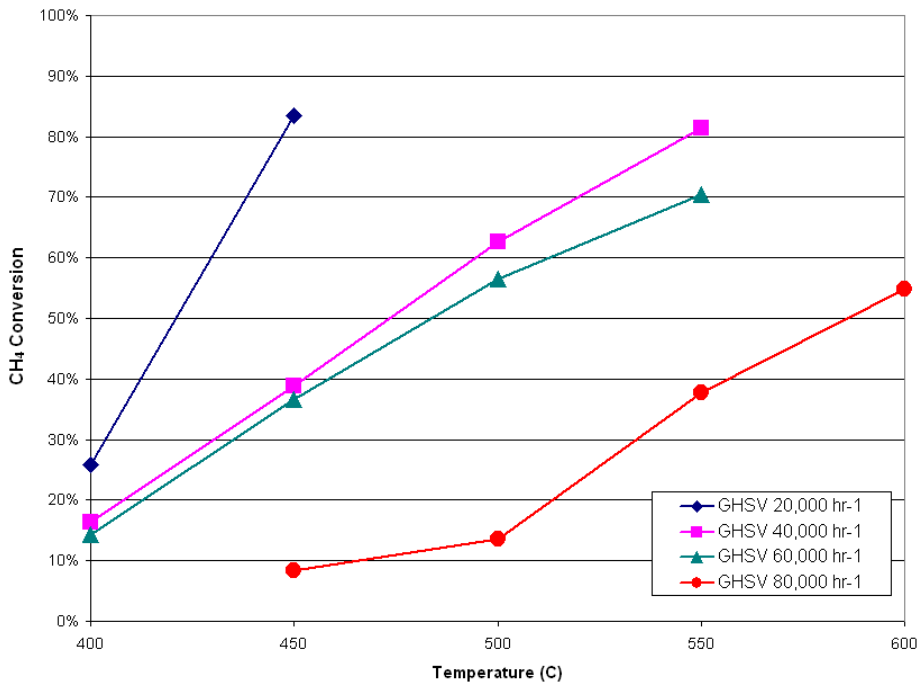

Figure A-7. Effects of Temperature on CH4 Conversion with GHSV as a Parameter at a ST of 30s.

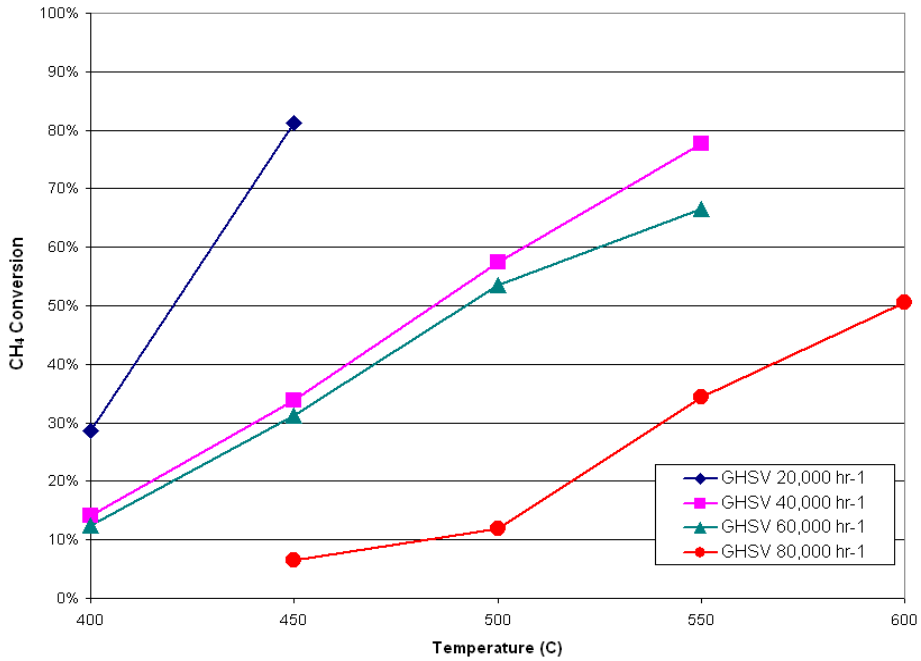

Figure A-8. Effects of Temperature on CH4 Conversion with GHSV as a Parameter at a ST of 45s.

VITA

Scott Smith was born in Phoenix, Arizona on December 19, 1975. Two weeks after completing high school in 1994, he enlisted into the U.S. Navy and served aboard the submarine U.S.S. Augusta (SSN 710) as a sonar technician from 1994 to 1998. Upon being honorably discharged from the Navy he entered the University of Tennessee's Mechanical Engineering Program. Subsequent to receiving his Bachelors of Science in Mechanical Engineering he enrolled in the graduate studies program at the University of Tennessee. Scott received his Masters of Science degree in Mechanical Engineering from the University of Tennessee in August 2005.